^{7}Li NMR studies of low-frequency motion of lithium ions in fast ion conducting glasses.

Tomoko Akai
Osaka National Research Institute, AIST

Abstract

Low frequency motion of ions in glassy ionic conductors was investigated by ^{7}Li NMR and the electrical conductivity measurements. Glassy system Li_2O-B_2O_3-Li_2SO_4, Li_2S-Ga_2S_3-GeS_2 and Li_2S-B_2S_3 system, which show high conductivities were prepared for the purpose to elucidate quantitative information on conduction mechanism in glasses from the microscopic point of view. The analyses of the line width of NMR spectrum have been attempted on the basis of standard theories for large number of materials including different kinds of glasses but the most of these analyses have let to invalid activation parameters (E_a and τ_0) for describing the molecular or ionic motion. Here, a new method of the analysis of the motional narrowing of the line width of ^{7}Li NMR spectrum incorporating the Kohlraush-Williams-Watt relaxation function was proposed. Application of the method to the ^{7}Li NMR spectra of fast-ion conductors, Li_2O-B_2O_3-Li_2SO_4, Li_2S-B_2S_3, Li_2S-Ga_2S_3-GeS_2, succeeded to elucidate reasonable activation parameters in comparison with those derived by the T_1 measurement. The present work clarified an important point that there are strict discrepancy in the activation parameters between those deduced by NMR and by the conductivity measurements for both the fast-ion conductors and oxide glasses with relatively low conductivity. The comparison of these data gave rise to a microscopic image for the electric conduction in glass that there occur very frequent random migration of ions in short-range, *i.e.*, a migration, back and forth in some restricted narrow region but a small fraction of ions among these ions find some long-distance path to transport through an intermediate structure of glassy system. The first success of the direct measurements of the diffusion coefficient in a few fast-ionic conducting glasses was very useful to establish the above image for the conducting glasses. In order to shed light on the hitherto unknown structure and properties so-called intermediate parts of the glass, the author attempted to measure alkali-oxide glass by varying the concentration of the dopant This method found to be promising for deducing microscopic information in the intermediate structure.

Contents

Chapter 1 Introduction 1

Chapter 2 Sample preparation 13
2-1 Preparation
2-1-1 Oxide glasses
2-1-2 Sulfide glasses
2-2 Characterization

Chapter 3 Electrical properties 19
3-1 Introduction
3-2 Experimental
3-3 Results and Discussion
3-3-1 DC conductivity
3-3-2 Modulus

Chapter 4 Temperature dependence of ^{7}Li NMR spectrum 41
4-1 Introduction
4-2 fundamental theories for the analysis
4-2-1 Bloembergen, Purcell and Pound (BPP) theory.
4-2-2 General theory of motional narrowing of the line width
4-3 Numerical Calculation of LW
4-4 Experimental
4-5 Results
4-6 Discussion

Chapter 5 Diffusion coefficient of Li 79
5-1 Introduction
5-2 Experimental
5-3 Results and Discussions

Chapter 6 Structural chug with doping salt 90
6-1 Introduction
6-2 Experimental
6-3 Results and Discussion

Chapter 7 Discussion and Summary 96

Appendix A
Appendix B

Chapter 1 Introduction

Ionic conduction in inorganic glasses has attracted great interests since it plays a key role in glass technology as well as glass science[1,2]. Usually, it occurs efficiently at high temperatures and very slow at room temperature. However, some class of glasses with high alkali content exhibits high conductivity at room temperature. These glasses are called "fast ionic conductor(FIC)". The study on glassy fast ionic conductor started in 1970's and various glassy ionic conductors were reported since then. Above all, Li glassy ionic conductors are of great interest because of their possible application as solid electrolytes in high energy-density batteries[3]. Glasssy ionic conductors are fascinating class of materials because they are isotropic, heat-stable and easily formed in bulk into any desired shape.

Glassy Li-conductors with various compositions hitherto are given in Figure 1-1. The binary oxide system, which is composed of network-former(SiO_2,P_2O_5,B_2O_3) and network-modifier(Li_2O), shows relatively low conductivity at 25°C(lower than $10^{-7}cm^{-1}$). One good method to increase the conductivity is to add some lithium salt to the system. Levasseur et al. found that the addition of LiX(X=F,Cl,Br,$(SO_4)_{1/2}$) drastically improves conductivity[4,5]. For instance, the conductivity of Li_2O-B_2O_3-LiCl or Li_2O-B_2O_3-Li_2SO_4 is increased up to10^{-6} Scm^{-1} at room temperatures[4,5,6]. However, this value seems to be the upper limit of conductivity that can be achieved by oxide-based glasses.

In pursuit of more conductive glasses, Pradel et al. considered on the bases of a weak electrolyte model that conductivity is greatly enhanced if the fraction of dissociated Li ion is increased by substituting O by S. They succeeded in preparing a Li^+ conductive sulfide glass that shows high conductivity as 10^{-4} Scm^{-1} at 25°C[7]. Conductivity of several other Li^+ conductive sulfide glasses have already been studied and reviewed[8,9,10]. It was later reported that the conductivity of $10^{-3}Scm^{-1}$ was succesfully achieved by doping of LiX. Though these glasses show much higher conductivity, they are very hygroscopic and can only be handled in an inert atmosphere where residual water content is decreased down to ppm level. Hence, some special apparatus and elaborate operation are necessary in preparation, so that the number of research group which works on studying the material successfully is not numerous to the author's knowledge.

As is shown above, the relation between the compositon and conductivity is well understood. However, the microscopic mechanism of conduction in these glasses is not well

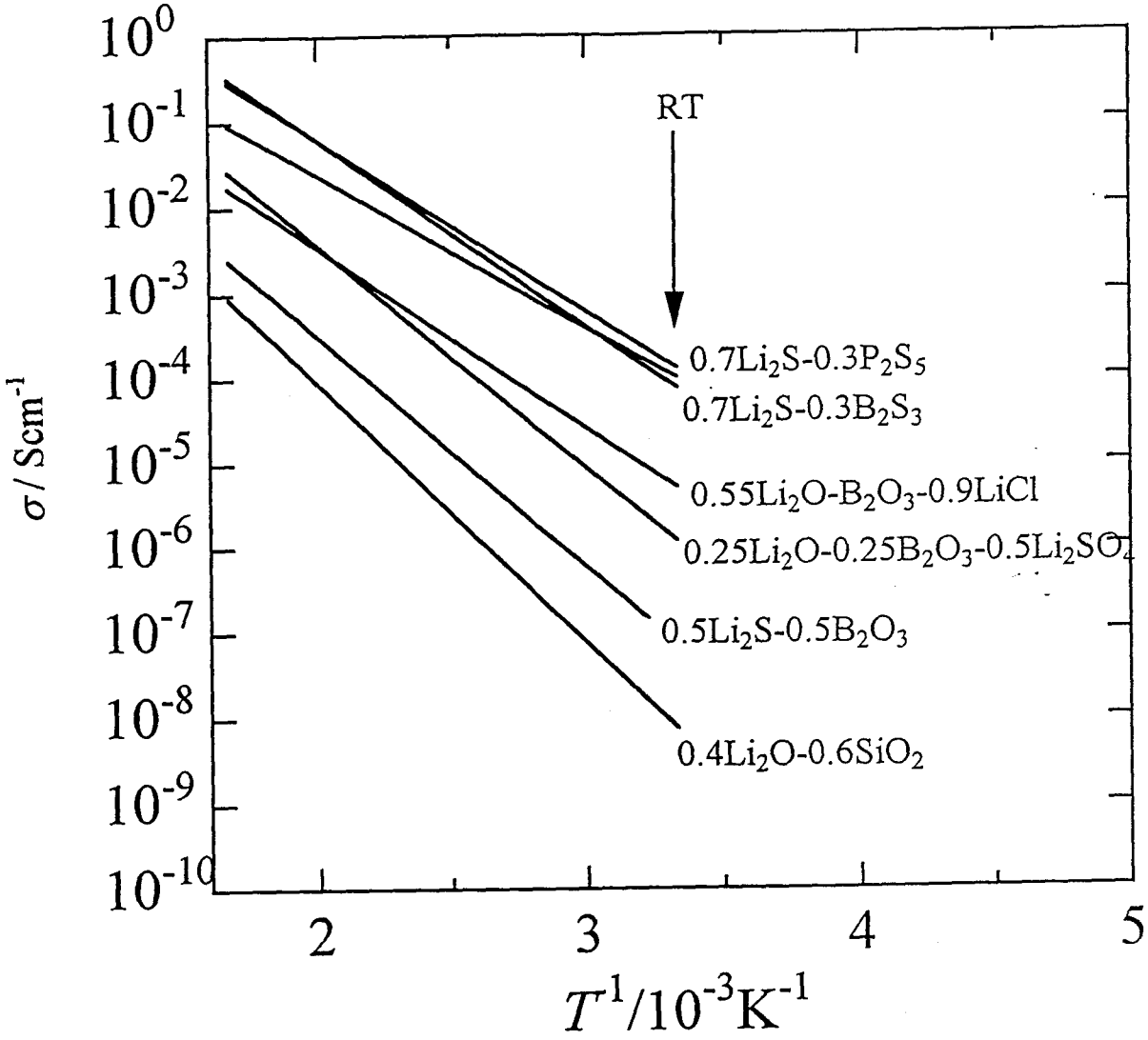

Figure 1-1 Conductivity of several Li conductive glasses.

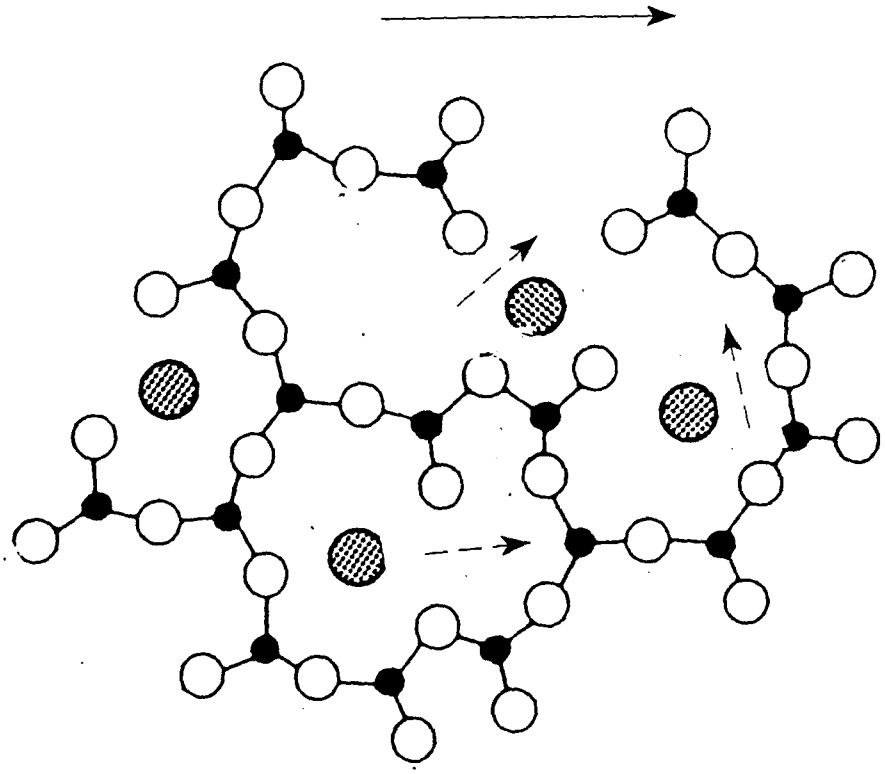

Figure 1-2 A model for ionic diffusion in glasses.

investigated. Figure 1-2 displays a model for ionic diffusion in glasses. Conductivity measurement observes the macroscopic current caused by the motion of indivisual ions, in other words, long range transport of charge carriers which are produced by the ensemble averaged local motion of huge number of ions (solid arrow). To understand the mechanism of ionic conduction in glassy material, the possible relation between microscopic motions (dashed arrow) and the macroscopic transport of carriers should be clarified. Nuclear magnetic resonance is one of the most powerful methods to investigate the local motion of ions.

To elucidate the motional mode concerning the ionic conduction by nuclear magnetic resonance, the temperature dependence of several characteristic parameters of NMR are commonly used. Spin-lattice relaxation time, T_1, spin lattice relaxation time in the rotating frame, $T_{1\rho}$, and line width, LW. To interpret these quantities, Bloembergen-Purcell and Pound(BPP) theory[11] is commonly used. In the analyses, a correlation function, $g(t)$, is used and this is assumed to be single exponential relaxation of single function time, τ_c, as

$$g(t)=\exp(-t/\tau_c). \qquad (1\text{-}1)$$

τ_c is assumed to obey the Arrhenius rule,

$$\tau_c=\tau_0 \exp(E_a/RT), \qquad (1\text{-}2)$$

where E_a is the activation energy for the atomic or molecular motion. In this case, the plot of T_1, $T_{1\rho}$, and LW varies with temperature as shown in Figure 1-3(a). T_1 and $T_{1\rho}$ vs. $1/T$ give symmetric V-shape curves with a slope of $-E_a/R$ and E_a/R on either side of T_1 minimum. Minimum in T_1 or $T_{1\rho}$ is observed at $\omega_0\tau_c\approx1$ or $\omega_1\tau_c\approx1$, where ω_0 is the Larmor frequency and ω_1 the frequency of oscillating field.

In the case of glasses or ionic conductors, these NMR parameters behave quite differently as shown in Figure 1-3(b) since correlation function, $g(t)$, deviates very often from the single exponential; These shapes can be reproduced by introducing a special form relaxation of [12],

$$g(t)=\exp(-(t/\tau_c)^{\beta}). \qquad (1\text{-}3)$$

Equation (1-3) is called Kohlraush-Williams-Watt(KWW) function. KWW function is a phenomelogical function and its physical picture is still unknown, although some models to interpret it are proposed[13,14]. In this case, slope of T_1 on the low temperature side (E_{T_1}) corresponds to βE_a, which is much lower than true activation energy.

In poor-conducting glasses such as binary oxide glasses, T_1 on the low temperature side of its minimum is only measureable below the glass transition point, T_g[15,16,17]. The lower

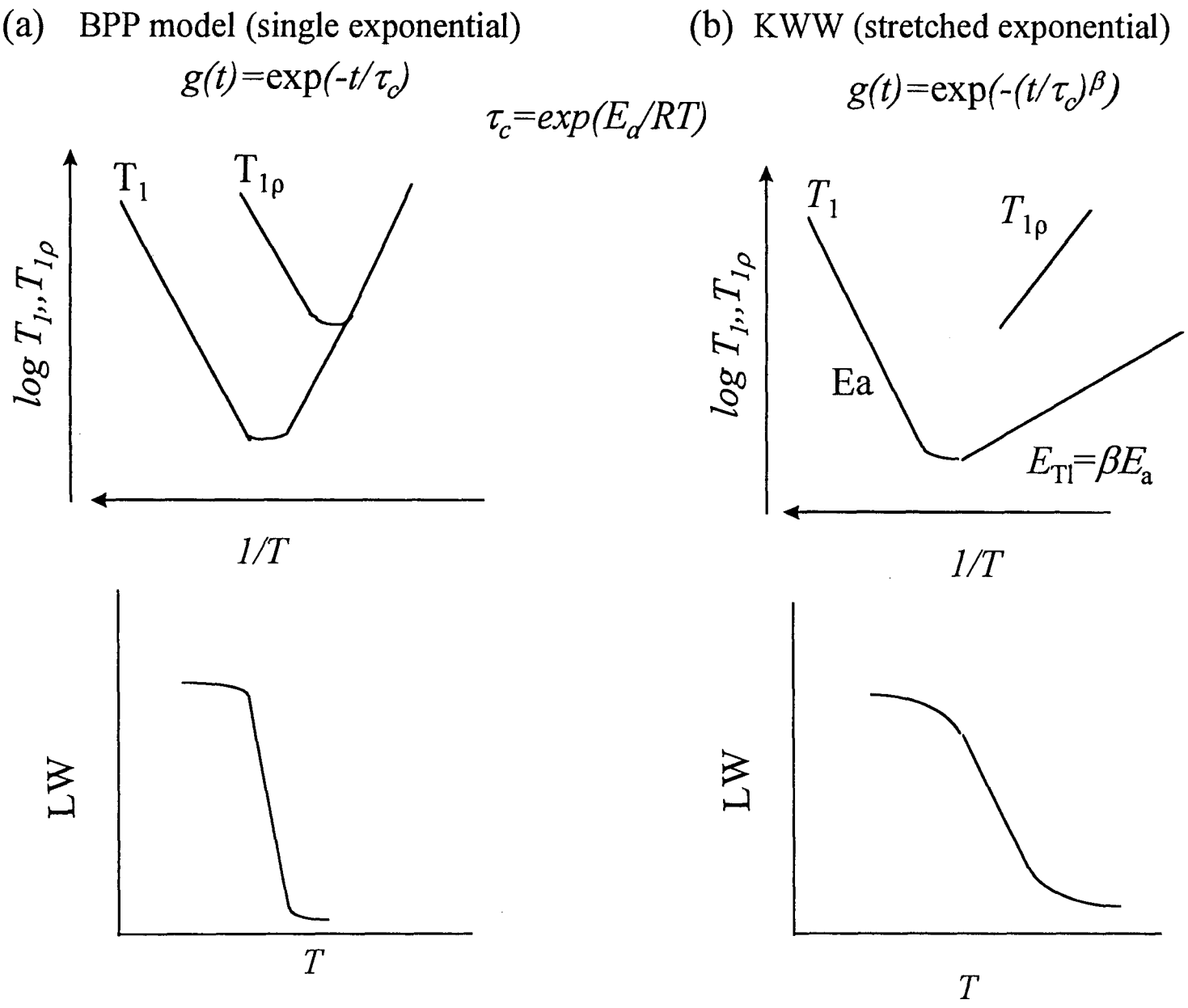

Fig.1-3 Temprerature dependence of NMR parameters.
(a)single exponential relaxation, (b) KWW relaxation observed in glasses.

activation energy observed by T_1 measurement was once explained by the existance of local motion that is not directly related to ionic conduction. In ternary oxide glasses which shows relatively high conductivity, such as Li_2O-B_2O_3-LiCl, T_1 minimum was observed, although high-temperature side of T_1 was not observed[18]. Since the motion of ions in sulfide glasses is considerably fast, it is expected that whole range of T_1 is observed in these glasses. Indeed, whole range of T_1 was observed in Li_2S-SiS_2 [19]. It was found that E_a nearly equals to that determined from conductivity measurement and it was concluded that these two measurements observe roughly the identical phenomenon.

Recently, new type of discrepancy between the above two measurements was reproted by Tatsumisago et al in Li_2O-B_2O_3-LiCl system[20]. They determined the relaxation time for the conductivity from the temprature dependence of modulus. The relaxation time was compared with that from T_1. It was found that correlation time from NMR(τ_{NMR}) is larger than the relaxation time from conductivity (τ_{cond}) from one to two ordres. Later, Borsa et al. studied the Li_2S-SiS_2 system and found that $\tau_{NMR}/\tau_{cond} \cong 10\text{-}10^2$ and $\beta_{NMR} < \beta_{cond}$[21]. The origin for such inconsistency has been the subject of controversy for the last few years [22,23]. However, no further experimental works which compares the electrical and NMR relaxation was reported because the number of glasses which gives T_1 minimum below T_g is limited and most of them have already been examined. For the universal understanding of conduction mechanism in ionically conducting glasses, it is promising to study $T_{1\rho}$ and LW which can monitor "slower motion" of ions.

The behavior of $T_{1\rho}$, however, is very questionable. Knart et al[24] studied the ^{7}Li $T_{1\rho}$ in Li_2O-GeO_2 glasses and found that the activation energy deduced from $T_{1\rho}$ is higher than that from T_1, E_{T1}. Similarly, Göbel[16] et al. measured $T_{1\rho}$ in several oxide glasses and found different activation energy from E_{T1}. $T_{1\rho}$ in Li_2O-Na_2O-B_2O_3 system also leads to a higher activation energy than E_{T1} on the low temperature side[17]. In this case, locked magnetization does not decay exponentially, but obeys the square of time, $\exp(-\alpha t^2)$. In Li_2S-Ga_2S_3-GeS_2 system $T_{1\rho}$ brings about a higher activation energy than that by T_1 and the minimum was observed in $T_{1\rho}$[25]. The author believes that these descrepancies is not intrisic of the relaxation behavior in ionic conductior since ^{19}F $T_{1\rho}(I=1/2)$ in fluorozirconate glass gives the activation energy which is consistnet with that from T_1 on low-temperature side[22]. The origin of this is unknown at present, but it may be brought about by nuclear quadrupole interaction.

The line width amounts usually to several kHz in glassy Li conductors in the absence of motion. It is decreased drastically by the onset of motion of ions of the order of kHz. In principle,

this phenomenon, so-called "motional narrowing of the line width (MNLW)", is effective in monitoring motions of the order of kHz. Although ^{7}Li MNLW in glasses was extensively studied, it is usually regarded as a meaningless parameter to describe the MNLW and abandoned in the studies of glassy ionic conductors. Bishop and Bray first studied ^{7}Li motional narrowing of the line width[26]. They analyzed the LW by using classical BPP method and found that the activation energy was three or four times lower than E_σ. Later, Hendrickson and Bray presented a phenomenological equation. Applying the equation, the situation was improved and much higher activation energy was obtained on the MNLW, but it was still much lower than E_σ[27]. Since then, numerous studies have been carried out on the MNLW, although each of works deduced much lower activation energy than E_σ and ended up with the conclusion that there exist local motion which is not associated with ionic conduction.

Among the works concerning MNLW, most workers analyze the LW data by the standard BPP-type method [28,29]. However few groups attempted to analyze the LW data. Chung et al. discussed the line width using KWW function. However, it is not adequate because they discussed only the well narrowed region based on Kubo-Tomita function but they obtained much lower activation energy.

As will be shown in chapter 4, it is difficult to incorprate stretched exponential function in BPP analysis. In fact, it was noted in reference 30, BPP analysis is crude for the analysis of line width. The relaxaion of magnetization, $G(t)$, Fourier transform of which gives absorption, $I(\omega)$, can be given expicitly from the theory. It was, however, difficult to solve mathmatically the Fourier transform of $G(t)$. Since $G(t)$ is a function of $g(t)$, it is in principle possible to incorprate the KWW function into the $G(t)$ through $g(t)$. Bjorkstam *et al.* calculated the temprature dependence of line width using $G(t)$ based on KWW equation, but they showed the result for only limited values of activation parameters[29]. For more definite calculation the author believes that accurate $G(t)$ can be calculated with numerical calculation. In Chapter 4, the calculation procedure of line width for the KWW function in general form will be proposed for the first time.

T_1 and MNLW give information only on a rate of motion. For detailed investigation of ionic motion which, the author believes, is closely associated with the long distance charge transport, aother parameter is needed to describes the motions in space. Self-diffusion constant is the most appropriate parameter for the purpose. If there is an appropriate radioisotope, it is not difficult to measure the diffusion coefficient by radioisotope tracer method. In fact, the diffusion coefficient of Na in solids is thoroughly studied using ^{22}Na. On the other hand, no radioisotope is

available for ^{7}Li. Therefore, the number of works on ^{7}Li diffusion coefficient is very few. The other difficulty in measuring the diffusion coefficient in fast ionic conductors is that they are generally hygroscopic and should be kept in inert atmosphere during the measurement.

Pulsed-field gradient spin-echo (PGSE) method[31] is a powerful method to measure the diffusion coefficient of the specified nucleus of interest. Hygroscopic samples can be measured in the form of powder, being sealed in sample tube in the experiment. It is a promising method to measure the diffusion coefficient of ^{7}Li and ^{1}H in the solid electrolyte. However, it is not often used in the study of ionic diffusion in solid state because of the limited experimental conditions. It requires very intense field gradient pulses(usually current used is more than 10A) with the good rectangular shape and the reproducibility in a material in which the T_2 of the nuclei is short and the diffusion is slow compared with that in liquid. If the diffusion coefficient can be measure in ^{7}Li ion conductive glasses, it would cast an new light on the studies of the macroscopic conduction mechanism.

The purpose of the present study is to investigate the low frequency motion of ions by nuclear magnetic resonance and compare the results with those of conductivity. Some Li^+ conductive glasses with several compositions are chosen for the study.

I. Li_2-B_2O_3-Li_2SO_4 (Glass forming region and the composition of sample studied are shown in Fig. 1-4).

II. $x$$Li_2S$-(1-$x$)$B_2S_3$ (The glass forming region is between 0.6 to 0.7). We chose x=0.6,0.65 and 0.7.

III. xLi_2S-Ga_2S_3-6GeS_2. (The purpose of the work is to prepare a glass with high T_g. The glass forming region is shown in Fig. 1-5)

The main objective of the study of each material is twofold:

(1) In order to investigate the motions of ions at low frequencies(~kHz) variation of the line width of ^{7}Li NMR spectrum with temperature is investigated. The procedure of data analysis based on the stretched exponential relaxation function is presented by using numerical calculation method. The result is discussed in relation to the results of the conductivity.

(2)Diffusion coefficient of ^{7}Li is measured by the pulsed-field gradient spin echo method. The mechanism of Li ion diffusions is discussed in relation to the mechanism of electric conduction.

Chapter 2 will describe the procedure of preparation of samples. Physical properties of these samples will also be given in chapter 2. Chapter 3 will give the result of the electrical conductivity measurements. The results of the DC conductivity and the electric modulus of some glasses will be presended. τ_{cond}, E_σ and β will be calculated from the result. In chapter 4, a method for numerical calculation of the line width by incorprating KWW function will be described. The temperature dependence of ^{7}Li LW were measured. It will be shown τ_{NMR} can be deduced from MNLW. The result will be discussed in relation to the parameters from conductivity measurements in Chapter 3. The experiment of the pulsed-field gradient spin-echo NMR will be presented in Chapter 5. The result will be discussed in relation to the rate of motion from LW in chapter 4. In chapter 6, the structural change due to salt-doping which enhance the conductivity is examined by ^{11}B and ^{7}Li NMR spectra. Chapter 7 gives general discussions and conclusion.

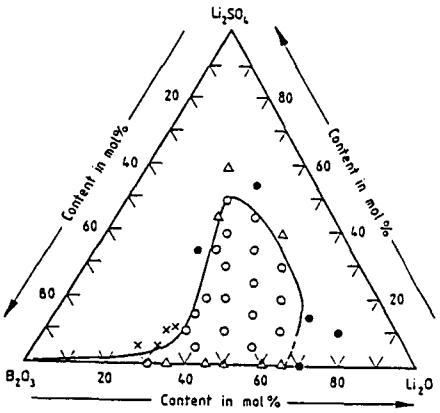

Figure 1-4 Phase diagram of Li_2O-B_2O_3-Li_2SO_4 system.
(After Yamashita and Terai [6])

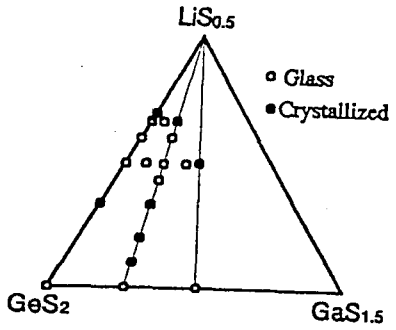

Figure 1-5 Phase diagram of Li_2S-Ga_2S_3-GeS_2 system.
(After Yamashita, *et al.*[32])

REFERENCES

[1] R. H. Doremus, "Glass Science", Willy, NY (1973).

[2] R. Terai and R.Hayami, J.Non-cryst. Solids, 18,217 (1975).

[3] J.Sarradin,R.Creus, A.Pradel, R.Astier and M.Ribes, "Solid State Microbatteries", pp102, ed by R. Akidge, Pleum press, NY (1990).

[4] A.Levasseur, J. Brethous, J. Reau and P.Hagemuller, Mat.Res.Bull,14,921(1979).

[5] A.Levasseur, M. Kbala, J.C. Brethous, J.M. Reau, and M.Couzi, Solid State Communications, 32, 839 (1979).

[6] M. Yamashita and R. Terai, Glastech. Ber. 63,13 (1990).

[7] M. Ribes, B.Barrau, and J.L.Souquet, J.Non-cryst. Solids, 38/39,271(1980).

[8] A. Pradel and M.Ribes, Mat. Chem. Phys., 23,121(1989).

[9] J. H. Kennedy, S.Sahami, S.W.Shea and Z.Zhang, Solid state Ionics, 18/19, 368 (1986).

[10] Z. Zhang and J. H. Kennedy, Solid State Ionics, 38, 217 (1990).

[11] N. Bloemgergen, E. M. Purcell and R.V. Pound, Phys. Rev., 75, 679 (1947).

[12]G. Williams and D.C. Watts, Trans. Faraday Soc., 66,80 (1971).

[13] K. L. Ngai, in "Non-debye relaxation in condensed matter", ed. by T.V. Ramakrishnan and M. Raj Lakshmi, World Scientific, Singapore (1986).

[14] S. R. Elliot and A. P. Owens, Phys. Rev. B, 44, 47 (1991).

[15] O. Knart, R. Küher, K.L.Ngai, Phys. Rev. B., 39,6071(1988).

[16] E.Göbel, W. Müller-Warmuth and H.Olyschläger, J. Magn. Reson., 36, 371 (1979).

[17] G.Balzer-Jöllenbeck, O.Knart, H.Jain, and K.L.Ngai, Phys.Rev.B, 36, 6071 (1989).

[18] M.Trunnel, D.R. Torgeson, S.W.Matin, and F. Borsa, J. Non-cryst solids., 139, 257 (1992)

[19] A. Pradel, M. Ribes, and M. Maurin, Solid State Ionics., 28, 762 (1988).

[20] M. Tatsumisago, C. A. Angell, and S.W. Martin, J. Chem. Phys., 97, 6968 (1992).

[21] F. Borsa, D. R. Torgeson, S. W. Martin and H. K. Patel, Phys. Rev. B, 46, 795 (1992).

[22] O. Knart, R. Kuher, K. L. Ngai, and H. Jain, Phys. Rev. B, 49, 76 (1994).

[23] I. Svare, F. Borsa, D. R. Torgeson, and S.W Martin, Phys. Rev. B, 48, 9336 (1993).

[24] O.Knart, J.Steiner, H. Jain, and K.L.Ngai, J.Non-cryst. solids., 130, 1001 (1991).

[25] T. Akai, M.Yamashita, H. Yamanaka, and H. Wakabayashi, Mat. Res. Soc. Proc., 321, 191 (1994).

[26] S.G. Bishop and P. J.Bray, J. Chem. Phys., 45, 1709 (1968).

[27] J. R. Hendrickson and P. J. Bray, J. Magn. Reson., 9, 341 (1973).

[28] S. H. Chung, K. R. Jerffrey, J. R. Stevens and L. Börjesson, Phys. Rev. B., 41, 6154 (1990).

[29] J. L. Bjorkstam and J. Listrud, J. Magn. Reson. 65, 383 (1985).

[30] A.Abragam, "Principle of Nuclear Magnetism", Oxford, NY, 1961, in Chapter X.

[31] J. E. Tanner and E. O. Stejskal., J. Chem. Phys., 49, 1768 (1968).

[32] M. Yamashita, T. Akai, J. Nishii, and H. Yamanaka, Amer. Ceram. Soc. Fall Meeting. Extended abstract (1994).

Chapter 2 Sample preparation

2-1 Sample preparation

2-1 -1 Oxide glasses

Li_2O-B_2O_3-Li_2SO_4

Starting materials were reagent grade Li_2CO_3, B_2O_3 and $Li_2SO_4.10H_2O$(Nakarai, GR). The appropriate amount of the materials were weighed, mixed and ground in the motor. The batch were melted in a platinum crucible at 1000 °C for 30min. Then, the melt was quenched by pouring it on to the brass plate and pressing it by a brass plate. The obtained glasses were transparent with the thickness of abouta 1mm. They were annealed at around their own T_g for about 3 hours. As the glass is hygroscopic, each sample was kept in a vacuum desiccator.

2-1-2 Sulfide glasses

Sulfide glass with high lithium concentration is very hygroscopic. Upon contact with H_2O, M_xS_y easily react as

$$M_xS_y + yH_2O \rightarrow M_xO_y + yH_2S,$$

to form metal oxide. To prevent the decomposition preparation and characterization were done in a dry Ar atmosphere by the use of a well sealed glove box. The glove box was filled with 6N Ar. To remove the residual oxygen and moisture the gas was circulated in column of platinum catalysis and molecular sieve. The content of the moisture was monitored by a H_2O sensor. The samples were more sensitive to H_2O than O_2. The residual H_2O in the glove box was as low as 2-3ppm.

Li_2S-B_2S_3

The preparation procedure is illustrated in figure 2-1 . First, Li_2S(Kishida, 3N) and B_2S_3(High Purity Chemicals, 2Nup) were carefully weighed in a glove box. They were mixed, ground and loaded into a silica tube, which is connected to the valve assembly. Then, the silica tube was evacuated and sealed by hydrogen torch.

Li_2S easily reacts with SiO_2 above 400°C, In particular, with high Li_2S loading, the silica tube is corroded within 30minutes. This often results in the burst of silica tube. To prevent the reaction of Li_2S and SiO_2, pyrocarbon film was coated inside of silica tube. by employing the method by Martin *et al.* [1]. The apparatus used for the coating is shown in

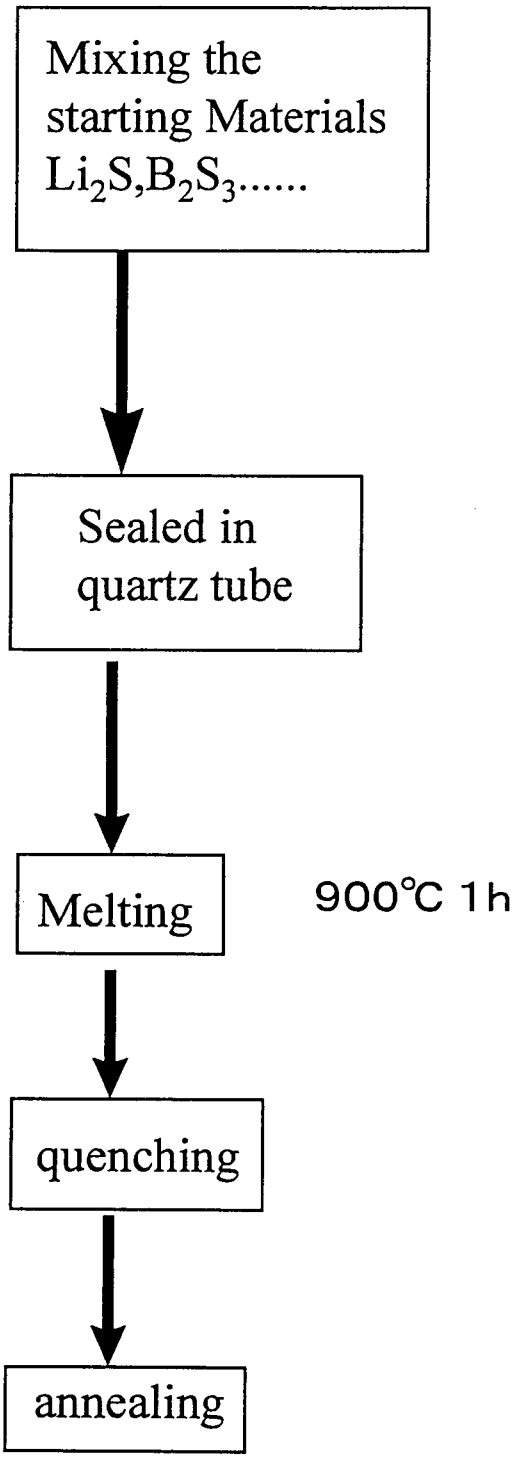

Fig. 2-1 Procedure for preapration of sulfide glasses.

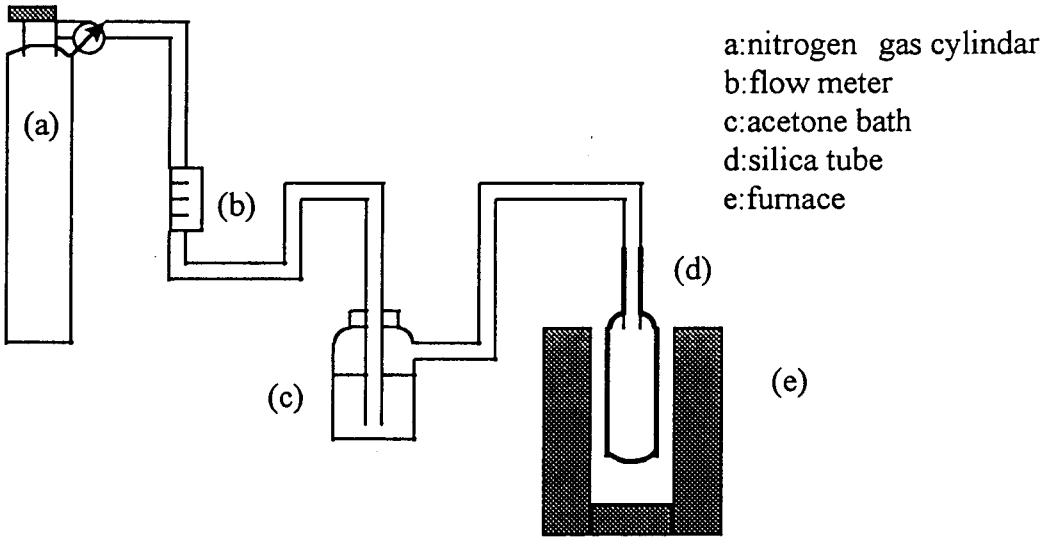

Fig. 2-2 Apparatus for coating carbon films inside the silica tube.

Figure 2-2. Nitrogen was first passed through acetone bath. The nitrogen with acetone was introduced into a tube heated at 800°C in a furnace. The durability of carbon film depends critically on the nitrogen stream pressure as well as flow rate previously pointed out[1]. Optimum pressure and flow rate were 2kgf/cm^{-2} and 150cc/min, respectively. After the carbon coating the tube was rinsed with acetone and dried at 150°C.

The batch sealed in the tube was melted and kept at 900°C for 30minutes. The melt was then quenched by cooling the tube in ice water. The glass was annealed at 170°C for 1h.

The glass was obtained in the region $0.6<x=<0.7$. It exhibits dark brown color and is very fragile. For x=0.7, the glass seems to be uniform, although crystallization seems to occur at the surface of the glass.

Li_2S-Ga2s3-GeS_2

The starting materials were Li_2S (99% high purity chemicals Nup), Ga_2S_3 (high purity chemicals 5N up) and GeS_2 (high purity chemicals 5N up). Since the melting point of Ga_2S_3 is 1300°C, the melting temperature for this system exceeds 1000°C. In this case, carbon film prepared by the above procedure is easily to be removed, probably because of the difference of thermal expansion coefficient. The surface of SiO_2 was reduced to Si by introducing H_2 in a microwave furnace.[2] The batch was melted at 1000°C for 15 minutes and quenched by putting the tube into the water.

2-2 Characterization

Differential thermal analysis was carried out by the use of Seiko TG/DTA 220 sysatem. Heating rate was about 5°C/min. T_g of several oxide glasses are listed in Table 2-1.

For sulfide glass T_g was determined by Differential scanning calorimeter(DSC). The measurement was carried out using Seiko DSC 320 system. The sample was sealed in aluminum can. Heating rate was also 5°C/min. The result are also shown in Table 2-2

Table 2-1 Glass transition temperature(T_g) of the samples.

Sample	T_g / °C
$(100-x)(0.5Li_2O-0.5B_2O_3)$ $-xLi_2SO_4$	
x=0	412
x=10	403
x=20	372
x=30	356
x=40	382
x=50	291
$xLi_2S-(100-x)B_2S_3$	
x=60	178
x=65	176
x=70	177
$xLi2S-Ga_2S_3-6GeS_2$	
x=4	338
x=6	340

References

[1] S.W.Martin and D.R. Blayer, J. Am.Chem. Soc, 73, 3481(1990).

[2] M. Yamashita, T.Akai, J.Nishii, and H. Yamanaka, Amer.Ceram. Soc. Fall Meeting, extended abstract (1994).

Chapter 3 Electrical properties

3-1 Introduction

In general, the ion-conductive glasses is the intermediate between the conductor and the insulator (as shown in fig. 3-1). In the discussion of its electrical property, equivalent circuit which is composed of resistor and insulator is postulated. The circuit depends on the nature of the conducting material. For glasses, where no grain boundary exit, the equivalant cirucuit by a simple parallel circuit of resistance R_p (conductance $1/G_p$) and capacitance C_p is used (Fig.3-2).

First, we consider the response of the circuit to an applied ac field from the phenomenological point of view. When the applied voltage is $V^*=V_0\exp(j\omega t)$, complex impedance Z^* is written by Ohm's law,

$$Z^*=V^*/I^* \tag{3.1}$$

It is a very simple problem to express the response of the circuit shown in Fig. 3-2 to the applied field.

The parameters often used in electrical studies are admittance $Y^*(\omega)$, conductivity $\sigma^*(\omega)$, capacitance $C^*(\omega)$, permittivity $\varepsilon^*(\omega)$, impedance $Z^*(\omega)$ and resistivity $\rho^*(\omega)$. All parameters can be determined when either $Y^*(\omega)$ or $Z^*(\omega)$ is known[1]:

$$Y^*(\omega)=G_p(\omega)+j\omega C_p(\omega), \tag{3.2}$$

$$\sigma^*(\omega)=Y^*(\omega)(d/A), \tag{3.3}$$

$$C^*(\omega)=C_p(\omega)+jG_p(\omega)/\omega, \tag{3.4}$$

$$\varepsilon^*(\omega)=[C^*(\omega)/\varepsilon_o](d/A), \tag{3.5}$$

$$Z^*(\omega)=1/Y^*(\omega)=\{Gp(\omega)/[G_p^2(\omega)+\omega^2C_p^2(\omega)]\} -j\omega C_p(\omega)/[G_p^2(\omega)+\omega^2C_p^2(\omega)]\}=Z'-jZ'', \tag{3.6}$$

and

$$\rho^*(\omega)=Z^*(\omega)(A/d), \tag{3.7}$$

where j is the imaginary unit and ε_0 permittivity of vacumm. It is understood from equation (3.6) that the plot of $Z'(\omega)$ versus $Z''(\omega)$ gives a semicircle that gives a semicircle with the diameter R_p as shown in Figure 3-3. The plot, so-called impedance Cole-Cole plot, is a commonly used to evaluate the d.c. conductivity of solid-state ionic conductor.

We now consider the problem how microscopic motion of ions affects $\sigma(\omega)$ or $\varepsilon(\omega)$. In the case of an ideal insulator, which is identical to a single capacitor $C(\omega)$, there is the well-known picture by Debye. Suppose that an altermating electric field is applied to some insulator that has a permanent dipoles in it. The dipoles in the insulator respond to the field and tend to take favorite oriantation in a manner that depends on the frequency of the field ω.

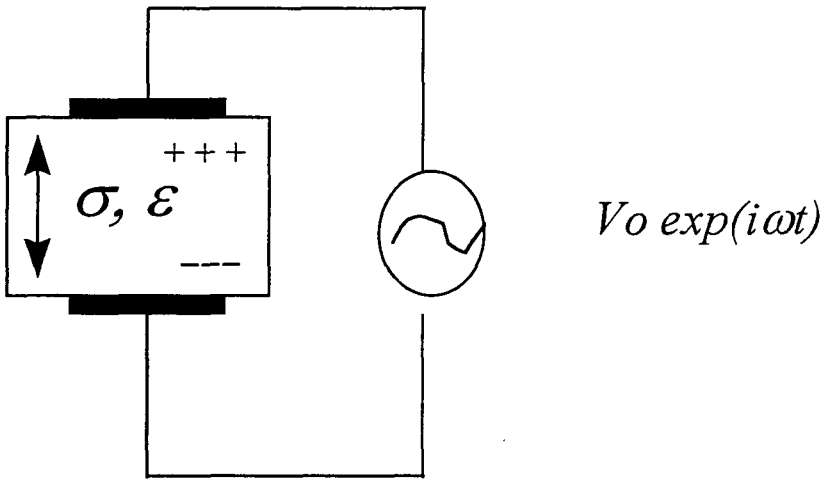

Fig. 3-1 Electrical property of inorganic material.

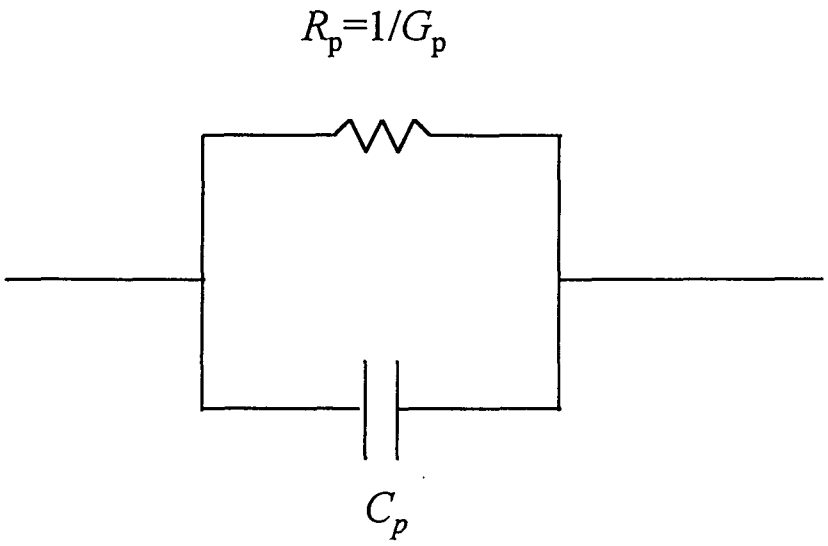

Fig. 3-2. Equivalent circuit of a dielectric material

The molecular dipoles depend on the frequency of the field ω. The molecular dipoles thus contribute to the macroscopic permmittivity but the degree of the contribution to ε is specified by the molecular reorientation and therefore the molecular rotational relaxation time τ. Such a situation is represented by the Debye equation,

$$\varepsilon^*(\omega)=\varepsilon_\infty+(\varepsilon_s-\varepsilon_\infty)/(1+\omega^2\tau^2)+j(\varepsilon_s-\varepsilon_\infty)\omega\tau/(1+\omega^2\tau^2), \quad (3.8)$$

where ε_∞ and ε_s is the permittivity of high-frequency and low-frequency, respectively.

Ion-conductive inorganic glasses do not usually have permanent molecular dipoles. Therefore, the ionic motion give rise to electrical dispersion. Stevens and Tayler proposed a model for such ionic motion in the presence of an electric field as shown in Figure 3-4[2]. At low frequencies, ions hop at higher energy site due to the field. It results in a macroscopic electric polarization. At high frequencies electric field, the ions cannot follow the reversal of the field, and have no polarization effect produced.

Using eqs.(3.2)-(3.5),

$$\varepsilon^*(\omega)=\varepsilon'-j\sigma/\omega\varepsilon_0 \quad (3.9)$$

Assuming that $\varepsilon'=\varepsilon_s$,

$$\varepsilon^*(\omega)=\varepsilon_s-j\sigma/\omega\varepsilon_0 \quad (3.10)$$

In analyzing the electrical properties in ionic conductor, Macedo *et al.*[2] introduced the concept of modulus M^*, inverse of permitivity.

$$M^*(\omega)=\varepsilon^*(\omega)^{-1} \quad (3.11)$$

$$=(\varepsilon'(\omega)+j\varepsilon''(\omega))/(\varepsilon'(\omega)^2+\varepsilon''(\omega)^2) \quad (3.12)$$

Form (3.10) and (3.12),

$$M^*(\omega)=M_s\left(\frac{(\omega\tau)^2}{1+(\omega\tau)^2}+j\frac{(\omega\tau)}{1+(\omega\tau)^2}\right) \quad (3.13)$$

where τ is the conductivity relaxation time, $\tau=\varepsilon_s\varepsilon_0/\sigma$ and M_s the modulus in the static field. It is very interesting that the modulus has the form of Fourier transform of a function which relaxes exponentially with the relaxation time τ. Indeed, the modulus plot gives curves as shown in figure 3-5 when it is plotted against ω.

In order to clarify the meaning of τ, we again consider the response of the equivalent circuit to the electric field. If the applied field is $V=V_o exp(j\omega\tau)$, the total current is the sum of I_R^* and I_c^*, so that

$$I^*=I_R^*+I_c^*=[V^*/R_p]+[C_p\, dV^*/dt]. \quad (3.14)$$

Integration of (3.14) leads to,

$$Z^*=V^*/I^*=R_p[1/\{1+j\omega\tau\}] \quad (3.15),$$

where $\tau=R_pC_p$. It is easily shown form eqs.(3.2)-(3.7) that R_pC_p equals $\varepsilon_s\varepsilon_0/\sigma$. Hence, τ shown in equation (3.13) is characteristic relaxation time of the circuit or the system.

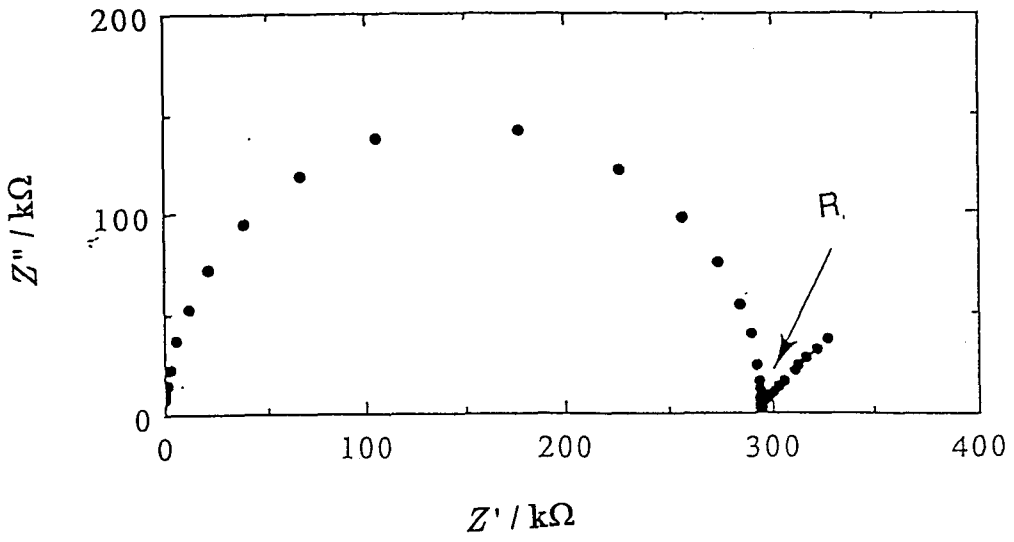

Figure 3-3 Example of impedance Cole-Cole plot.

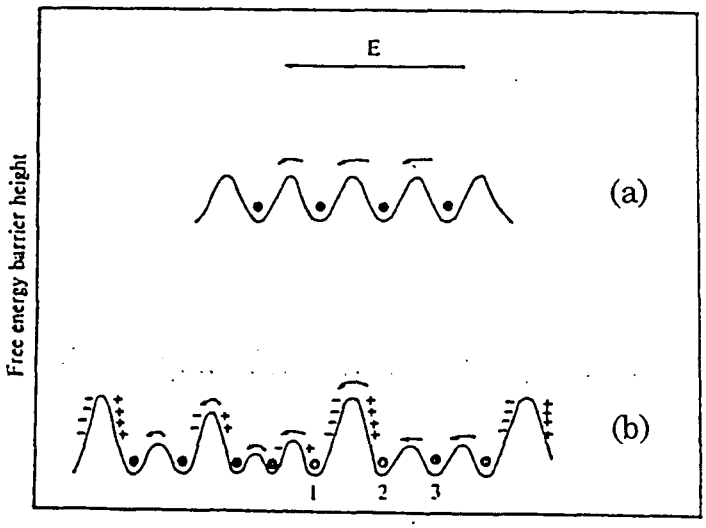

Figure 3-4 A model by Stevens and Taylor (After Stevens and Tayler [2])
(a) crystals (b) inorganic glasses.

From the phenomenological point of view, it can be written as from eq(3.5)-(3.8),

$$M^*(\omega)=1/\varepsilon^*(\omega)=\varepsilon_0(A/d)j\omega Z^* = M' + jM'' \qquad (3.16)$$

$M^*(\omega)$ can be obtained simple operation of the data.

The modulus is useful in studying relaxation process, and so it is often used in the study of glassy ionic conductor. In the real glasses, the modulus usually deviate from the ideal symmetrical behavior with respect to the applied frequency implying that the relaxation process cannot be described by a single exponential relaxation. Therefore, in order to elucidate useful informations from the non-ideal modulus data we must introduce some suitable relaxation function which reproduce the experimental modulus. One promissing candidate is the KWW function[3] and, if we can perform the Fourier transformation of KWW function, we can reproduce the observed $M^*(\omega)$ (See in Fig. 3-6). However, Fourier transform of KWW function can be explicitly solved only in the case of β=0.5 and 0.3. To calculate the equation (3.13), Moynihan et al. approximated the stretched exponential function by expanding it as

$$g(\tau)=\exp(-(t/\tau)^{\beta})= \Sigma\, g_i \exp(-t/\tau_i). \qquad (3.17).$$

More than 10 τ_i extending more than 4 orders centered at τ_c are chosen and g_i were calculated to fit the stretched exponential function for the given β by least-squares' method. Fig. 3-6 shows an example of the result of the analysis. Thus, β and τ can be determined from the experiment.

In this chapter the impedance and the DC conductivity of Li-conducting glasses are first examined. Then, the modulus of a few glasses are shown and the analysis is carried out by the method proposed by Moynihan. The results in this chapter will be discussed in chapter 4 and 5 in relation to NMR parameter.

3.2 Experimental.

Figure 3-7 shows the scheme of the apparatus used in the measurement of the impedance. The alternating voltage was applied to the sample placed in a cell and the current was monitored and analyzed by HP4192. The $Y^*(\omega)$ was transferred to a personal computer through GPIB and converted to $Z^*(\omega)$. The impedance due to the cell was subtracted. The schematic of the cell was shown in Fig, 3-7. Gold wire was used for the lead . At high frequencies, the interference between the cell and the surrounding is not negligible. To avoid the effect, the wire was covered by aluminum or Au coated alumna tube. The wire was connected to BNC connector. Coaxial cable was used to connect the cell to an impedance analyzer. Two different types of cells were used in the measurement: For the measurement of sulfide glasses, the cell need to be placed in the glove box, so that the limitation of the seize

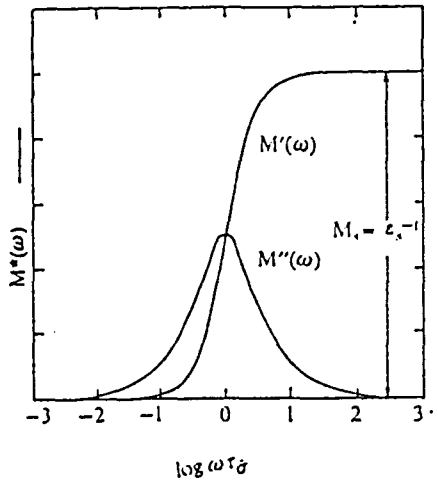

Figure 3-5 Modulus plotted agains logarithmic of τ.

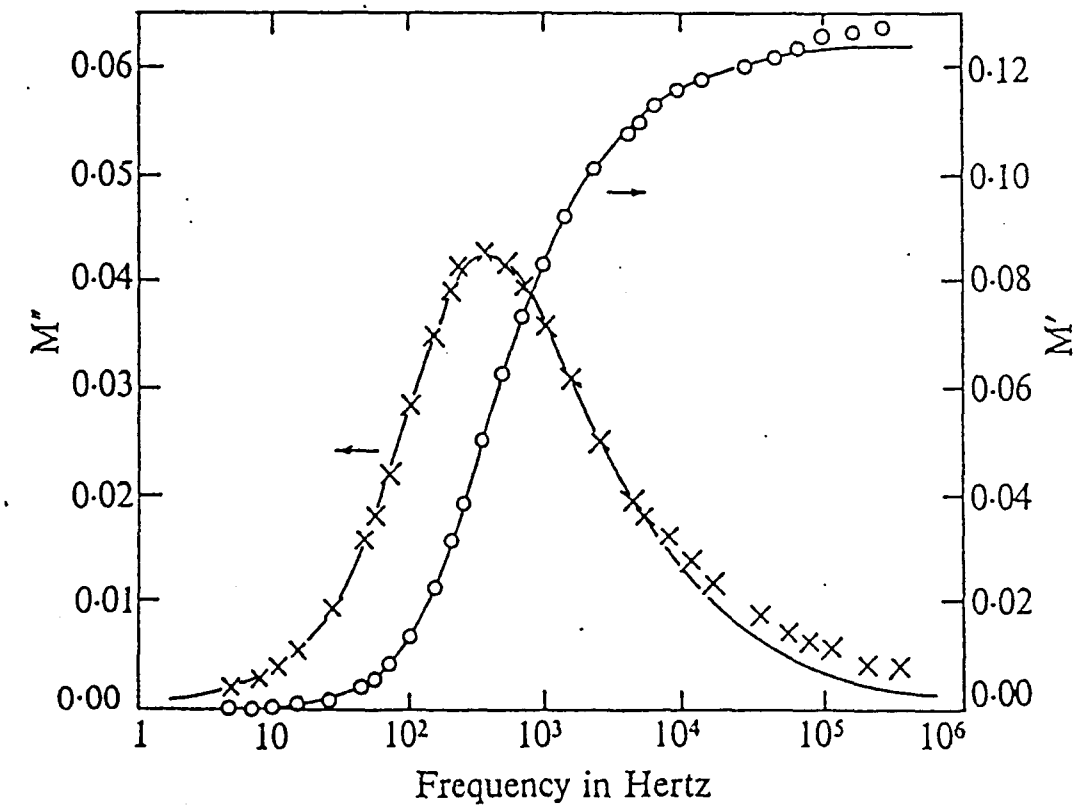

Figure 3-6 Modulus plot for a glass. (After Moynihan *et al.*[3]).

was quite severe. The length of the cell was approximately 20cm. Temperature was controlled using a heater wound around the bras can which was placed around the sample. The diameter of the can was about 6cm and the height was 6cm.

For the measurement of modulus, the accurate temperature control and the measurement of high frequency is very important. So, the cell as long as 40 cm was used. Part A in Fig. 3-7 was made of silica glass, and it was introduced into a furnace.

Li_2O-B_2O_3-Li_2SO_4 glasses were shaped and polished to disks. The diameter and the thickness of the disk was 1cm and 0.5cm, respectively. Gold electrodes (ϕ=0.9cm) were deposited on to the disk by the vacuum evaporation method.

For Li_2S-Ga_2S_3-GeS_2 system, the samples were shaped to disks (ϕ=6mm,d=1mm) by polishing. As the glass was very fragile, organic solvent such as toluene was used as lubricant. These solvents were dried over molecular sieve 5A, which was previously dried at 150°C under vacuums. Ag paste was painted on the disk for the electrodes.

3-3. Results and Discussion

3-3-1. DC conductivity

Figure 3-8 shows an impedance Cole-Cole plot of $50Li_2O$-$50B_2O_3$. A good semicircles were obtained for this case. The conductivity σ was calculated from the value of the resistance R. At temperatures lower than T_g, σ obeys the Arrhenius' law,

$$\sigma=\sigma_0\exp(-E_\sigma/RT). \qquad (3.18)$$

The value of σ is plotted against the inverse of temperature in figure 3-9. The activation energy, E_σ, preexponential factor σ_0, and the conductivity at 25°C, $\sigma_{25℃}$, is 50.7kJ/mol, $1.49\times10^2 Scm^{-1}$ and $2.0\times10^{-7} Scm^{-1}$, respectively.

The other glasses doped with Li_2SO_4 were already measured by Yamashita and Terai as shown in Table 3-1 [5]. The activation energy is almost independent of the doping but the conductivity varies on doping of Li_2SO_4.

For a sulfide glass, xLi_2S-Ga_2S_3-$6GeS_2$, semicircles are not ideal as shown in figure 3-10, as is often observed in sulfide glasses. Especially such a pattern is observed in hygroscopic samples. It may be caused by the denaturation of the surface of the samples, but it was possible to estimate R by extrapolating the observed circle. However, we recently found that the sample denaturation brings about a significant error in the absolute value of the conductivity while it contains considerable error, while it affects the activation energy only slightly [5].

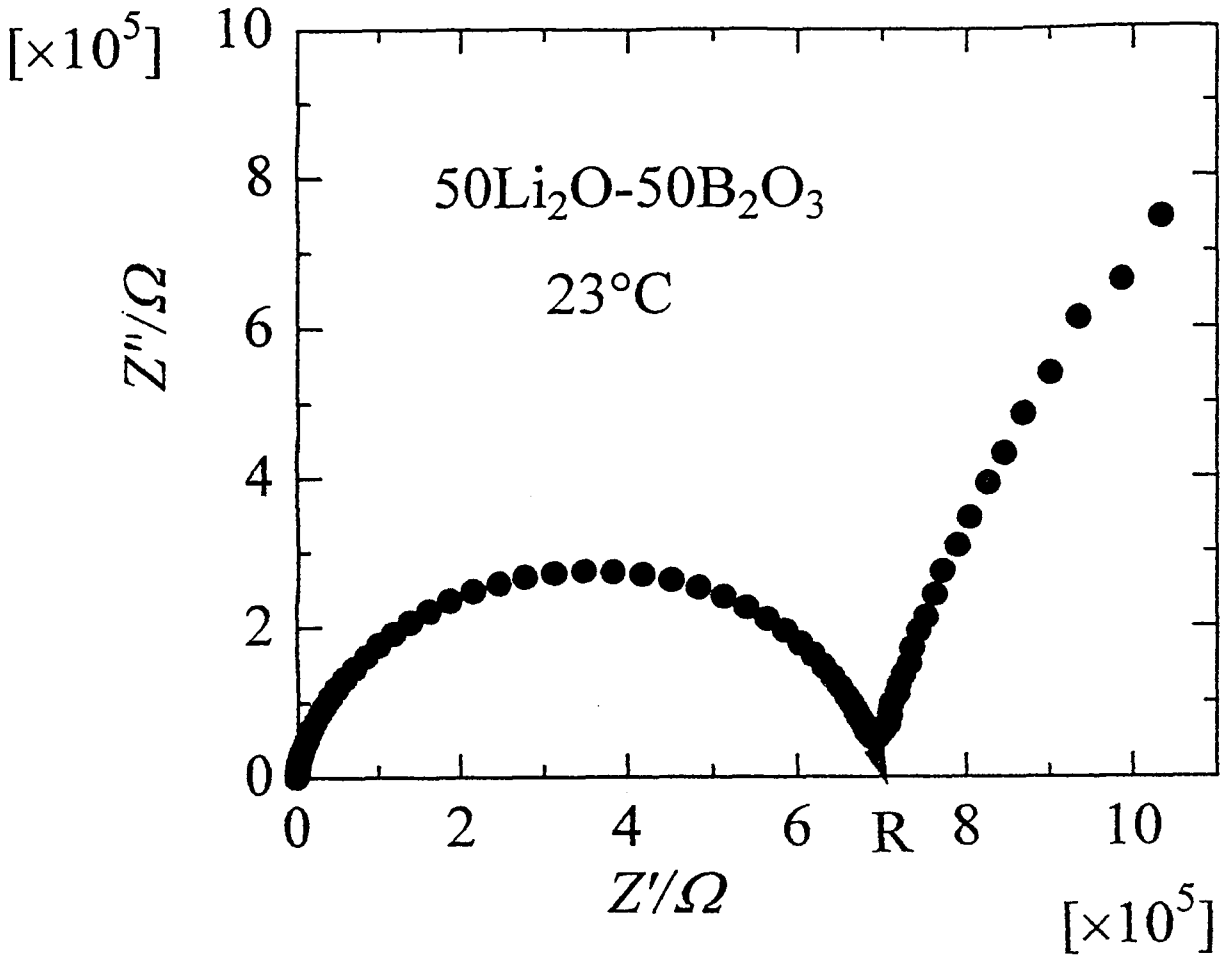

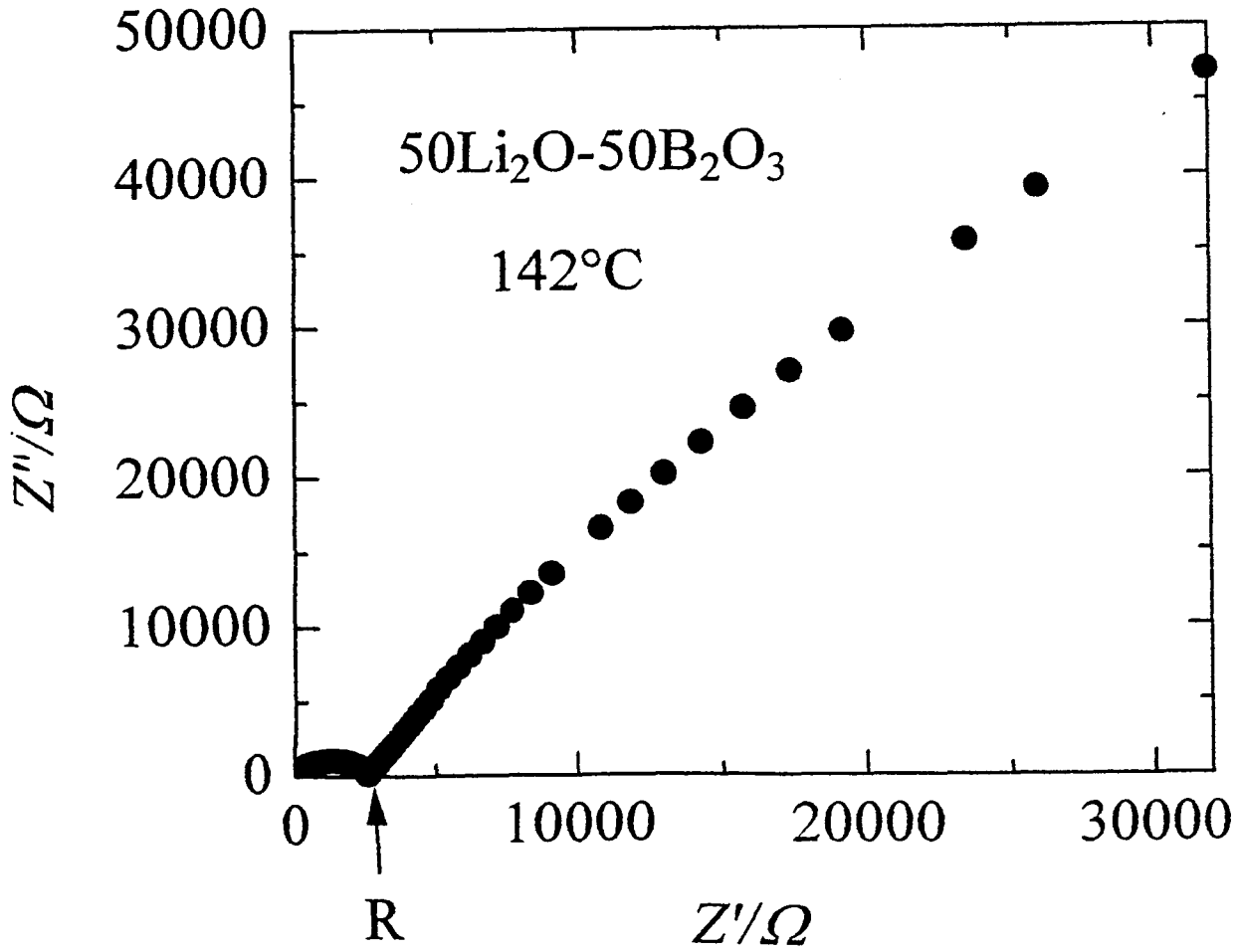

Figure 3-8 Impedance Cole-Cole plot for $50Li_2O$-$50B_2O_3$ at 23°C and 142°C.

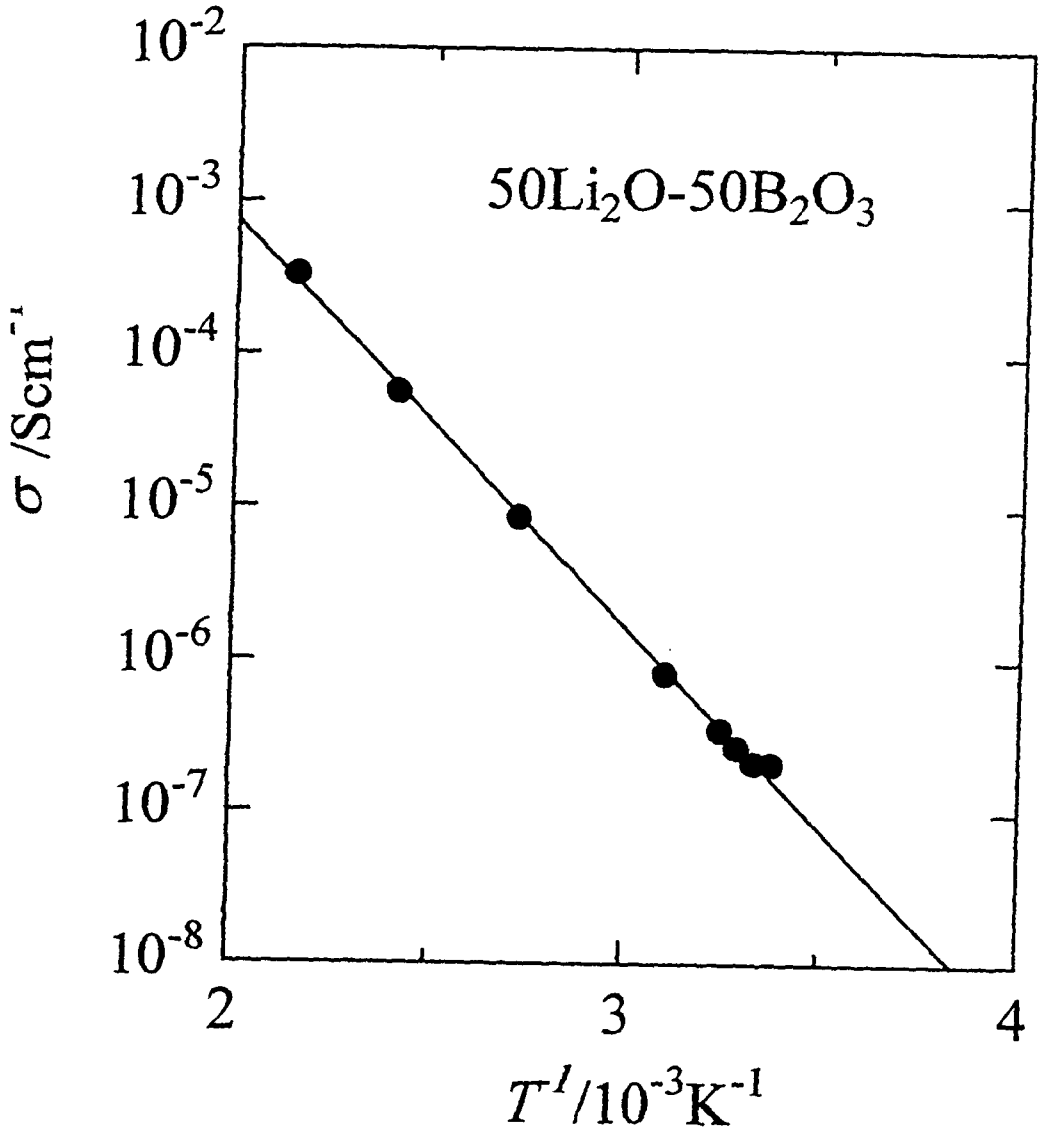

Figure 3-9 The conductivity of $50Li_2O$-B_2O_3 is plotted against the reciprocal temperature.

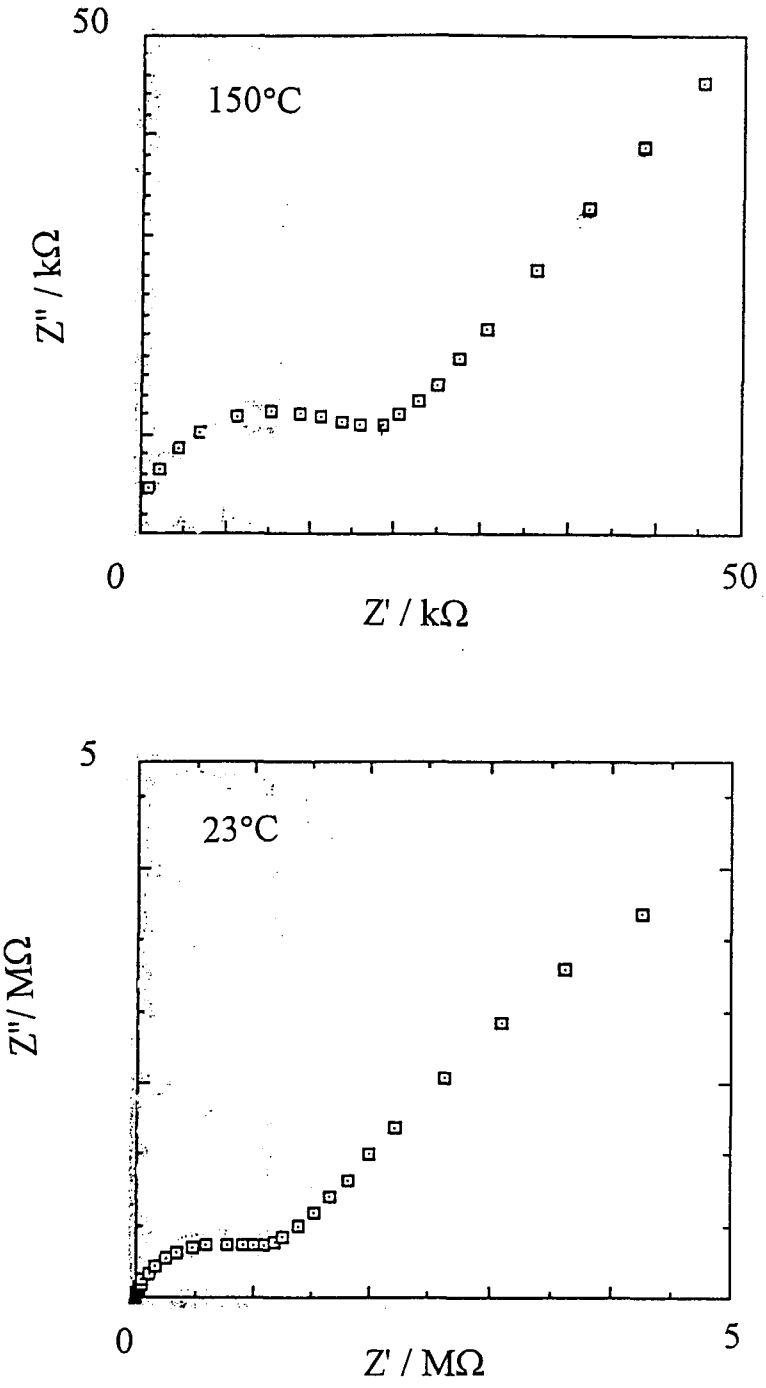

Figure 3-10 Impedance Cole-cole plot of $4Li_2S$-Ga_2S_3-$6GeS_2$.

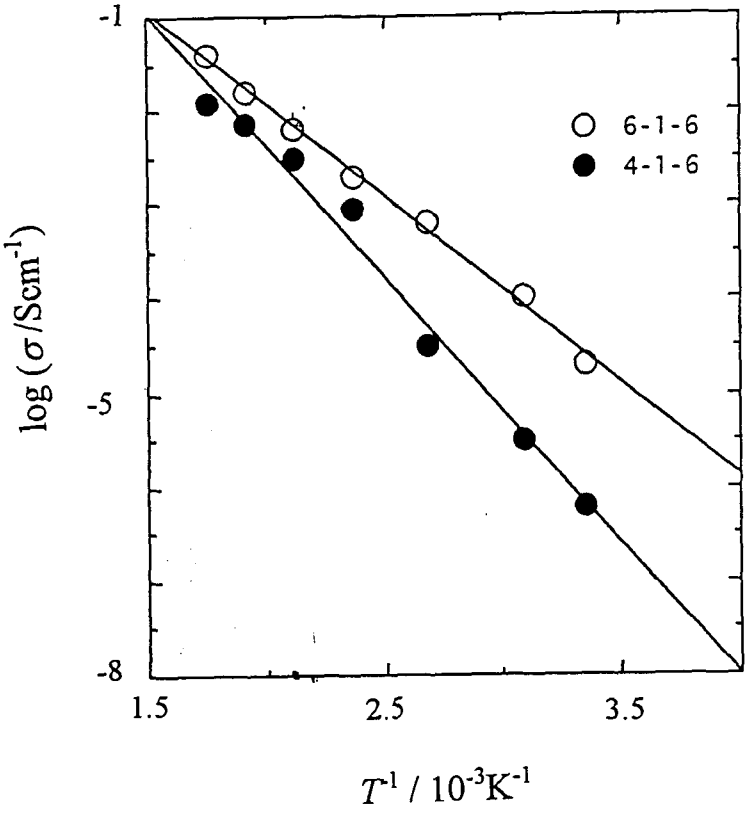

Figure 3-11 Conductivity of xLi_2S-Ga_2S_3-$6GeS_2$.
Open circles: x=6; closed circles: x=4.

Table 3-1 Conductivity at 25°C($\sigma_{25°C}$) and activation energy (E_σ).
of (100-x)($0.5Li_2O$-$0.5B_2O_3$)xLi_2SO_4.

x	$\sigma_{25°C}$	E_σ /kJmol^{-1}
10	8.0x10^{-7}	50
20	1.0x10^{-6}	50
30	1.3x10^{-6}	50
40	1.3x10^{-6}	50
50	1.0x10^{-6}	52

Table 3-2 Conductivity at 25°C($\sigma_{25°C}$) and activation energy (E_σ).
of $x$$Li_2S$-$Ga_2S_3-6GeS_2$.

x	$\sigma_{25°C}$	E_σ/kJmol^{-1}
4	2.0x10-6	54.4
6	2.0x10-5	38.8

The conductivity of $x$$Li_2S$-$Ga_2S_3$-$GeS_2$ (x=4,and 6) is plotted as a function of the reciprocal temperature in figure 3-11. The E_σ and $\sigma_{25℃}$ derived from this Arrhenius plot is given in table 3-2. These values are close to those for Li_2S-GeS_2 system [6].

3-3-2. Modulus

Figure 3-12 and 3-13 show the frequency dependence of the real and the imaginary part of the modulus of $50Li_2O$-$50B_2O_3$ and $40Li_2O$-40-B_2O_3-$20Li_2SO_4$, respectively, at room temperature. The peak in M'' of $50Li_2O$-$50B_2O_3$ occurs at around 20kHz. The peak appears at the higher frequency in $40Li_2O$-$40B_2O_3$-$20Li_2SO_4$. This means that the relaxation time τ becomes shorter with the addition of Li_2SO_4. The frequency limit for the bridge (HP4192) is below 1-2MHz, so the uncertainty increases above 1MHz can be attributed to experimental errors: Thus, the apparatus cannot be used to measure the modulus for higher conductivity than in $50Li_2O$-$50B_2O_3$ with the cell used here.

In order to analyze modulus plot, a computer program was coded according to the procedure of Moynihan. As already shown in introduction of this chapter, the KWW function is first expanded as (3.17) by least square method. g_i is normalized by

$$\Sigma g_i=1. \qquad (3.19)$$

Then, modulus M_i for each τ_i is calculated by using (3.13), and they are summed as follows.

$$M=\Sigma g_i M_i . \qquad (3.20)$$

Thus, M for given τ and β is calculated and fitted to experimental data.

The program for the fitting was written in NEC N88-BASIC. An algorithm of the program is shown in Figure 3-14. The program list is shown in Appendix A.

First, KWW function is expanded by (3.17) for a given β and τ by determining g_i using least squares' method. Number of expansion terms τ_i used for the analysis is 14. The range of τ_i is 8 orders centered at τ. 100 points are used for the non-Linear least square fitting. The method used here was Mardquest method. The initial condition for g_i is as follows. g_i at $\tau_i=\tau$ is set to 1 and other g_i are set to 0. Conversion factor is critical in determining g_i. Too large value results in a discrete shape of distribution of g_i which reflects the inadequateness of initial condition, but too small value results in diversion. Therefore, the conversion factor was first chosen as 0.5, which seems to be very large, and it is reduced step by step manually by monitoring the g_i versus τ_i and it was fixed when the change becomes stable. After determining g_i for a given β and τ, M is calculated according to eq.(3.20) and compared with the experimental result.

The result for the fitting is shown in Figure 3-15. The obtained parameters for $40Li_2O$-$40B_2O_3$-$20Li_2SO_4$ are $\tau=7.0\times10^{-7}$ s and $\beta=0.55$.

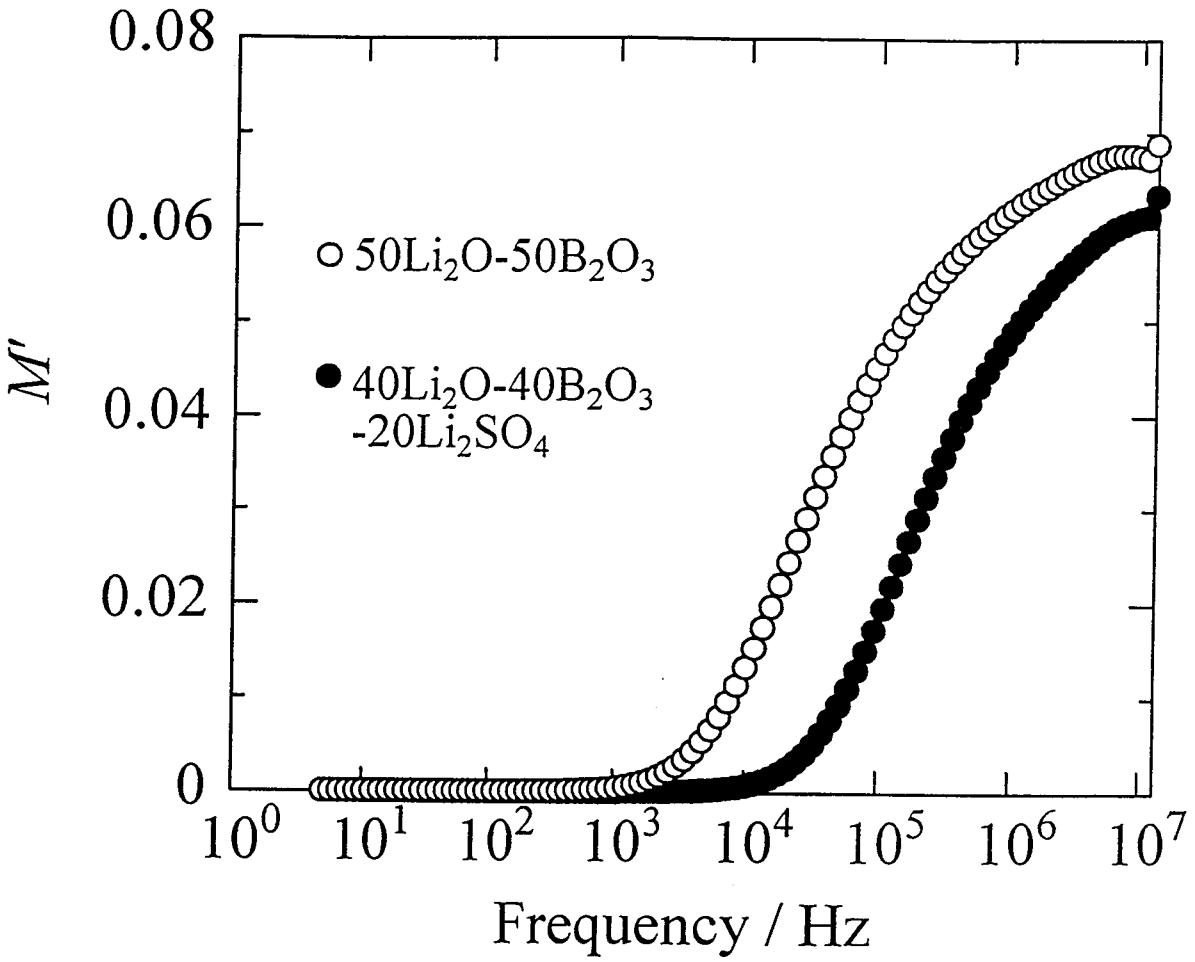

Figure 3-12 Real part of modulus plotted against logarithmic frequency. Open circles: $50Li_2O\text{-}50B_2O_3$; closed circles: $40Li_2O\text{-}40B_2O_3\text{-}20Li_2SO_4$.

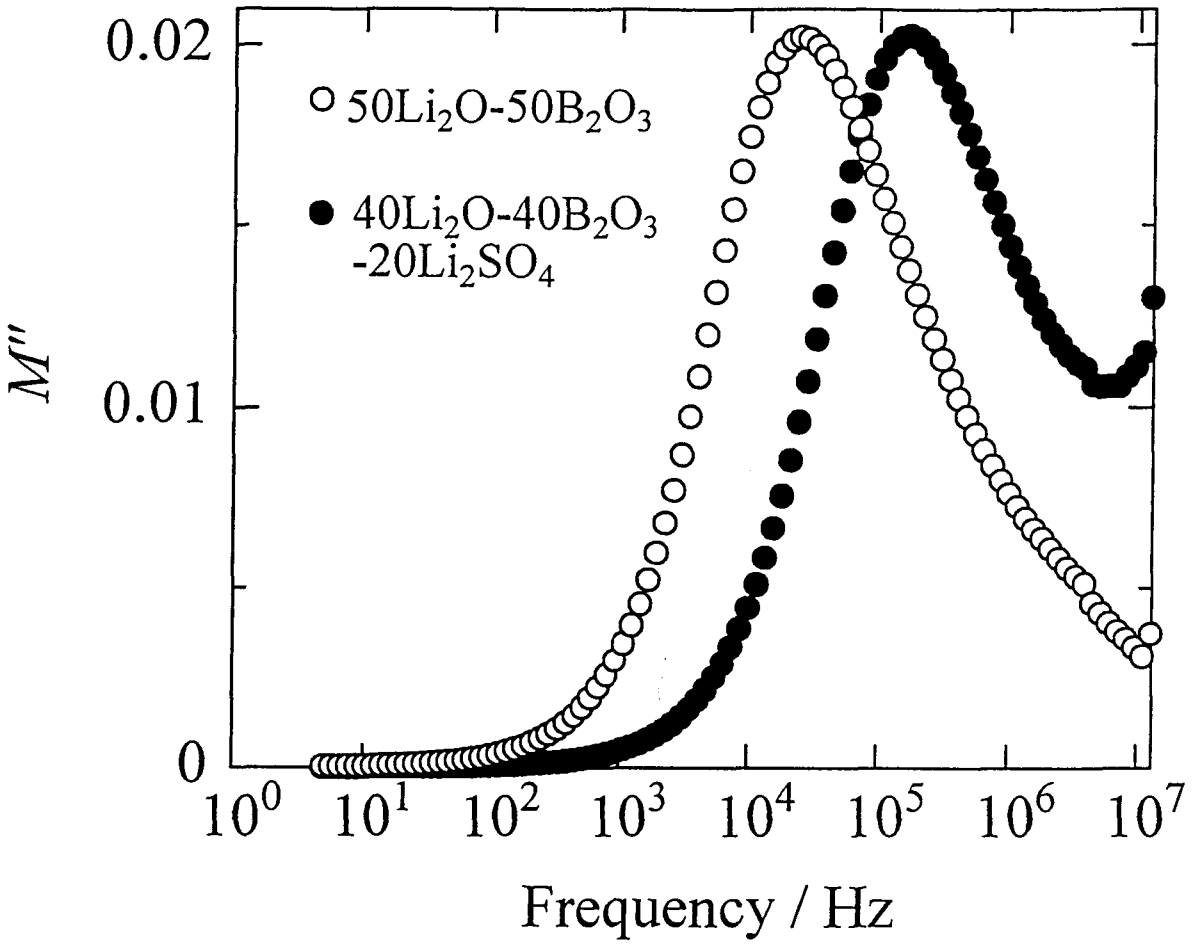

Figure 3-13 Imaginary part of modulus plotted against logarithmic frequency. Open circles: $50Li_2O$-$50B_2O_3$; closed circles: $40Li_2O$-$40B_2O_3$-$20Li_2SO_4$.

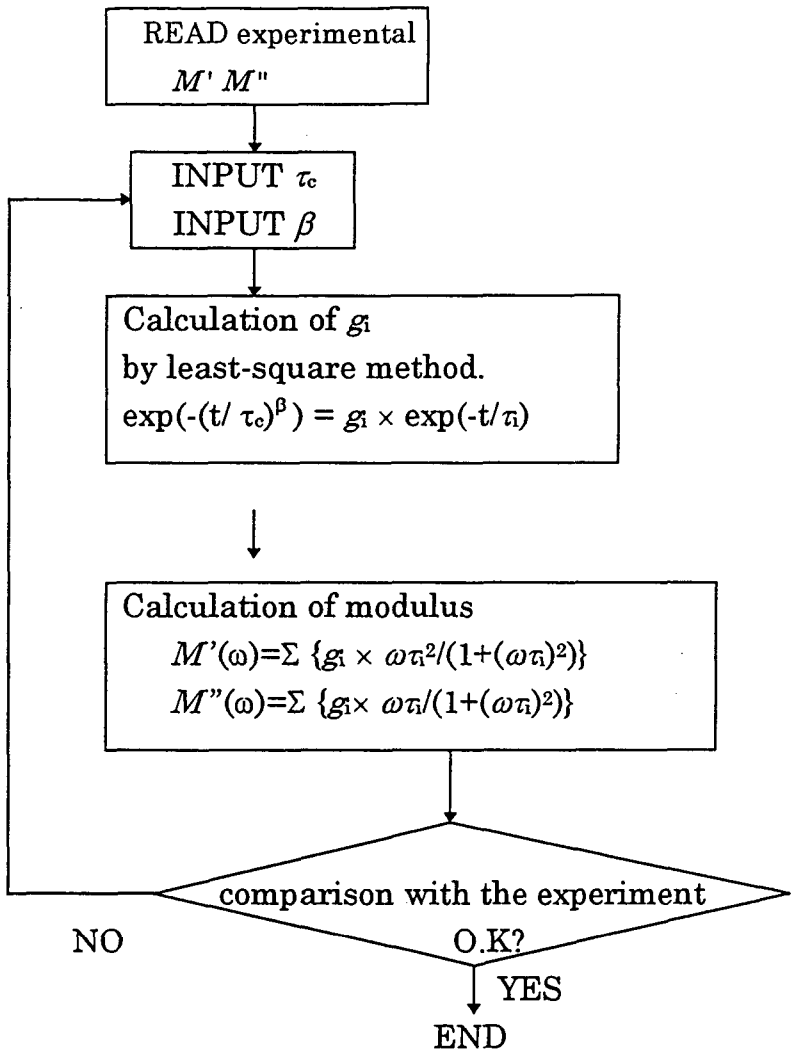

Figure 3-14 Algorithm of data anaylysis

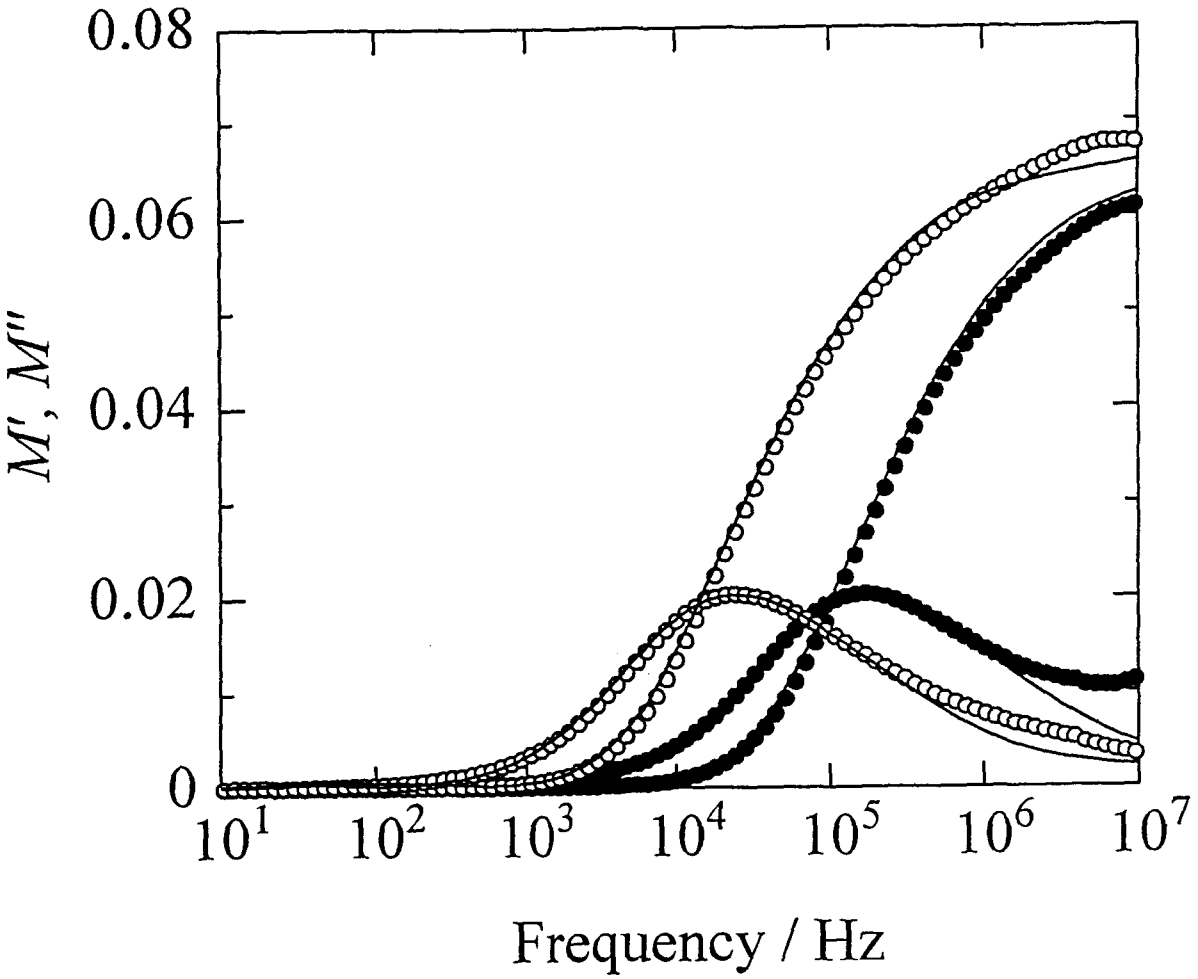

Figure 3-15 Fitted results of 3-12 and 3-13
Open circles: $50Li_2O$-$50B_2O_3$.
Closed circles: $40Li_2O$-$40B_2O_3$-$20Li_2SO_4$.
Solid line: theoretical

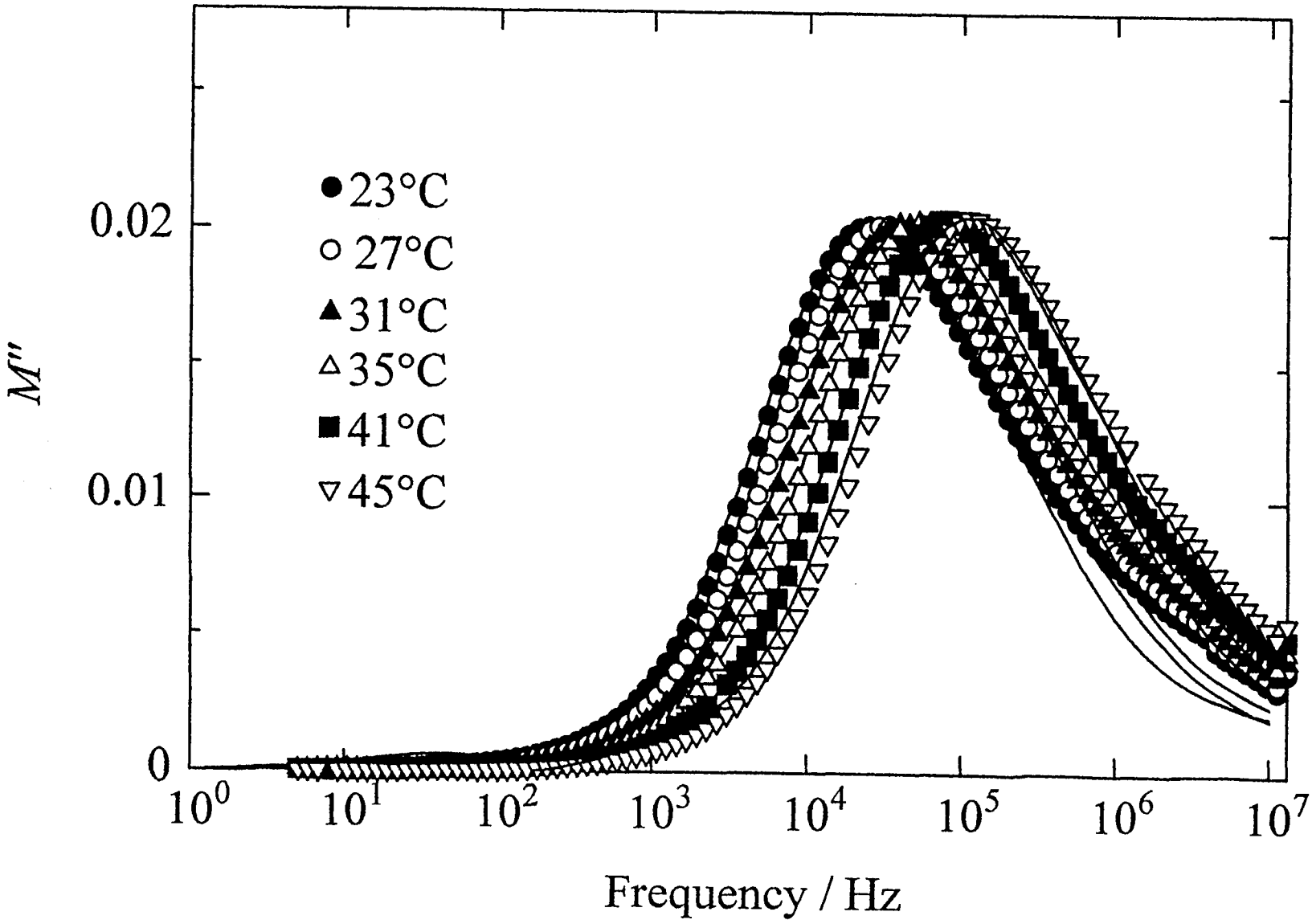

Figure 3-16 Temprature dependence of M" in $50Li_2O$-$50B_2O_3$. Temperatures are shown in the figure. Open and Closed circles show the experimental values and solid curves represents the calculated modulus.

The obtained parameters for $50Li_2O$-$50B_2O_3$ are τ =6.0x10^{-6}s and β=0.54. In high-alkali content, β from modulus usually shows a values below 0.6. Compared with other glasses, these values seem reasonable.

Due to the frequency limitation of the measurement, only the temperature dependence of M for $50Li_2O$-$50B_2O_3$ is investigated. Figure 3-16 shows the temperature dependence of the imaginary part of modulus. The peak position shifts gradually to higher frequency as temperature increases because of the increase of the rate of motion of ions. With the same procedure described above, the value of τ at each temperature is calculated. Theoretical curves are also shown in Figure 3-16 by solid curves. As, τ obeys the Arrehenius rule,

$$\tau = \tau_0 \exp(E_a/RT) . \qquad (3.21)$$

τ obtained here is plotted versus reciprocal temperature in figure 3-17. From the plot, we determined the values τ_0=2.52x10^{-15}s and E_a=52kJ/mol. Tatusmisago et al. found that τ_0 is about 10^{-15}s for Li_2O-B_2O_3-LiCl glass[8]. The present value of τ_0 agree well with their value.

The values of τ_0 and E_a will be compared to NMR parameter in the next section.

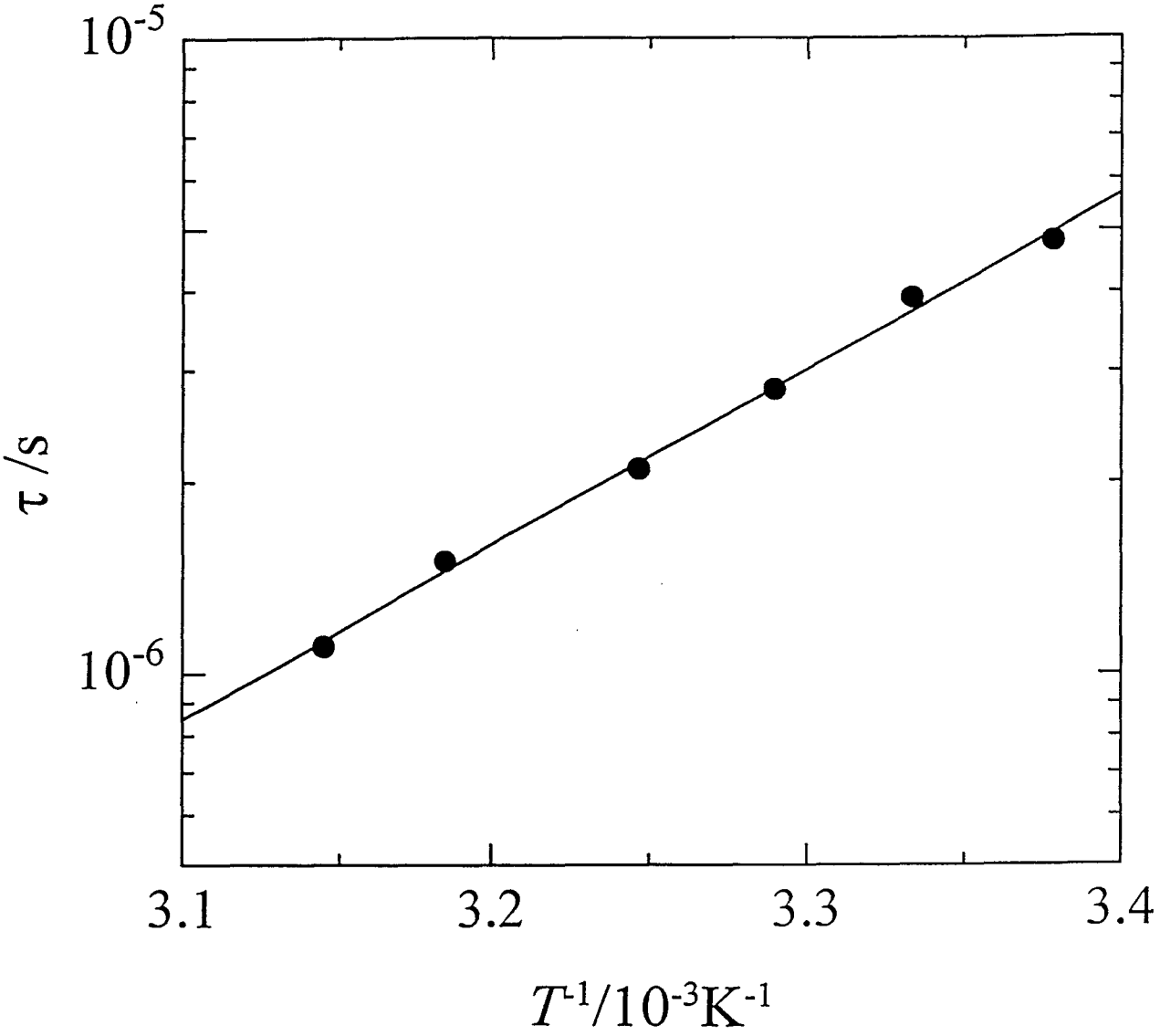

Figure 3-17 Relaxation time τ plotted against the reciprocal temperature.

References

[1] A.K.Varshneya, "Fundamentals of Inorganic Glasses"; Chapter 15, Academic Press, NY(1994).

[2] P. B. Macedo, C. T. Moynihan, and R. Bose, Phys. Chem. Glasses., 13, 171 (1972).

[3] G. Williams and D. C. Watts, Trans Faraday Soc., 66, 80 (1971).

[4] C. T. Moynihan, L. P. Boesch, and N. L. Laberge, Phys. Chem. Glasses., 14, 6 (1973).

[5] M. Yamashita and R. Terai, Glastech Ber., 63, 13 (1990).

[6] T. Akai, Y. Saitoh, H. Yamanaka, O. Oishi and S. Miyajima, in preparation.

[7] A. Pradel and M. Ribes, Mat. Chem. Phys., 23, 121 (1989).

[8] M. Tatsumisago, C. A. Angell, and S.W. Martin, J. Chem. Phys., 97,6968 (1992).

Chapter 4 Temperature dependence of ^{7}Li NMR spectra

4-1. Introduction.

The motional narrowing of the line width of NMR spectrum is well known from the early stage of magnetic resonance. However, as already referred in Chapter 1, most of the studies of line width in glassy ionic conductor seems to end in failure. This chapter reviews theories of motional narrowing and consider reasons why MNLW do not provide with useful information for inorganic glasses. Then, a method to solve the problem will be presented.

4-2 Fundamental theories for the analysis.

4-2-1 Bloembergen, Purcell and Pound (BPP) theory

Theory on the longitudinal relaxation time, T_1, and the transverse relaxation time, T_2, in nuclear magnetic resonance has been established by Bloembergen, Purcell and Pound[1]. Their theory is called BPP theory and has been widely applied to interpret the nuclear magnetic relaxation. BPP theory considers the spin relaxation caused by dipole-dipole interaction between two spins. In the theory, the inverse of line width, T_2, is given by,

$$1/T_2 = \frac{3}{2}\gamma^2\hbar[I(I+1)/3]^{1/2} \times \left[\int_{-1/\pi T_2}^{1/\pi T_2} J_0(\nu)d\nu\right]^{1/2} \qquad (4.1),$$

where γ is the gyromagnetic ratio of nuclei and I the spin operator. $J_o(\nu)$ is the spectral density of the secular term of the dipole-dipole interaction between nuclear spins, and is defined as follows,

$$\int_{-\infty}^{\infty} J_o(\nu)d\nu = \left\langle \sum_j [1-3\cos 2\vartheta_{ij}(t))r_{ij}(t)]^2 \right\rangle_{AV} \qquad (4.2)$$

, where the θ_{ij} is the azimuthal angle between the inter-spin vector, r_{ij} is the distance between spins i and j. If the fluctuation of vectors between two spins, $F(t)$, is assumed to be

$$\langle F(t)F^*(t+t_1)\rangle_{AV} = \langle F(t)F^*(t)\rangle_{AV}\, g(t_1), \qquad (4.3)$$

$$J_0(\nu) = \langle F(t)F^*(t)\rangle^2 \int_{-\infty}^{\infty} g(t_1)\exp(i2\pi\nu t_1)dt_1. \qquad (4.4)$$

$g(t_1)$ is the correlation function for molecular motion, which is assumed to be single

exponential,

$$g(t_1)=\exp(-t_1/\tau_c), \qquad (4.5)$$

where τ_c is the correlation time for the nuclear motion.

In this case, we obtaine that $J_o(\nu)= 2\tau_c/(1+4\pi^2\nu^2\tau_c^2)$ (4.6)

Eq. (4.1) was written as,

$$(1/T_2)^2=(1/T_{2RL})^2\,(2/\pi)\,\tan^{-1}(\alpha\tau_c/T_2), \qquad (4.7)$$

α is from the limit of integration (4.7) and cannot be exactly defined.

Frequency of the motion, ν_c, can be expressed as,

$$\nu_c=\tau_c^{-1} \qquad (4.8)$$

Eq. (4.7) can be written as,

$$\nu_c = \alpha W \cot[\frac{1}{2}\pi(W / A)^2], \qquad (4.9)$$

where W is the observed line width and A the width of rigid lattice.

Assuming ν_c is obeys the Arrhenius activation process, $\nu_c=\nu_0\exp(-E_a/RT)$, the logarithmic plot of ν_c versus reciprocal temperature eq. (4.9) gives an straight line with the slope of E_a/RT and with the intercept of ν_0.

Bishop and Bray[2] first examined the motional narrowing of ^{7}Li in some lithium borate glasses. Figure 4-1 shows the temperature dependence of the line width of ^{7}Li in lithium borate glasses. Figure 4-2 shows the result of the analysis of the data in Fig. 4-1 using eq.(4.9) from reference 2. It was found that E_a determined by the use of eq.(4.9) is always much smaller than E_σ by a factor of about 3. At this stage, it was concluded that the motion of the lithium ions observed in glasses by NMR is restricted in a narrow space. It was interpreted as "local" motion and does not represent the lon-range motion which contributes to the electric conduction.

Now we can consider that the discrepancy between E_a and E_σ is not intrinsic to the material but originated from unappropriate application of the theory for the line-width transition. In BPP theory the single relaxation process is assumed.

In an attempt to overcome the problem, Hendrickson and Bray proposed a phenomenological equation [3,4]. Their model assumes two species of ions. One is very static ion (A) and the other is very mobile ion(B). T_2 and fraction of ions A and B is T_{2A}, T_{2B}, f_A, and f_B, respectively. Each of ions, A and B, moves between two sites. They assumed that total T_2 can be expressed as follows,.

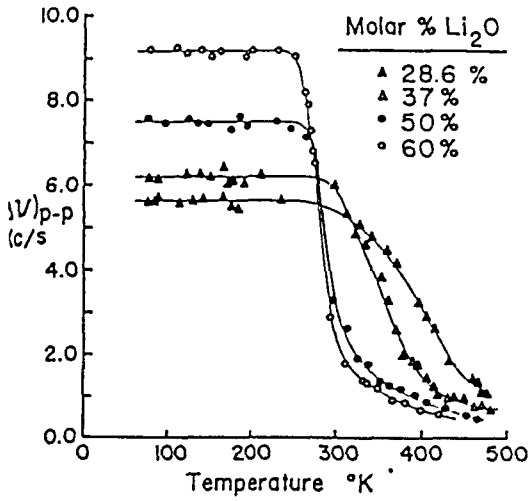

Fig. 4-1 Motional narrowing of the line width of ^7Li in Li_2O-B_2O_3 system. (After Bishop and Bray[2])

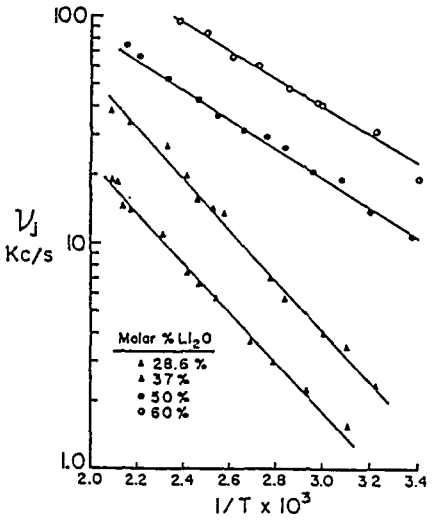

Fig. 4-2 BPP plot from Fig. 4-2.(After Bishop and Bray.[2])

$$T_2=f_aT_{2A}+f_BT_{2B}=1/W. \quad (4.10)$$

They associated the origin of KWW function as the distribution in glasses and considered that the distribution in T_2 and f_b can be compensated in (4.10).

f_B can be represented by,

$$f_B=\exp(-E_a/RT). \quad (4.11)$$

f_A and f_B must satisfy the condition

$$f_A=1-f_B. \quad (4.12)$$

Combination of Eqs. (4.10)-(4.12) yields,

$$\ln(W^{-1}-A^{-1})=-(E_a/RT)-\ln(B^{-1}-A^{-1}), \quad (4.13)$$

where A is the rigid lattice line width and B is the line width at extreme narrowing. The plot of W^{-1}-A^{-1} vs. the inverse of temperature gives a straight line the slope of which gives the activation energy. Figure 4-3 shows examples of Hendrickson-Bray plot. The activation energy obtained from region II in Fig.4-3(a) is usually higher than that by BPP method, but still lower than E_σ. Though the Hendrickson-Bray method brought about an improvemnt in the analysis of the line width transition, their model is rather artificial in the sense that they specified "two" largely different fast ions in glasses. The author believes the analysis should be based on more explicit theory which conforms to the structure and properties of ionic glasses.

Recently, new anomalous behavior of the temperature dependence of Ag in AgI-Ag_2O-B_2O_3 glasses[5]. The reciprocal line width, T_2^{-1}, shows an irregular variation as shown in figure 4-4. This is a noticable anomaly in the process to discuss LW with respect to its ion conductive glasses.

To sum up, analysis by classical BPP method leave three main defects.

(i) E_a by LW is much smaller than E_σ. (ii)preexponential factor (τ_0) is usually of the order of 10^{-6} to 10^{-7} s which is too large. (iii) the plot sometimes shows an irregular variation at high temperature.

As already noted, the line width of ionic probe in glasses should be analyzed on the bases of a model which incorprates the diversity of probable motion of ions distributed ober numerous inequivalent position and compelled to move in diverse potential energy manifold in ionic

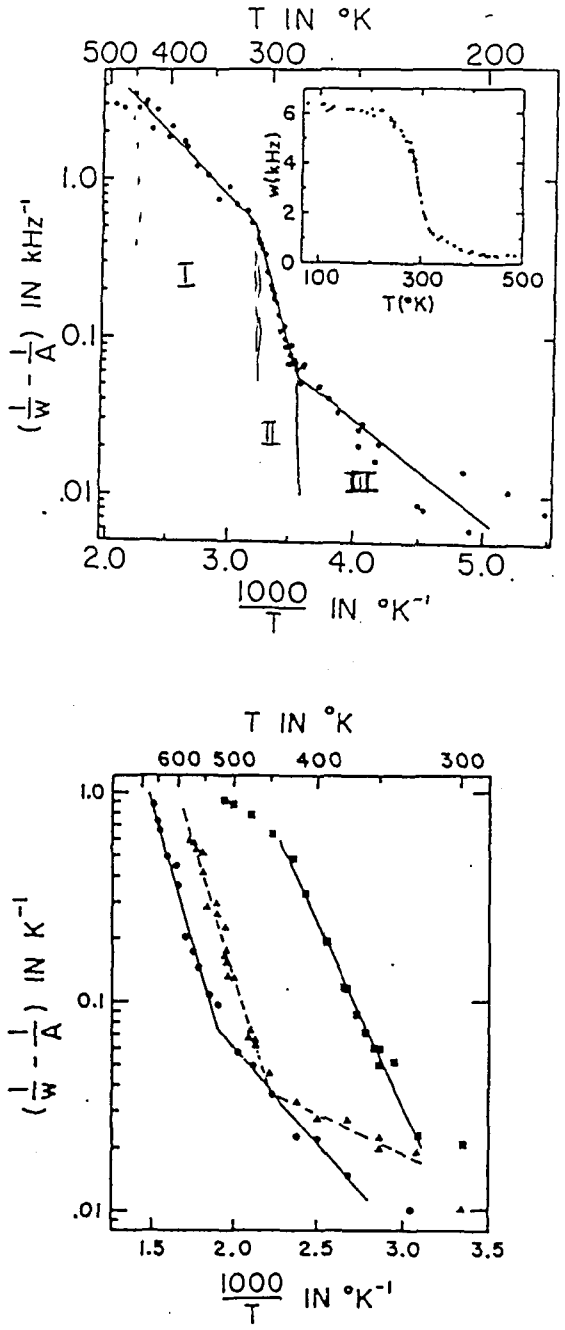

Fig. 4-3 Hendrickson-Bray analysis for (a)alkali-borate glasses.(b) mixed alkali glasses.(After Hendrickson and Bray [3][4])

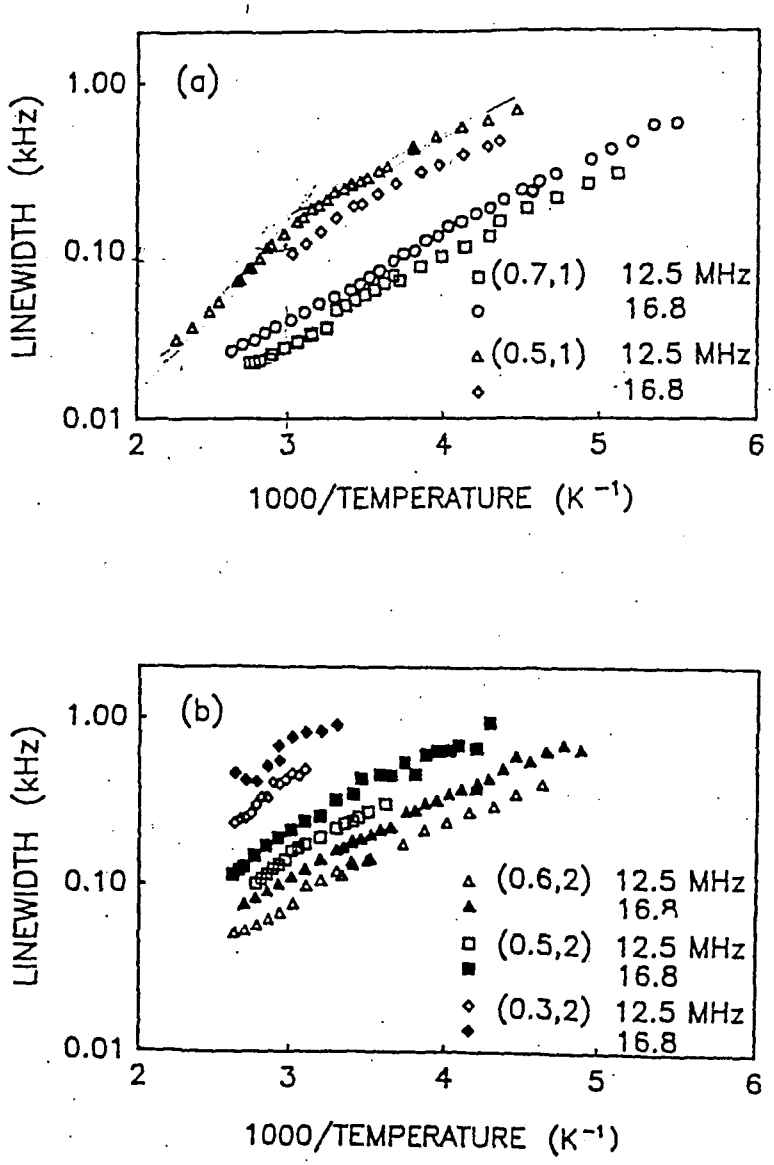

Fig. 4-4 (a) Temprature dependence of line width of ^{109}Ag in $AgI\text{-}Ag_2O\text{-}B_2O_3$. (after Chung et al[5])

glasses. It is therefore appropriate to develop a method of analysis of LW based on the KWW functions which coincide the large inhomogenity of structure and physical properties.

4.2-2 General theory of motional narrowing of line width

Explicit time domain relaxation function of magnetization, $G(t)$, is derived in chapter X in reference 6.

The absorption, $I(\omega)$, is the Fourier Transform of the relaxation function:,

$$G(t)=\mathrm{tr}\{M_x(t)M_x\}=\mathrm{tr}\{e^{i\mathcal{H}t}M_x e^{-i\mathcal{H}t}M_x\}, \qquad (4.14),$$

where $\mathcal{H}$ is the total Hamiltonian of the system, M the magnetization operator. We assume that $\mathcal{H}$ is composed of the unperturbed Hamiltonian $\mathcal{H}_o^T$ and a small perturbing term $\mathcal{H}_1$. Unperturbed Hamiltonian $\mathcal{H}_o^T$ is composed of Zeeman Hamiltonian $\mathcal{H}o$, and an operator F, which separates the lattice effect, for example, Brownian motion, $\mathcal{H}_l$ is supposed to be an interaction operator between spins, for instance dipole-dipole coupling.

As the calculation of eq.(4.14) needs a long procedure, only the result and the assumption adopted in formation procedure will be given here.

$$G(t) = e^{i\omega_0 t}\exp\left(-\left\langle\omega_p^{\,2}\right\rangle\int_0^t (t-t_1)g(t_1)dt_1\right), \qquad (4.15)$$

where $g(t_1)$ is the correlation function and ω_p is the r.m.s. line width in the rigid, *i.e.*, static, lattice. A few assumptions were introduced in the procedure:

i) $[\mathcal{H}_0^T,F]=0$, $[M,F]=0$, and $[\mathcal{H}_1,F]\neq 0$

ii) $\langle\omega_p^2\rangle$ corresponds to the values in the absence of the ionic motion.

iii) τ_c is sufficiently long compared to the inverse of Larmor frequency.

If $g(t_1)$ is expressed by a single exponential function as $g(t_1)=\exp(-t_1/\tau_c)$, $G(t)$ can be expressed as ,

$$\exp(-i\omega_o t)G(t) = \exp\left\{-\omega_p^{\,2}\int_0^t (t-t_1)g(t_1)dt_1\right\} \qquad (4.16)$$

$$= \exp\left\{-\omega_p^2\tau_c[\exp(-t/\tau_c)-1+t/\tau_c\right\}.$$

In the case of glassy ionic conductor, we assume that $g(t_1)=\exp(-(t_1/\tau_c)^{\beta})$ in eq.(4.15).

The Fourier transform of (4.15) gives the absorption line shape, but it is difficult to solve it explicitly even in the case of (4.16). Abragham stated in reference[6] that eq. (4.16) gives more precise description for motional narrowing but BPP theory is used only for its

simplicity.

There has been only one inadequate attempt to interpret the LW by (4.15) incorprating KWW function[7]. Bjorkstam *et al.* assumed that T_2 is the time at which $G(t)$, which is proportional to free-induction decay of the magnetization, reachs its $1/e$ value and estimated the variation of line width with temperature from T_2^{-1} thus obtained. They only showed how temperature dependence of line width varies with β. Figure 4-5 shows how temperature dependence of line width changes with β, keeping $\tau_0=10^{-13}$ s, E_a/R=2000K and $<\omega_p^2>=10^8 s^{-2}$. The region where motional narrowing occurs is broadned as β is decreased. They also calculated τ_c from BPP equation (4.9) and plotted them in logarithmic scale as a function of reciprocal temperature as shown in Fig. 4-6. In all cases, the plot shows linear dependence on reciprocal temperature when the line width is between 0.25 to 0.75 for the rigid static width and the slope becomes smaller with the decrease of β. They found that slope of this region is approximately βE_a. Their analysis has not been used since then, though it seems promissing. Presumubaly, there are a few reasons for this. First, calculation procedure of (4.15) incorprating KWW function was not cleary shown and only the results were shown. The other reason is that the line width is estimated from T_2^{-1}, so that the line width cannot be accurately determined when the line shape is close to Gaussian shape.

For a rigorous analysis of LW data, it is essential to establish a method to calculate the FWHM of (4.15) incorporating KWW function. In the next section, we newly propose the method.

4-3 Numerical calculation of LW

In this section, the procedure of the calculation of LW by Fourier transforming (4.15) incorporating KWW function. The basic scheme of calculation is straightforward. The right hand side of eq. (4.15) for given smapling time, t, is computed by calculating the integration by numerical calculation method. Then, $G(t)$ is digitally Fourier transformed to yield a spectrum. From the spectrum, LW is easily obtained.

Figure 4-7 shows the algorithm of the program. First, τ_c and β is input. 1024 points for t of equal spacing was chosen to calculate $G(t)$. Integration of each $G(t)$ was calculated by Sympson method. The division number in the integration was set to more than 3000 in the computation. Next $G(t)$ is digitally Fourier transoformed to give a spectrum. From the

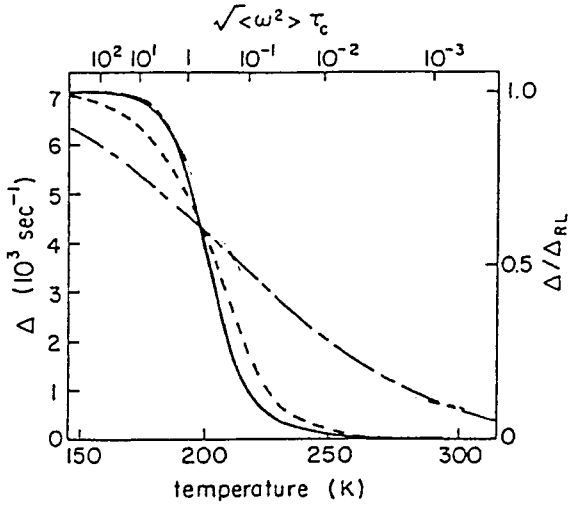

Fig. 4-5 Line width Δ as a function of temprature. (a) exponential (solid), (b)KWW(β=0.5) (Short dashes). (c) KWW(β = 0.2) (Short-long dashes). (after Bjorkstam *et al.*[7])

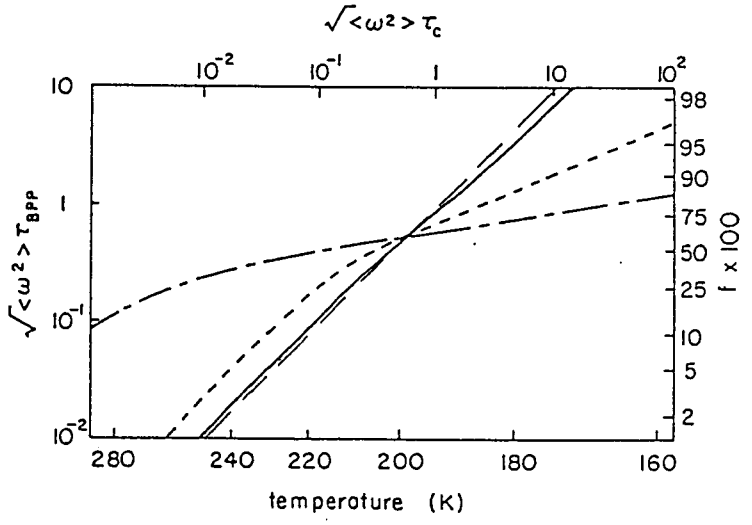

Fig. 4-6 Bilogarithmic plot of τ_{BPP} calculated using Δ in Fig.4-5 from eq. (4.9) vs. τ_c in KWW function with β=1 (solid line), β=0.5(short dashes) and β=0.2(short and long dashes). f =(line width/static width) × 100. (After Bjorkstam *et al.*[7])

spectrum full-width at half maximum(FWHM) was obtained. Temperature dependence of FWHM was calculated assuming that τ_c obeys Arrhenius rule. Calculation was not carried out when τ_c^{-1} is shorter than 1/10 of Larmor frequency, taking into account the assumption (iii) in 4-2-2. Thus, MNLW for given τ_0, E_a, β can be calculated. Programm is coded by NEC-N88BASIC. The source code of the program is shown in Appendix B.

Figure 4-8 shows the simulated spectra in the case of β=0.5 and 0.1 when $\tau_c = 10^{-4}$s and ω_p=10000 Hz. It is easily sean that line width differs greatly with the value of β.

Figure 4-9 shows the temperature dependence of line width for β=1, 0.5 and 0.3, when $\tau_0=10^{-14}$s, E_a=50kJ/mol and ω_p=24000Hz. The region of motional narrowing extends with the decrease of β. Figure 4-10 shows how behavior of MNLW changes with τ_0 when E_a, ω_p, and β was kept constant as 50kJ/mol, 24000Hz and 0.5, respectively. As τ_o decreases, the temperature at which motional narrowing occurs (T_{MN}) decreases. Figure 4-11 shows the temperature dependence of line width for E_a=40kJ/mol, 50kJ/mol and 60kJ/mol when other parameters are kept constant. T_{MN} decreases with the decrease of E_a.

To clarify how these theoretical MNLW incorprating KWW function differs from single exponential case (β=1) in BPP analysis, FWHM thus obtained was substituted for W in eq. (4.9) and temperature dependence of ν_c was calculated. Figure 4-12 shows logarithmic plot of ν_c against the reciprocal temperature for the case of β=0.3, 0.5 and 1, assuming E_a=50kJ/mol and $\tau_0=10^{-14}$s. Similar behavior was observed as that by Bjorkstal et al in Fig. 4-6. The plot shows linear region and apparant activation energy(E_{app}) can be obtained from the slope. Hence, the apparant activation energy drastically decreases as the β decreases. As the temperature increases, the slope becomes more steeper, and the slope for β=0.3 and β=0.5 become similar to that for β=1. Therefore, at high temperature, it is expected that BPP behavior is observed. However, experimental results are diffrent from the expectation, as will be shown later.

The apparent activation energy obtained from the linear region from the plot as shown in Fig. 4-12 is plotted against β in figure 4-13. Solid line shows the line that holds βEa. They well coincide with the solid line. This means that βEa can be obtained if the temperature dependence of line width for in the case of KWW relaxation function is analyzed by BPP method.

Now, we will turn to the experimental result for motional narrowing of the line width

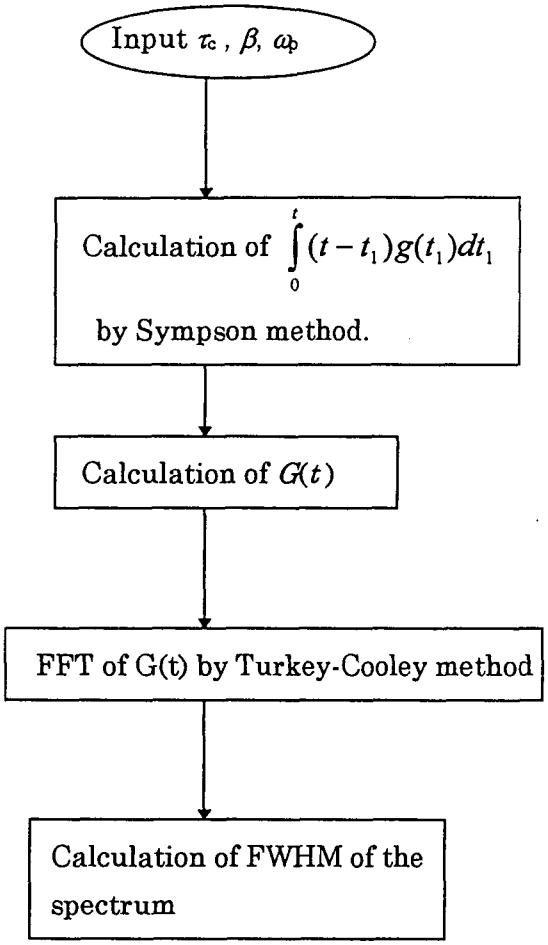

Figure 4-7 Algorithm for the calculation of FWHM

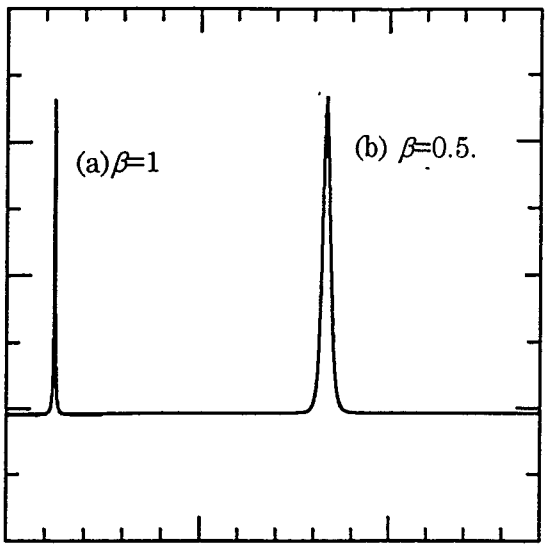

Fig. 4-8 Simulated spectra.(a)β=1 and (b) β=0.5. ω_b=10000Hz and τ_c=10^{-4}s is used for the calculation. τ is shown in the figure.

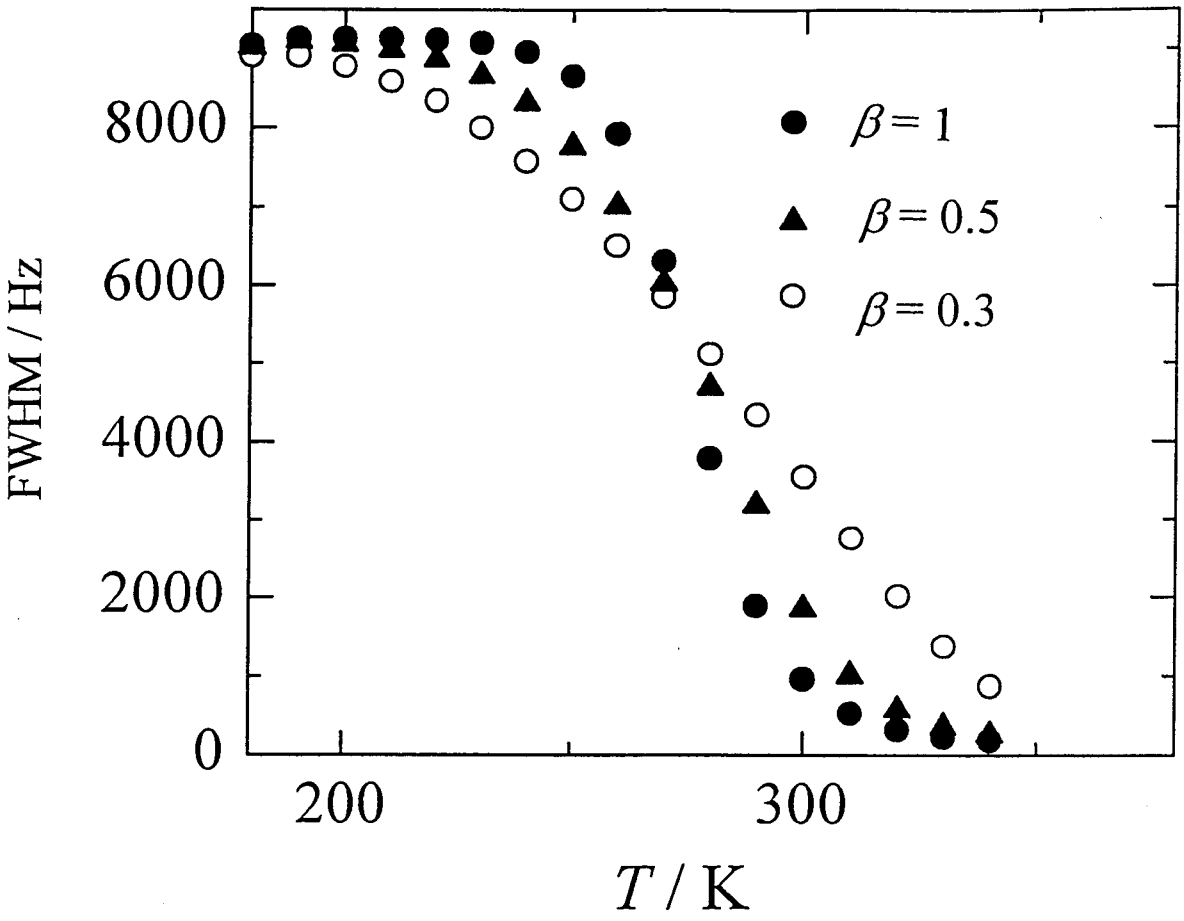

Figure 4-9 Theoretical temprature dependence of line width. τ_0=10^{-14} s, E_a=50kJ/mol and ω_p=24000Hz is used for the analysis. The values for the β used for the calculation are shown in the figure.

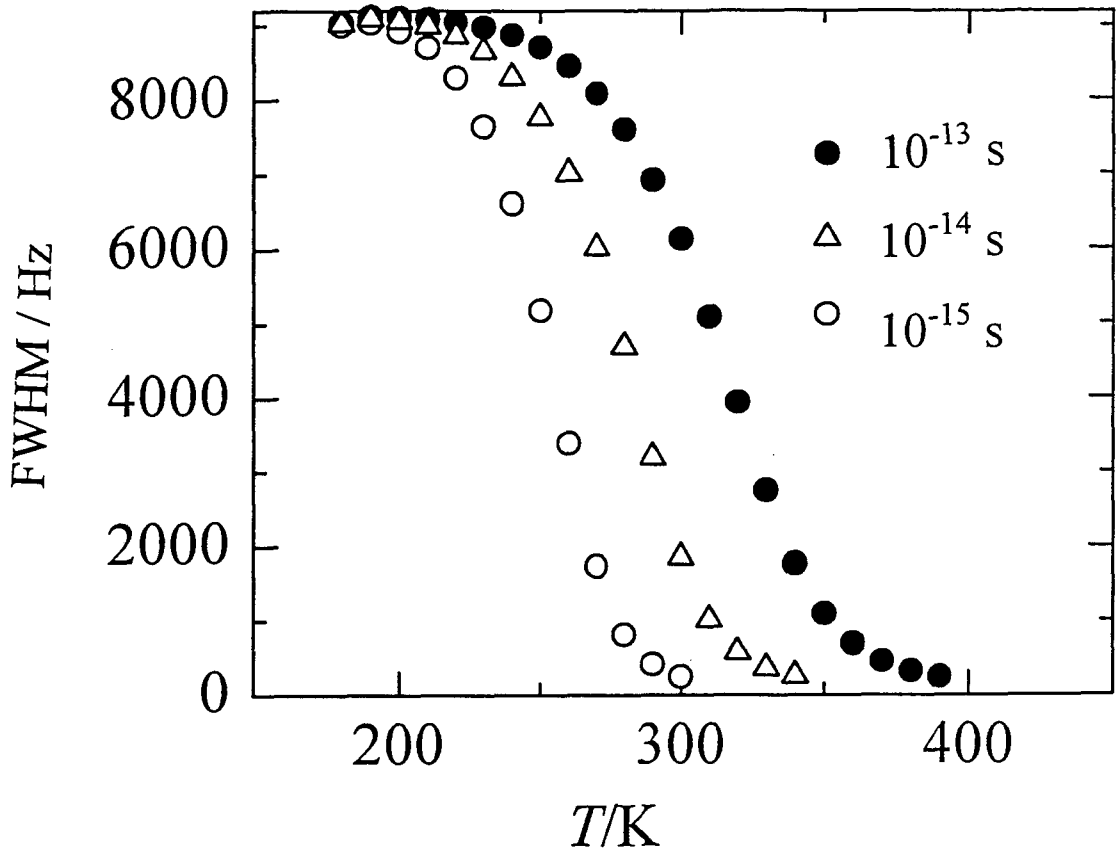

Figure 4-10 τ_0 dependence of FWHM vs. Temprature. E_a=50kJ/mol, ω_p=24000Hz and β=0.5 is used for the calculation.

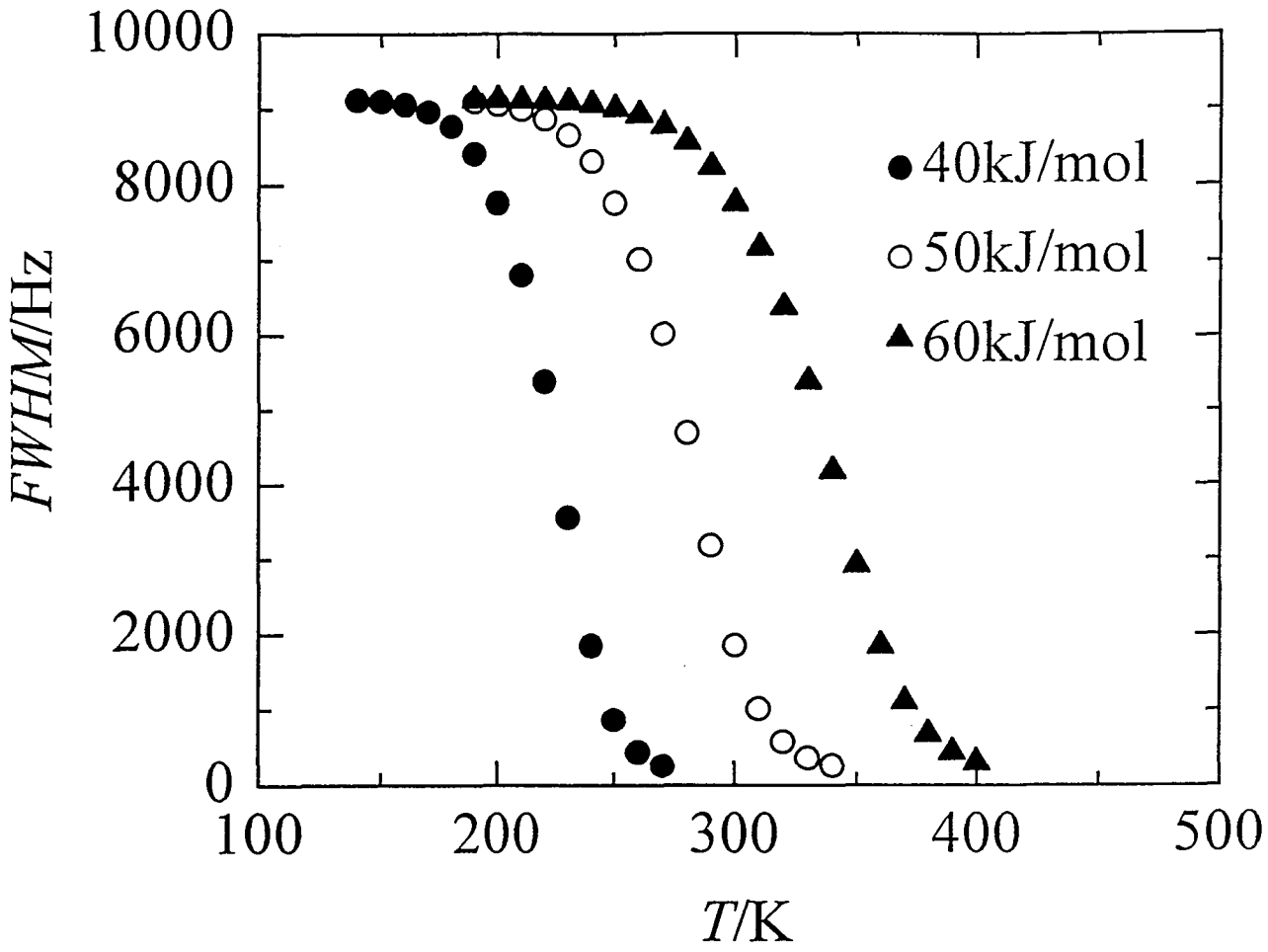

Figure 4-11. E_a dependence of FWHM vs temprature. $\tau_0=10^{-14}$s, $\omega_p=24000$Hz and $\beta=0.5$ is used for the calculation.

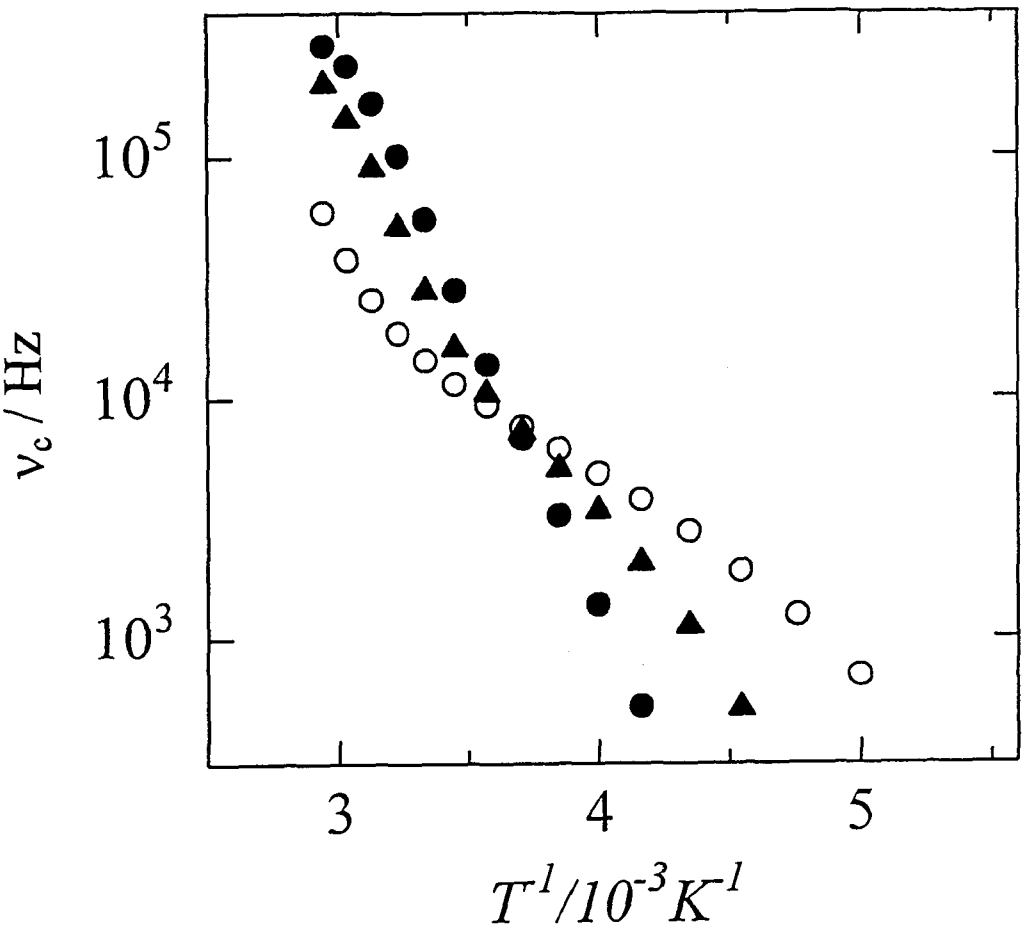

Figure 4-12 ν_c calculated from eq.(4.9) from FWHM in Fig. 4-9 and plotted against reciprocal temperature.

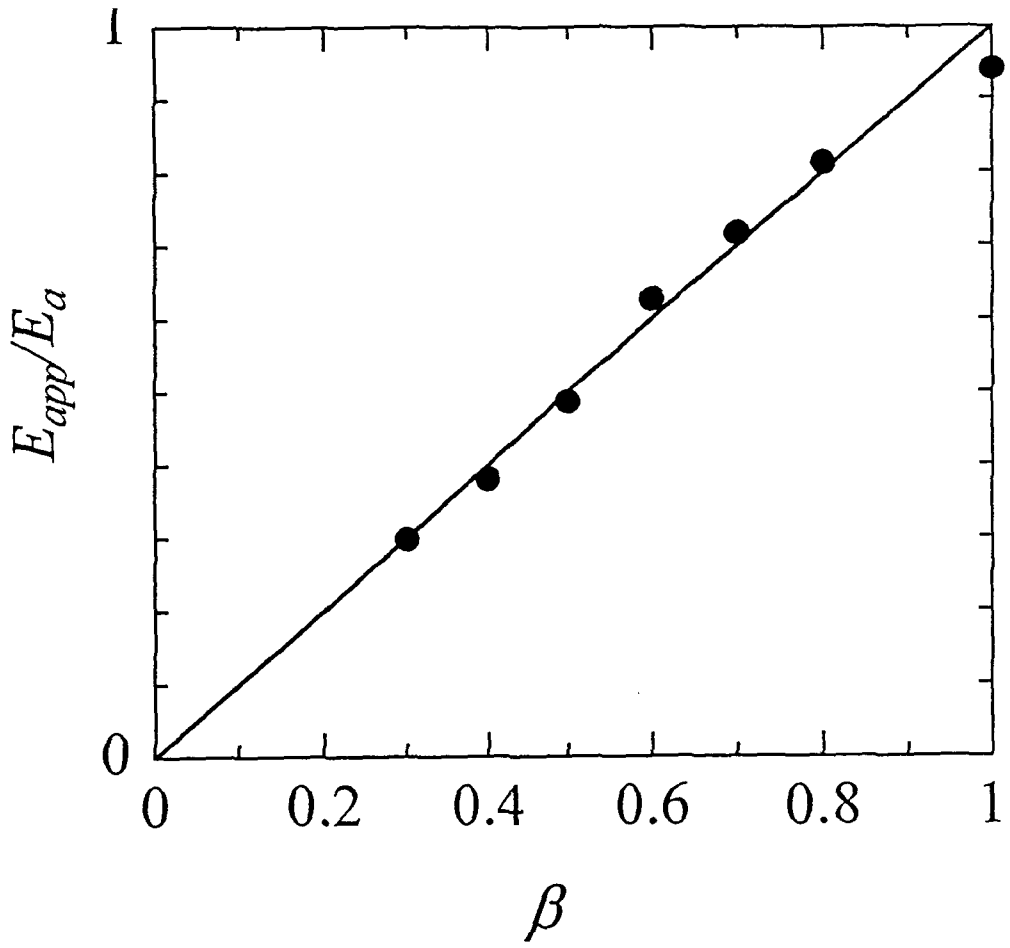

Figure 4-13 The activation enegy in linear region as in Fig.4-12 E_{app} is normalized by E_a is plotted against β.

of several glasses presented in Chapter 2. First, the result was analyzed by BPP region. The adiabatic motional narrowing region is discussed for each glasses. At high temperature region, it is possible T_1 becomes comparable to T_2 to affect the line width. Therefore, the measurement of spin-lattice relaxation time was also carried out. Next, the experimental MNLW are compared the relaxation function from electrical measurement. After examining the validity of the analysis, relaxation parameters are calculated and presented for all glasses in Chapter 2.

4-4. Experimental

^{7}Li NMR was measured with Chemagnetics CMX 200 NMR system at the Larmor frequency of 78MHz. Temperatures were controlled by introducing the cooled or heated nitrogen into a dewar made of teflon placed in the probehead. Spectra were obtained by Fourier transforming the free-induction decay signal after the excitation pulse. The pulse used here was 0.5μs, which is equal to $\pi/18$ pulse. Spin-lattice relaxation times were measured by inversion recovery method. Duration of $\pi/2$ used was 4.5μs.

4-5 Results

Fig. 4-14 shows the temperature dependence of ^{7}Li NMR spectrum of $40Li_2O$-$40B_2O_3$-$10Li_2SO_4$ glass system. Only the central transition(-1/2 ↔ 1/2) is clearly observed in the spectrum. Fig. 4-15 shows the temperature dependence of ^{7}Li NMR spectra of xLi_2S-$(100-x)B_2S_3$. Fig. 4-16 shows the temperature dependence of ^{7}Li NMR spectraof xLi_2S-Ga_2S_3-$6GeS_2$.

FWHM of $(100-x)(0.5Li_2O$-$0.5B_2O_3)$-xLi_2SO_4 is plotted against temperature in Fig. 4-17. T_{MN} are almost independent of the content of Li_2SO_4(230K). With the doping of Li_2SO_4, the LW changes faster with temperature. It should be noted that slower change with temperature is again observed for the glasses with highest doping content of Li_2SO_4(X=50).

Fig. 4-18 shows the variation of *FWHM* with temperature of xLi_2S-$(100-x)B_2S_3$. T_{MN} for the glasses is around 150K, which is much lower than that of Li_2O-B_2O_3-Li_2SO_4. This means that the motion of lithium is much faster in these glasses.

Fig. 4-19 shows the temperature dependence of the line width of xLi_2S-Ga_2S_3-$6GeS_2$. T_{MN} lies between 170K and 180K, which is very low compared with T_{MN} in oxide glasses.

Temperature dependence of the spin-lattice relaxation times of above three samples

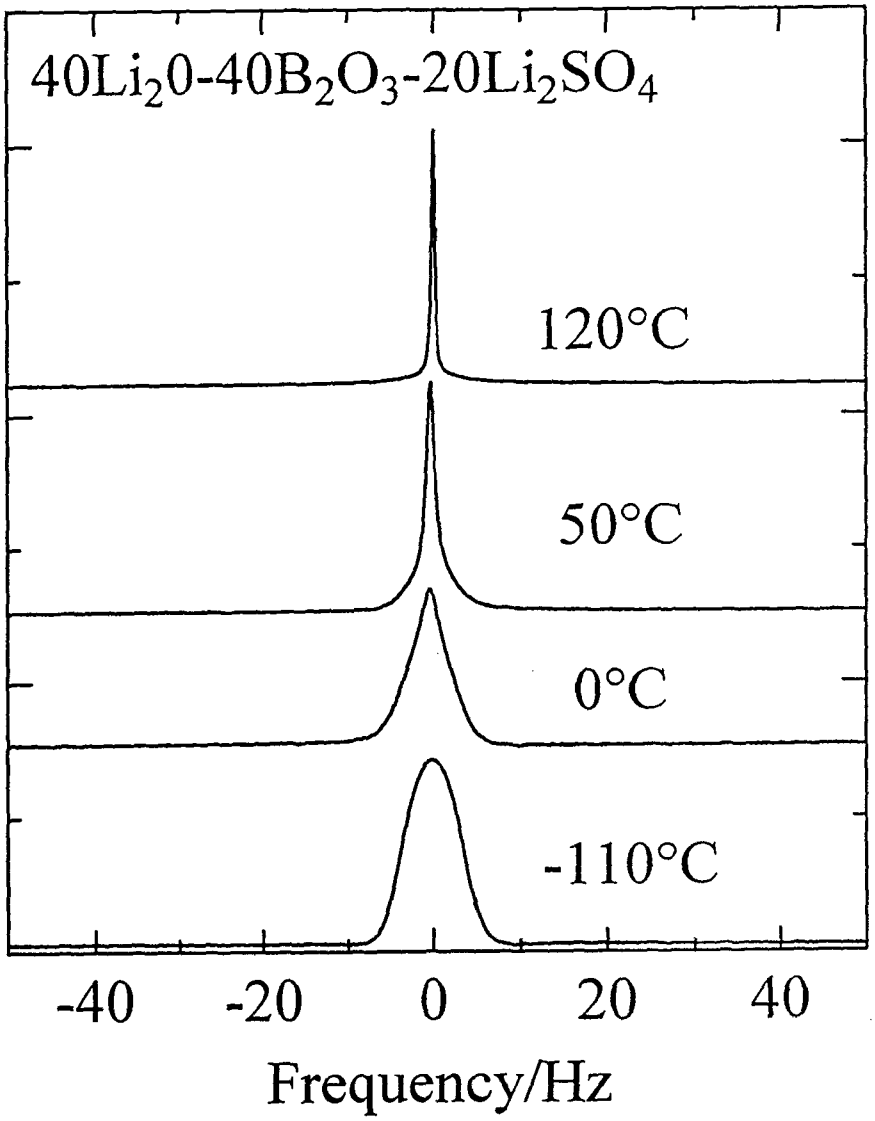

Figure 4-14 Temprature dependence of ^{7}Li NMR spectrum of $40Li_2O$-$40B_2O_3$ - $10Li_2SO_4$.

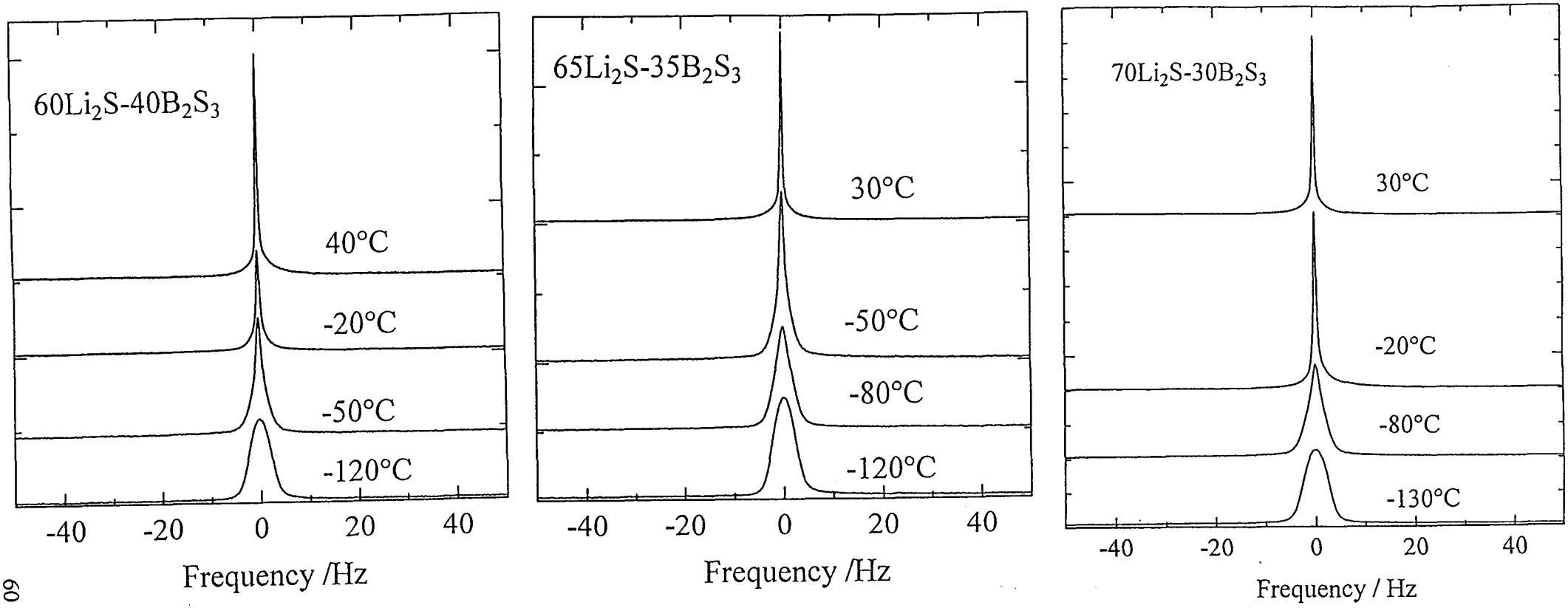

Figure 4-15 Temprature dependence of ^{7}Li NMR of xLi2S-(100-x)B2S3. (a)x=60, (b)x=65 and (c)x=75.

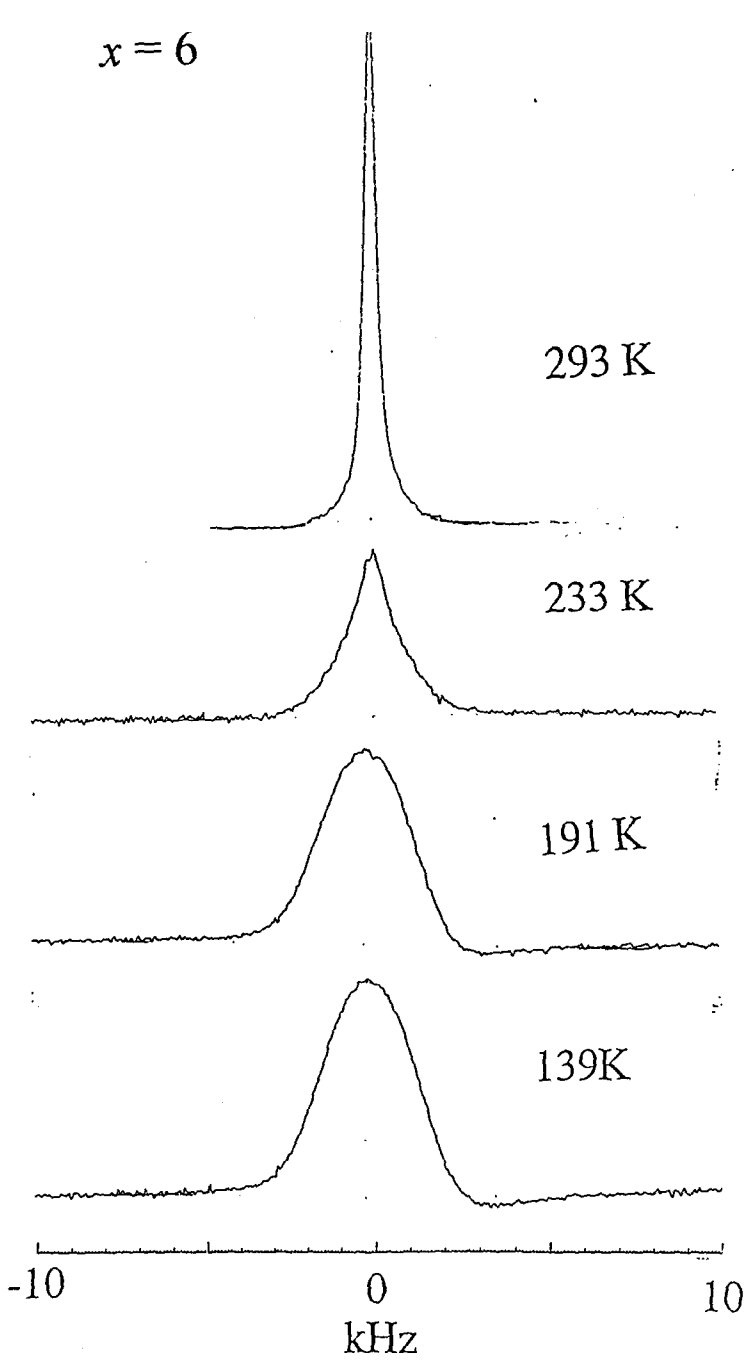

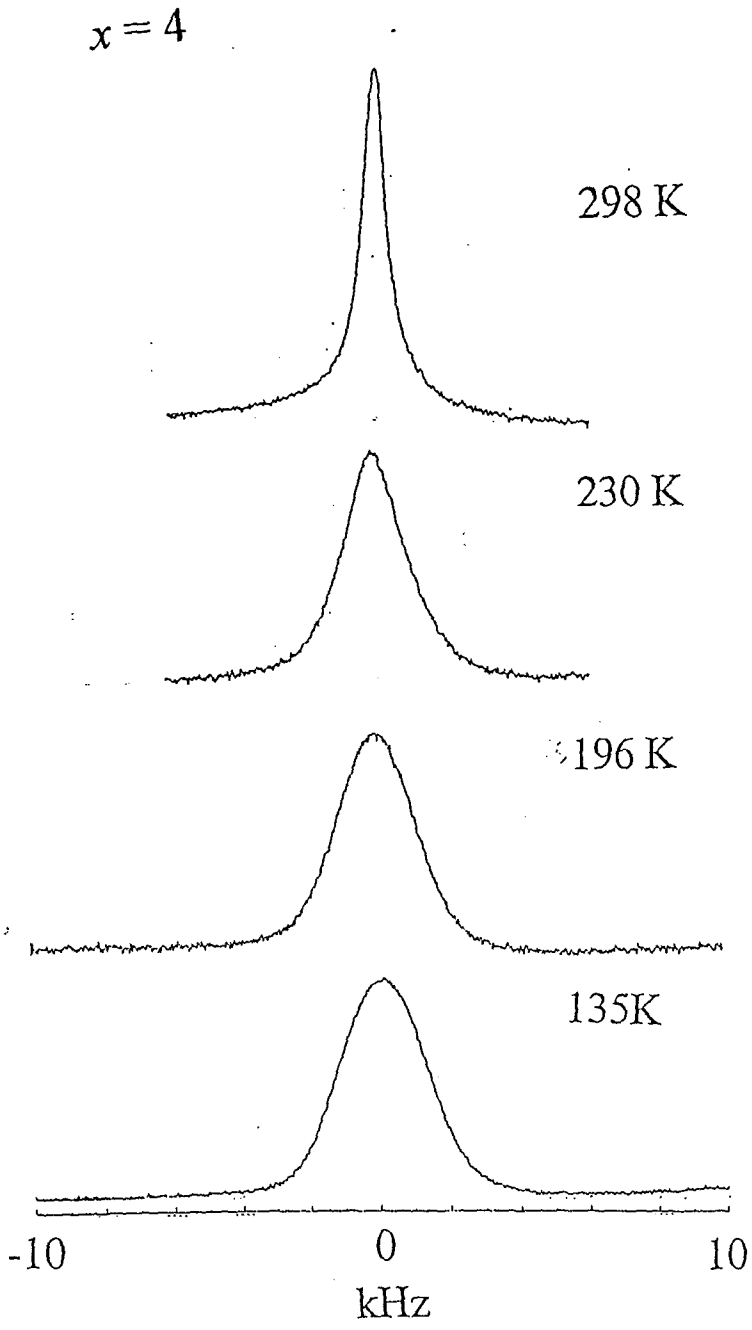

Figure 4-16 Temprature dependence of ^{7}Li NMR of xLi$_2$S-Ga$_2$S$_3$-6GeS$_2$. (a)x=6 and (b)x=4.

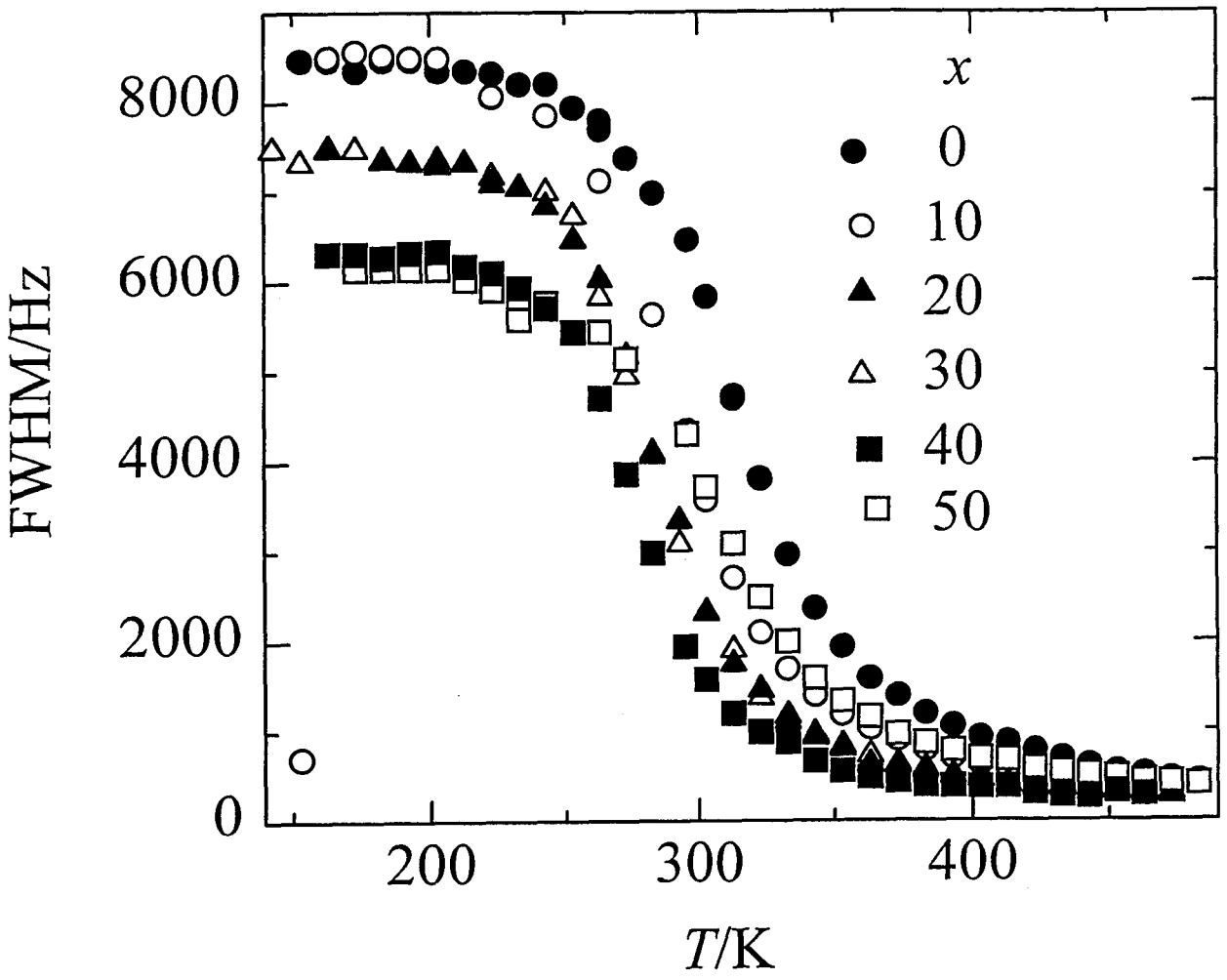

Figure 4-17 FWHM of ^{7}Li NMR spectra are plotted as a function of temprature in $(100\text{-}x)(0.5Li_2O\text{-}0.5B_2O_3)\text{-}xLi_2SO_4$.

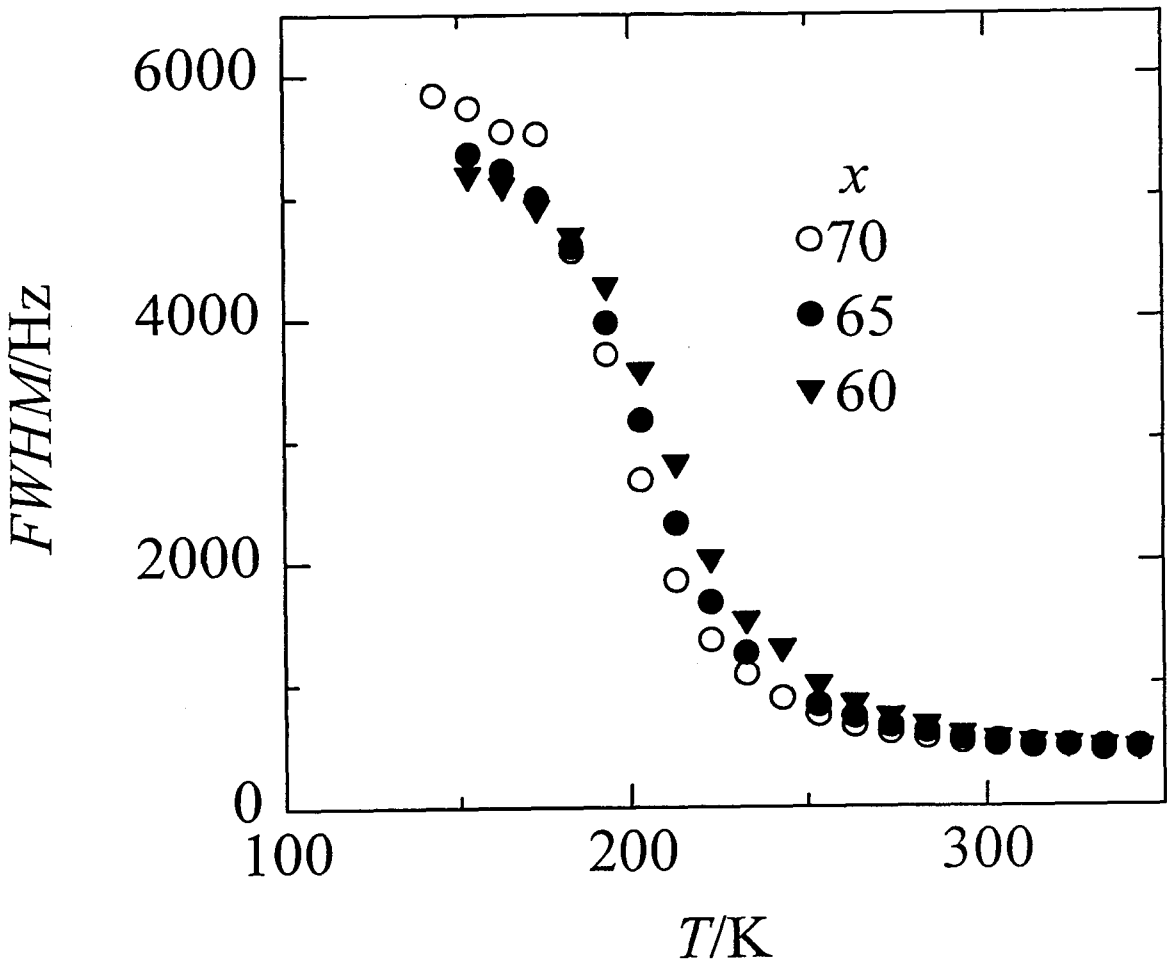

Figure 4-18 FWHM of ^{7}Li NMR spectra of xLi_2S-$(100-x)B_2S_3$ are plotted against temperature.

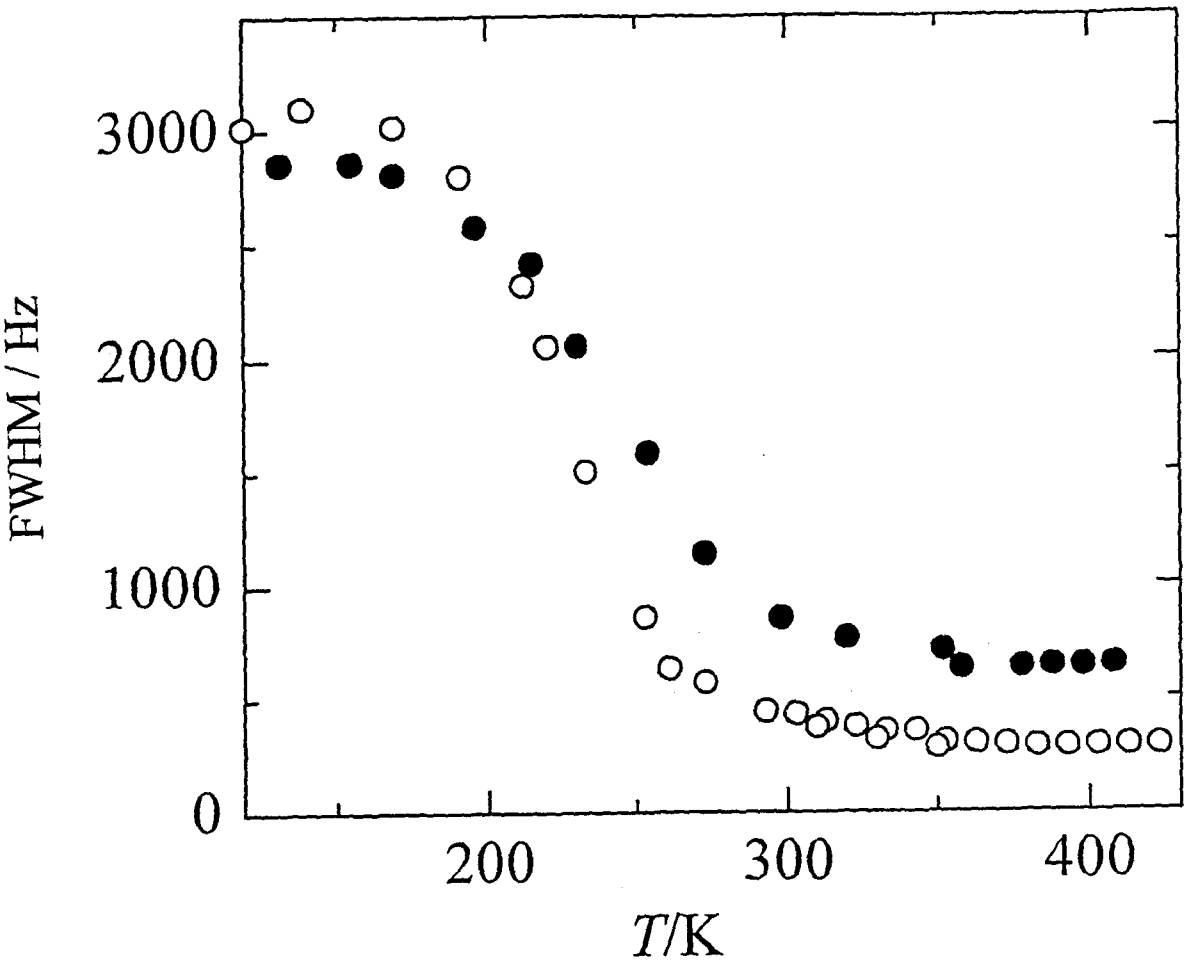

Figure 4-19 FWHM of ^{7}Li NMR spectra of xLi_2S-Ga_2S_3-$6GeS_2$.
Open circles: x=6 ; Closed circles: x=4

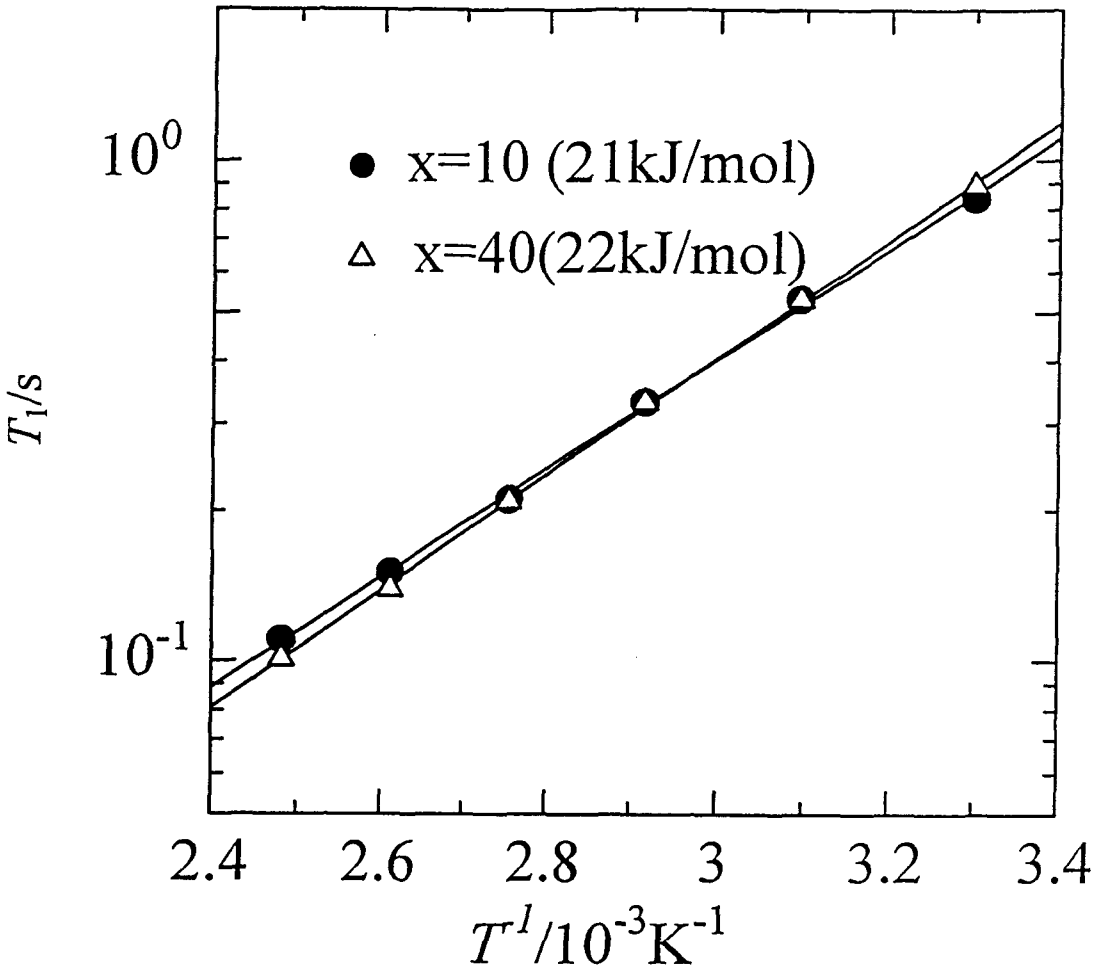

Figure 4-20 Spin-lattice relaxation time(T_1) of ^{7}Li at 78MHz in Li_2O-B_2O_3-Li_2SO_4.

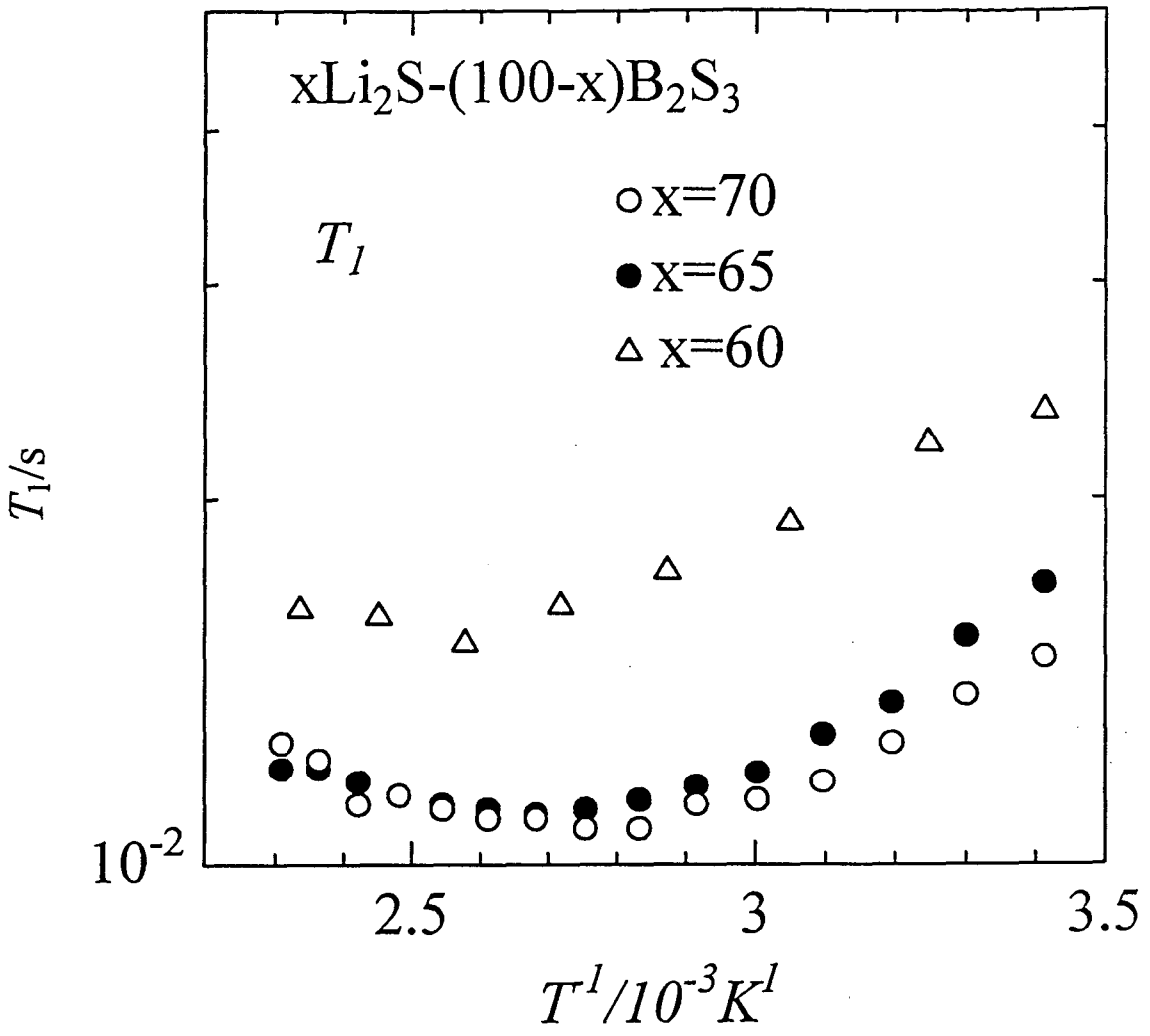

Figure 4-21 Spin-lattice relaxation time(T_1) of ^{7}Li at 78MHz in xLi$_2$S-(100-x)B$_2$S$_3$.

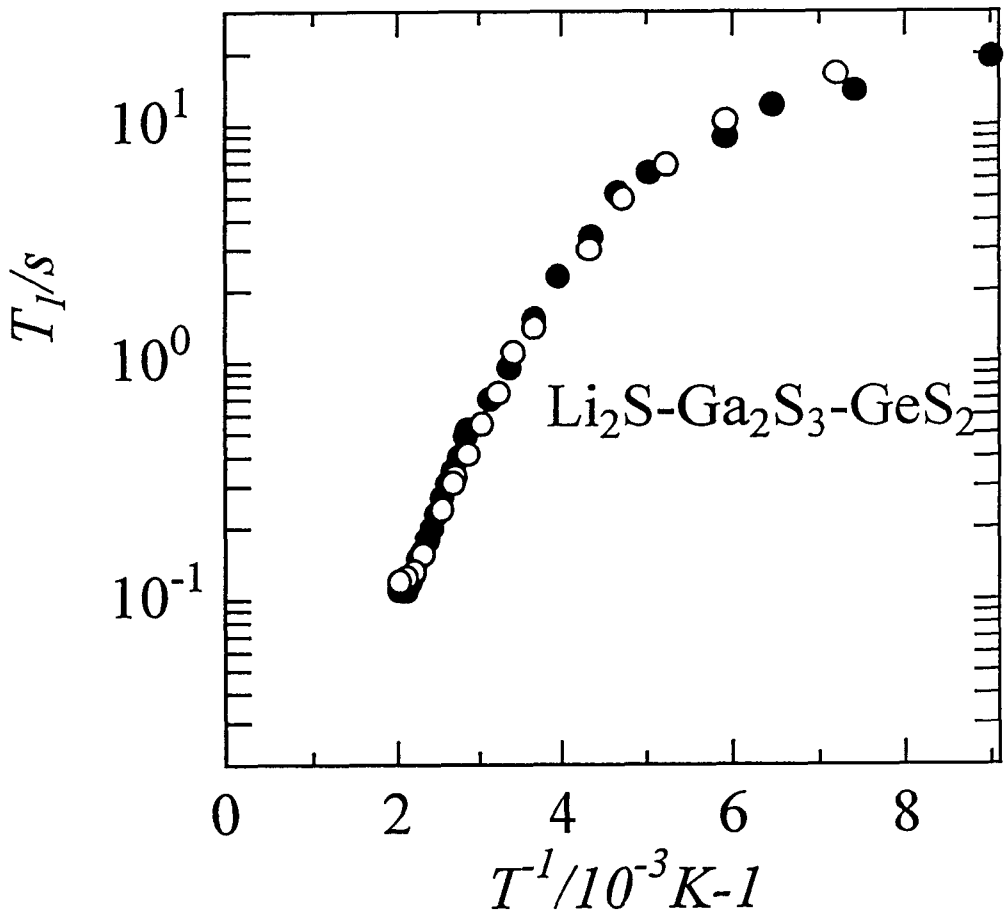

Figure 4-22 Spin-lattice relaxation time (T_1) of ^{7}Li at 78MHz in xLi_2S-Ga_2S_3-$6GeS_2$
Open circles: $x = 6$; Closed circles: $x = 4$.

are shown in Figs. 4-20, 4-21 and 4-22. For each of Li_2O-B_2O_3-Li_2SO_4 and Li_2S-Ga_2S_3-GeS_2, only the lower temperature side of the temperature where T_1 minimum value is observed. For each of Li_2S-B_2S_3 glasses with different compositions, the T_1 minimum was observed. The position of the minimum shifts to the lower temperature as x increases, which means the motion of ions becomes fast with increase of x. The temperature at which T_1 minimum observed is 400K, 385K, and 370K, for x=60, 65,and 70, respectively.

4-6 Discussion.

In Figs. 4-23, 4-24 and 4-25, ν_c was calculated from the line width using (4.9) and log ν_c is plotted as a function of reciprocal temperature. In all samples, linear regions are observed. From the discussion in 4-3, the slope corresponds to βE_a. The sample (100-x)(0.5 Li_2O-0.5B_2O_3)-xLi_2SO_4 shows an apparent activation energy of 17.2kJ/mol. For $x$$Li_2S$-(100-$x$)$B_2S_3$, an apparent activation energy is 9.70kJ/mol. For $x$$Li_2S$-$Ga_2S_3-6GeS_2$, the obtained apparent activation energies are E_a=10.0kJ/mol and 12.0kJ/mol for x=4 and 6, respectively.

As discussed in Fig. 4-12 in 4-3, it is expected that the slope becomes larger at high temperature region and true activation energy E_a is observed from the slope. However, such behavior is never observed at high temperature region. The slope gradually decreases at high temperature. For $x$$Li_2S$-(100-$x$)$B_2S_3$ and $x$$Li_2S$-$Ga_2S_3-6GeS_2$, irregular changes are observed at higher temperature region. It is possible that as τ_c^{-1} approaches the Larmor frequency and spin-lattice effect gives contribution to the line width.

In this case, observed life time, T_2', can be written as[1],

$$1/T_2' = 1/2T_1 + 1/T_2. \qquad (4.18)$$

Assuming T_2'=1/(2π·FWHM), T_2' was calculated and compared with T_1 in logarithmic scale in figure 4-26. In all cases, T_1 is much longer than T_2'. For Li_2S-B_2S_3 glasses, T_2 shows similar behavior around T_1 minimum[8]. The similar behavior of T_1 and T_2 was reported for Li_2S-SiS_2 and AgI-Ag_2O-B_2O_3 glassy systems[5,8]. The similar behavior was also observed in some ion-conductive crystals such as Li_5AlO_4[9]. One explanation which is often used is the coupling of ^7Li to paramagneitc impurities[10]. Ions cannot reach in the vicinity of paramagnetic impurities when the motion is slow. When the motion becomes fast, they encounter the impurities and the impurities affect the magnetic relaxation of lithium. If the mechanism of the similarity of T_1 and T_2 at high temperature occurrs by the coupling to

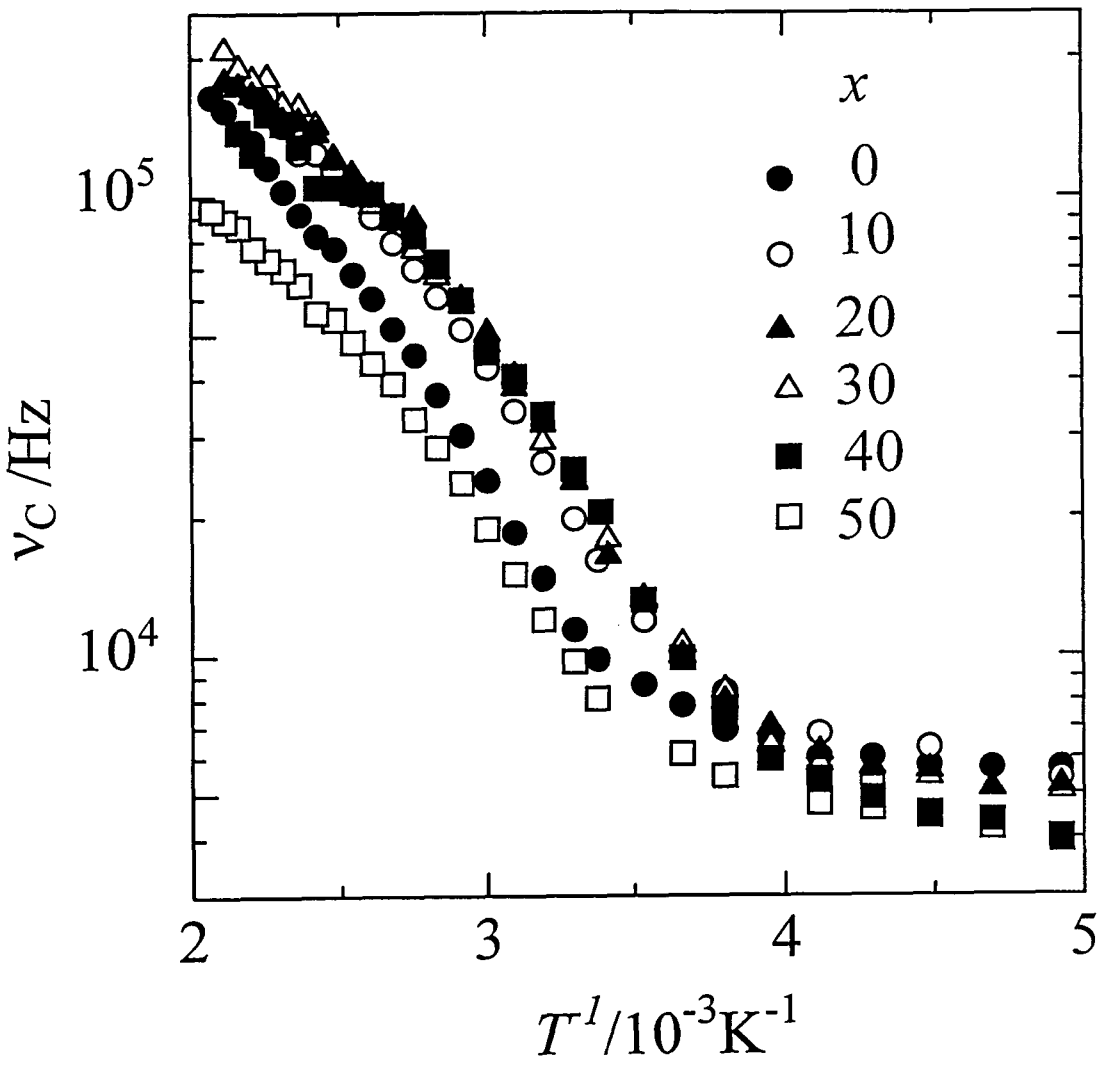

Figure 4-23 ν_c calculated from eq.(4.9) from FWHM in (100-x)(0.5Li_2O-0.5B_2O_3)-xLi2SO4. x is shown in the figure.

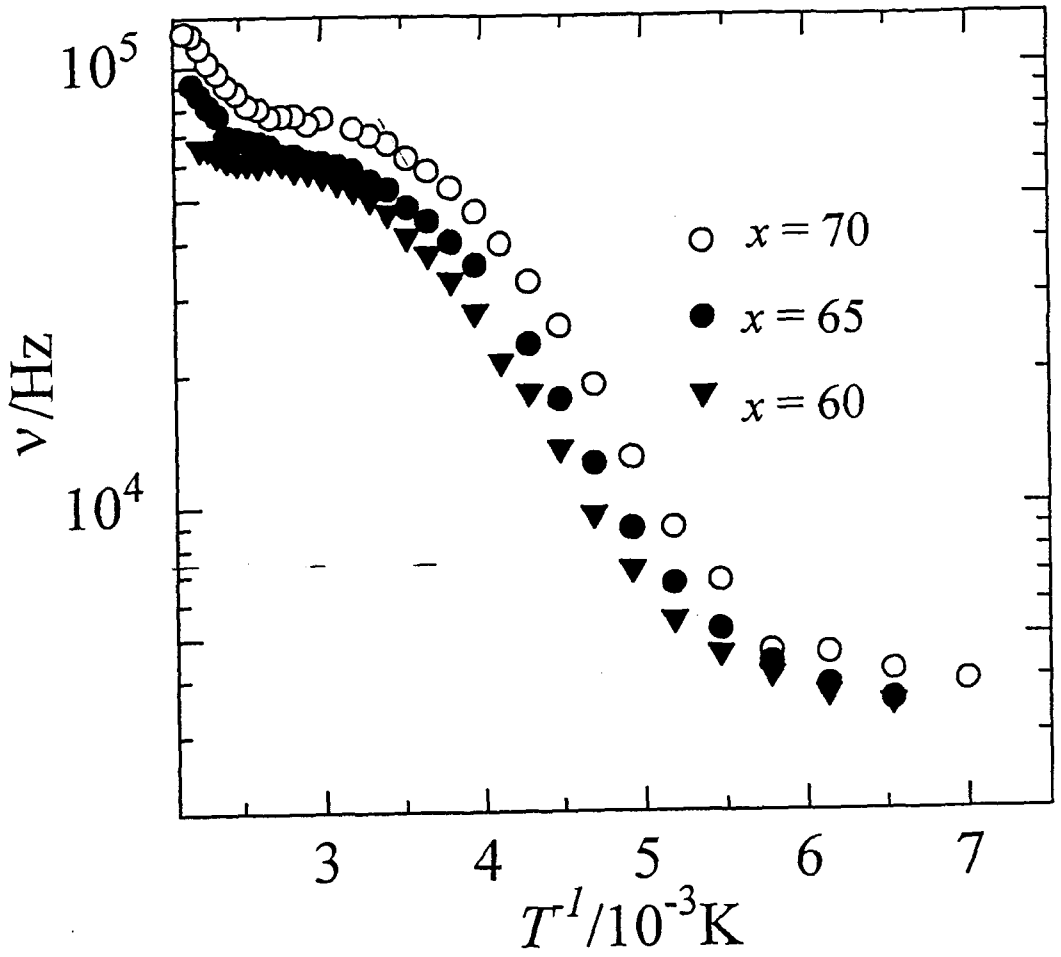

Figure 4-24 ν_c calculated from eq.(4.9) from FWHM in xLi$_2$S-(100-x)B$_2$S$_3$.. x is shown in the figure.

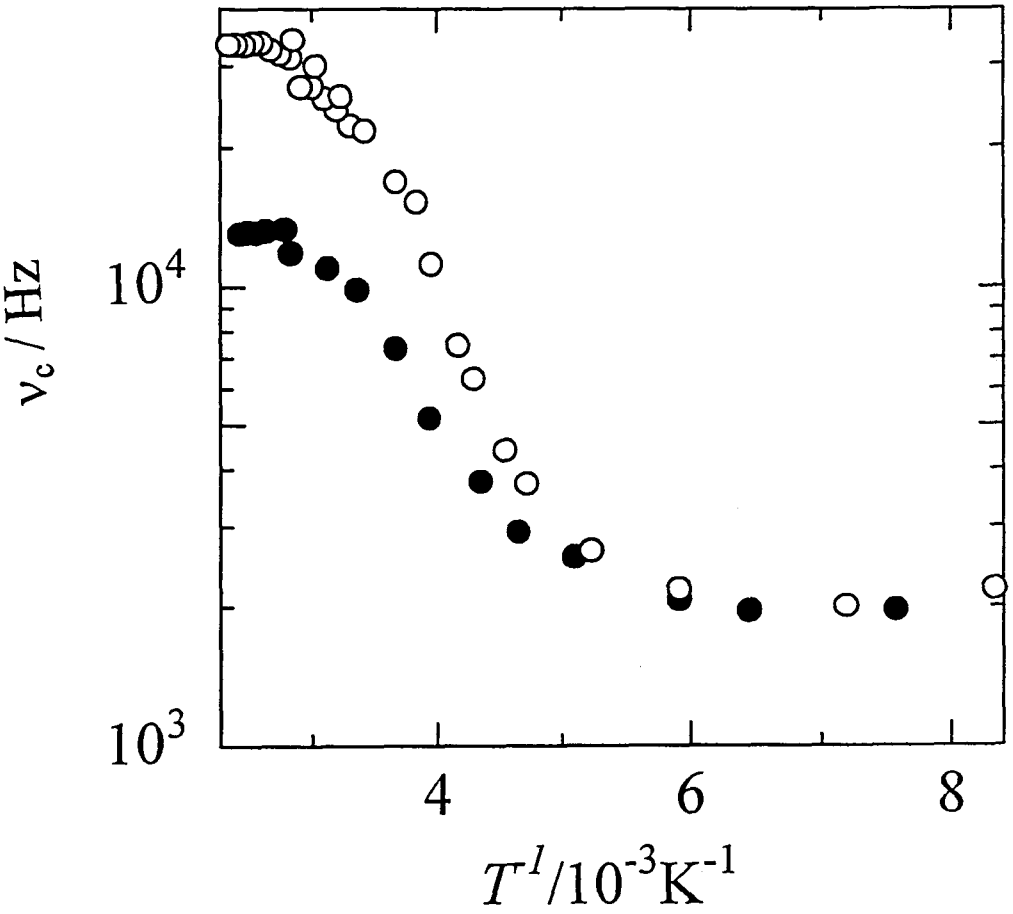

Figure 4-25 ν_c calculated from eq.(4.9) from FWHM in xLi$_2$S-Ga$_2$S$_3$-6GeS$_2$.
Open circles: x=6; Closed circles:x= 4

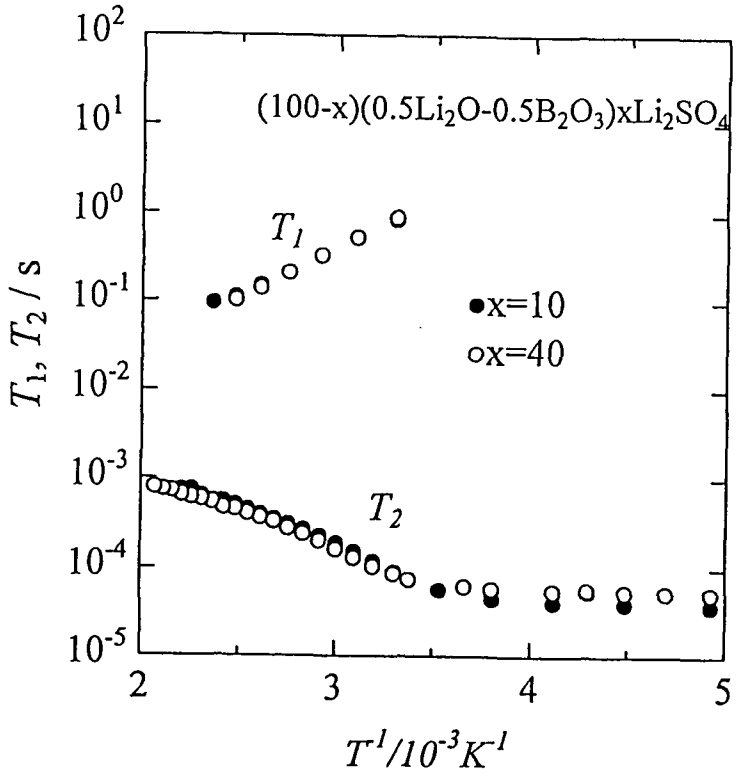

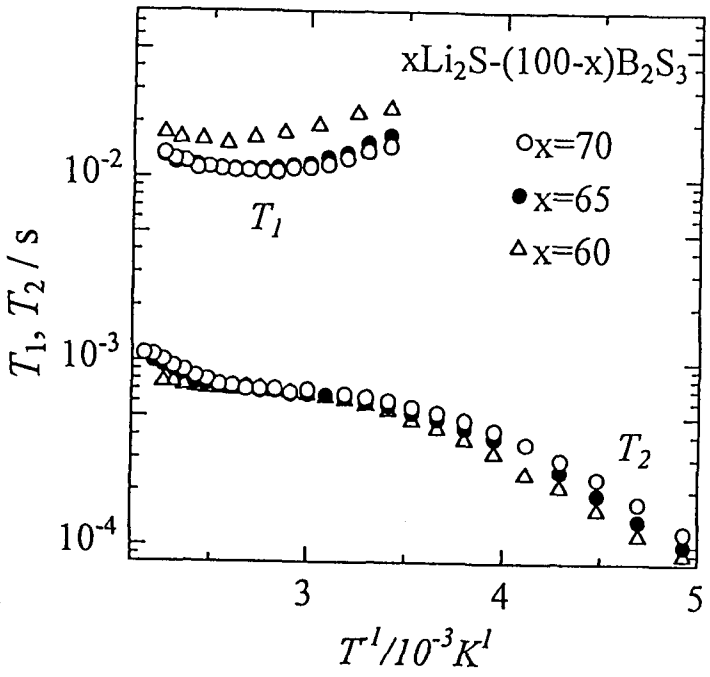

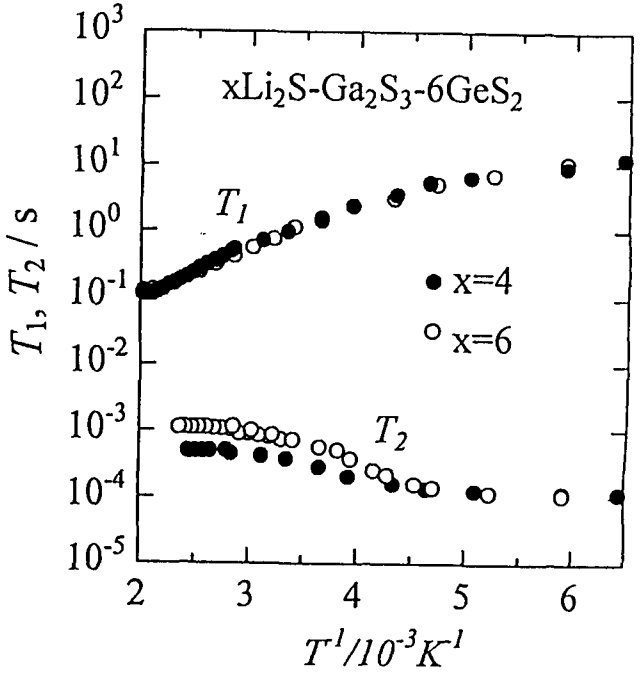

Figure 4-26 Comparison between T_1 and T_2.

(a) Li_2O-B_2O_3-Li_2SO_4 (b)Li_2S-B_2S_3 (c) Li_2S-Ga_2S_3-GeS_2.

paramagnetic impurities, the behavior is very different for every sample since the concentration of paramagnetic impurities is greatly different for each samples. However, the behavior seems to be common in all super-ion conductive glasses. Therefore, the author believes that the another explanation should be considered. One possibility is that T_1 effect on LW cannot be interpreted by the eq.(4.18) in ionic conductor where the relaxation process is complicate.

Next, the measured FWHM for $50Li_2O$-$50B_2O_3$ is examined using the relaxation parameter τ_o, β, and E_σ in chapter 3. Using the values of these parameters deduced from the conductivity measurement (τ_0=2.52x10^{-15}s, E_σ=52kJ/mol, β=0.54), the theoretical motional narrowing is calculated by the procedure described in 4-3. The result is shown in Fig. 4-27 by the solid line. It is obvious that the experimental FWHM results cannot be reproduced by these parameters from conductivity. Then, FWHM was simulated by varying τ_0 and β, keeping the E_a to be 52kJ/mol. The best fit was obtained with τ_o = 6.0x10^{-14}s and β =0.33. The theoretical FWHM is shown by the dotted curve in Fig. 4-27. It is found that the incorpration of KWW relaxation function into the line width analysis leads to a greatly improved result. However, there remains a serious consistency between the activation parameters deduced by NMR and conductivity measurements. Similar discrepancy in τ_o and β are also reported for Li_2S-SiS_2 and Li_2O-B_2O_3-LiCl by T_1 measurements[11,12].

The result shows that the discrepancy between the activation parameters by NMR and by conductivity measurement is not only characterstic of superionic-conductor but also of poor-conducting glasses. There are two possilble interpretation for this discrepancy. Ngai *et al.* stated that the discrepancy is intrisic and not related to conduction mechanism because nuclear spin relaxation observe the correlation between two spins, while conductivity observe relaxation time of single ion[13,14]. On the other hand, Svare et al. attributed it to the mechanism of conduction[15]. They considered that NMR observes all motion of ions while conductivity observe limited fraction of ions associated with conduction.

Recently, very suggestive result was reported by Fan et al. [16]. They investigated the value of τ_e/τ_σ in some polyelectrolyte system which can be varied from salt-in polymer electrolyte to polymer-in-salt solution by changing continuously the fraction of the electrolyte salt. For low content of salt (salt-in-polymer) τ_e/τ_σ is nearly equal to 1. As the salt concentration increases, this ratio gradually increases and it abruptly increases at the transition

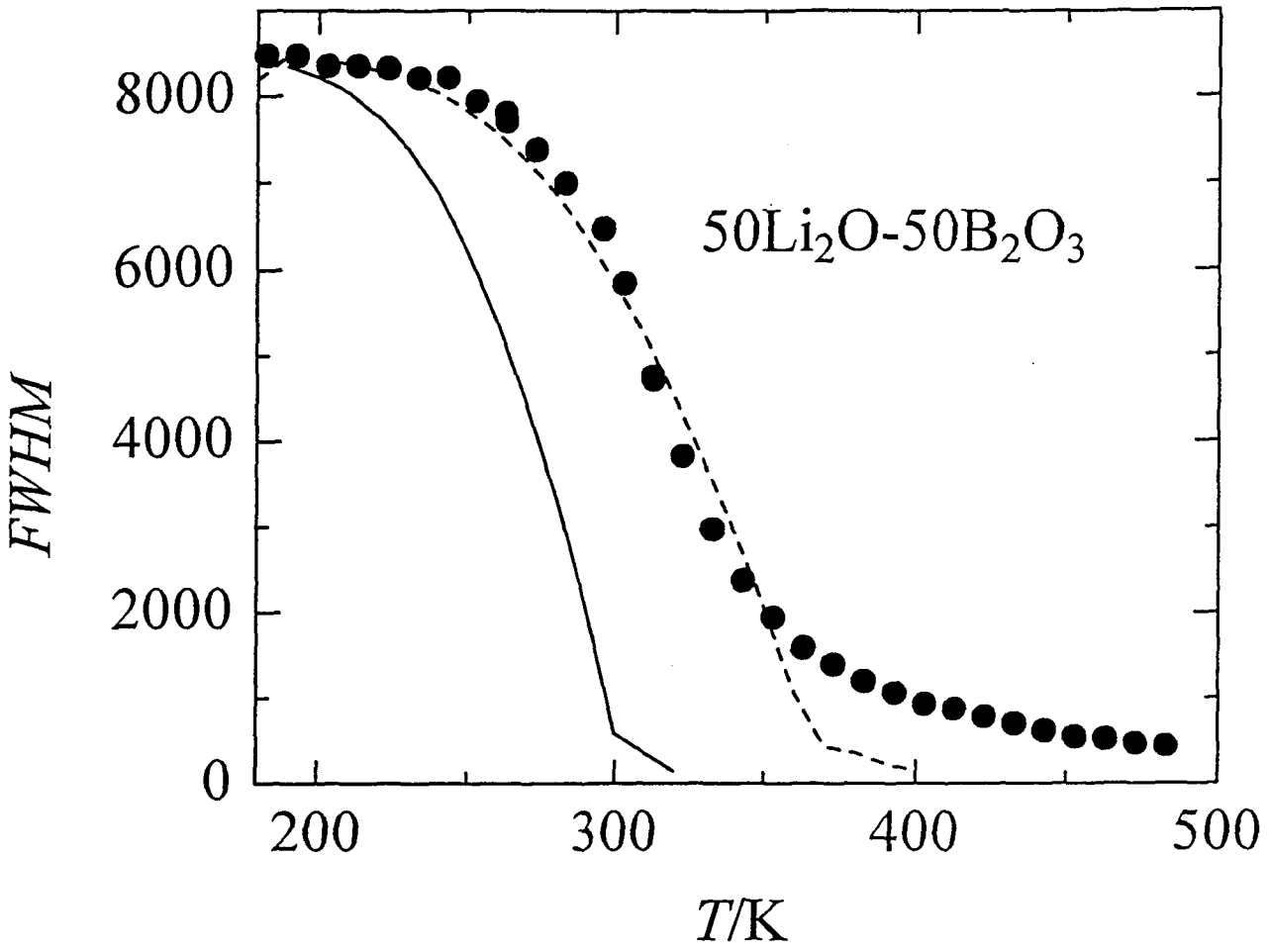

Figure 4-27 Temprature dependence of FWHM of ^{7}Li NMR of $50Li_2O$-$50B_2O_3$. Solid line is calculated using τ_0=2.48x10^{-15}s, E_a=52kJ/mol, and β=0.54. Dashed line shows that calculated assuming, τ_0=6.0 x10^{-14}s, E_a=52kJ/mol, and β=0.33.

point from salt-in-polymer domain to polymer-in-salt domain. This result indicates that the difference between the correlation times deduced from NMR and conductivity is not caused by the difference of relaxation and correlation since there is a case where τ_c and τ_σ coinsides with each other. Also, it is suggested that considerable increase of the ratio at the transition point is caused by some percolation because τ_c/τ_σ drastically increase at the transition to polymer-in-salt region. The result suggests strongly that the number of ions which is responsible for the conduction is much smaller than whole number of ions.

It should be noted that the conductivity σ can be given by $ne\mu$, where e is the electron charge, μ the mobility and n is the number of carrier ion. The fact that τ depends on the physical properties should be mainly associated with n. The fact that there is a same order of discrepancy in poor-conducting glass suggests that n is not greatly different between superionic glasses and poor conducting glasses. The difference in conducitivity may be attributed to the difference of mobility μ. In order to examine this point in more quantitative manner, the direct measurement of lithium mobility is highly desirable and therefore the measurement of diffusion coefficient which is directly related to the mobility will be conducted in the next chapter.

Finally, it is remarked that the rate of ionic motion can be determined by analyzing of MNLW below T_g for all the glasses. As already shown in section 4-3, MNLW depends on both τ_0 and E_a, so that it is impossible to determine E_a and τ_0 simultaneously. Hereafter, we analyze the data assuming that $E_a = E_\sigma$. The assumption is reasonable because it was confirmed that E_a coninsides with E_σ within almost 10% by analyzing the T_1.

On the above assumption the line widths are analyzed for all the glass samples. Parameters used to fit the data are shown in Table 4-1. To show the validity of analysis, obtained parameters from the MNLW for Li_2S-B_2S_3 are compared with those by T_1 measurements. In xLi_2S-$(100-x)B_2S_3$ system minimum was observed in the T_1 at 400K, 385K and 370K for x=60, 65 and 70, respectively. Using the relation that $\omega_o\tau_c=0.64$ at the temperature of T_1 minimum, we know that τ_c reaches 1.3×10^{-9}s at the temperatures. On the other hand the calculated values of τ_c using the parameters in Table 4-1 are 9.2×10^{-10}s, 1.3×10^{-9}s and 9.2×10^{-10}s for x=0.6, 0.65 and 0.7, respectively. Taking into account uncertainty in the determination of minimum point and in the data analysis in FWHM, the value of τ_c agrees excellently with the expected value, 1.3×10^{-9}s.

Table 4-1 Parameters determined in this work.

Sample	Conductivity			NMR		
	E_a/kJmol^{-1}	τ_0/ s	β	E_a/kJmol^{-1}	τ_0/ s	β
$(100-x)(0.5Li_2O-0.5B_2O_3)-xLi_2SO_4$						
x=0	52	2.5×10^{-15}	0.54	(52)	6.0×10^{-14}	0.33
x=10	50	-	-	(50)	3.0×10^{-14}	0.34
x=20	50 [1)]	-	-	(50)	1.5×10^{-14}	0.34
x=30	50 [1)]	-	-	(50)	1.2×10^{-14}	0.34
x=40	50 [1)]	-	-	(50)	3.0×10^{-14}	0.34
x=50	52 [1)]	-	-	(52)	5.0×10^{-14}	0.33
$x\ Li_2S-(100-x)\ B_2S_3$						
x=60	38 [2)]	-	-	(38)	1.0×10^{-14}	0.26
x=65	38 [2)]	-	-	(38)	9.0×10^{-15}	0.26
x=70	38 [2)]	-	-	(38)	4.0×10^{-15}	0.26
$xLi_2S-Ga_2S_3-6GeS_2$						
x=6	38	-	-	(38)	6.0×10^{-14}	0.32

1) M. Yamashita and R. Terai, Glastech Ber., 63, 13 (1990)

2) M. Menetrier, A.Hojjaji, C. Estournes and A. Levasseur, Solid State Ion, 48, 325 (1991)

As can be seen in Table 4-1, in the Li_2O-B_2O_3-Li_2SO_4 system the rate of motion of lithium ions are increased with addition of Li_2SO_4 up to x=30 then begins to decrease at x=40. This tendency observed in NMR is consistent with the conductivity.

References.

[1] N. Bloembergen, E.M. Purcell and R.V. Pound, Phys. Rev.; 75, 679 (1947).

[2] S. G. Bishop and P. J. Bray, J. Chem. Phys., 48, 1709 (1968).

[3] J. R. Hendrickson and P. J. Bray, J. Magn. Reson., 9, 341(1973).

[4] J. R. Hendrickson and P. J. Bray, J. Chem. Phys., 61, 2754(1974).

[5] S. H. Chung, K. R. Jeffery, and J. R. Stevens, Phys. Rev. B, 41, 6154 (1990).

[6] A. Abragham, " Principle of nuclear magnetism", Chapter X, Oxford, N.Y.1961

[7] J. L. Bjorkstam, J. Listerud, M.Villa, and C. I. Massara, J. Magn. Reson., 65, 383 (1985).

[8] A. Pradel, M. Ribes, and M. Maurin, Solid State Ionics, 28, 362 (1988).

[9] B. A. Huberman and J. B. Boyce, Solid State Commun., 25, 759 (1978).

[10] P. M. Richards in "Super-ionic conductor" Springer

[11] M. Tatumisago, C.A. Angell, and S.W. Martin, J. Chem. Phys., 97, 6968 (1992).

[12] F. Borsa, D. R. Torgeson, S.W. Martin and H.K. Patel., Phys. Rev. B, 46, 795 (1992).

[13] O. Kanert, R.Küchler, K. L. Ngai, and H. Jain, Phys. Rev. B, 49, 76 (1994).

[14] K. L. Ngai, J. Chem. Phys., 98, 6424 (1993).

[15] I. Svare, F. Borsa, D. R. Torgeson, and S. W. Martin, Phys. Rev. B, 48, 9336 (1993).

[16] J. Fan, R. F. Marzke, E. Sanchez, and C. A. Angell, J. Non-cryst solids., 172, 1178 (1994).

Chapter 5 Diffusion coefficient of Li

5-1 Introduction

In Chapter 4 it was shown that the rate of motion of ions can satisfactory deduced by analyzing the MNLW in every glass assuming $E_a=E_\sigma$. However it is extremely difficult to relate the activation parameters directly to the long-range transport of ions which is responsible for the electric conductivity because the motion observed in NMR can be highly localized one whereas electric conduction necessitate a very long range transitional motion of ions

In order to find any possible relation between the motional parameters by NMR and those by conducting experiments and then to shed light on the molecular mechanism of electrical conduction in inorganic glassy materials, it is desired to measure some physical properties which is closely associated with the electric charge transport. Self-diffusion coefficient of ions is one of such properties and, we expect that it can be measure directly by a special technique of NMR, *i.e*, by pulsed-field gradient spin echo method(PGSE).

If the ions of interest has any appropriate radioisotope, *e.g.*, ^{22}Na for ^{23}Na, its diffusion coefficient can easily be measured by monitoring the radioactivity of diffused nuclide in glasses[1]. However, no such radioisotope exist for the lithium ion which is the main interest of the present work. In principle, diffusion coefficient of lithium can be measured by an ion-exchange technique and monitoring the fraction of seeded ^{6}Li by MAS spectroscopy or ion micro analysis, but the experiment is very difficult and the experimental uncertainty is very large. Moreover, the lithium-conductors are usually hygroscopic and their surfaces are easily damaged on exposure to air.

Pulsed-field gradient spin-echo NMR is an excellent method to measure the diffusion coefficient[2,3,4]. Figure 5-1 shows a basic time-chart of the pulsed-field gradient spin-echo method proposed by Stejeskal and Tanner[2]. Two identical static magnetic field gradient are applied to the sample in the series of well-known spin-echo measurement. The principle of the measurement is very simple: After the first $\pi/2$ rf pulse, a magnetic field gradient zH_g, where z is the position of nuclei along the static field, is applied to the sample, each nucleus experiences an different magnetic field, $Ho+zH$, depending on z. The inhomogeneous field causes the dephasing of the nuclear spin signal, and results in the

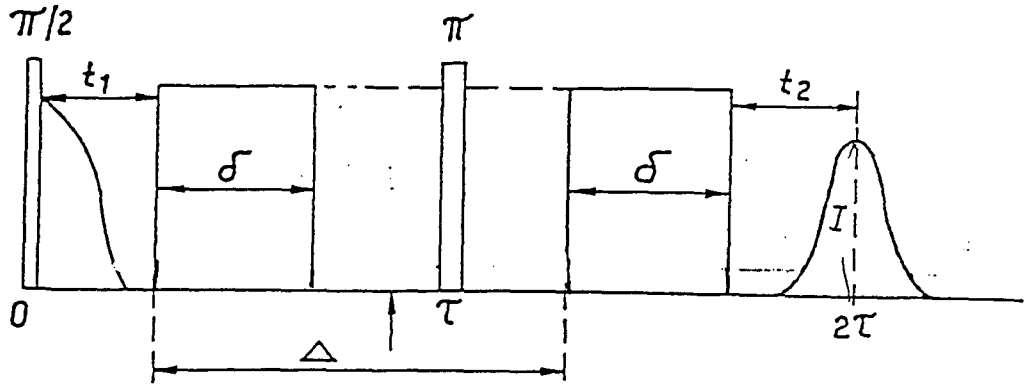

Fig. 5-1 A time chart of the typical pulsed-field gradient spin echo sequence.

decay of the signal. Next, the π rf-pulse is applied to invert the phase of the signal. Then, the field gradient with the same strength as the first one is applied. In the absence of rapid ionic motion, the effect of first gradient pulse is canceled by the second one, and the echo amplitude is the same as that in the absence of field gradient. When there exits a transitional motion of nucleus in the time interval between two field gradient pulses, the moved nucleus experience the 2nd field gradient the strength of which is different from that of the 1st field gradient. In this case the canceling by the second pulse is imperfect, causing the dephasing of the signal, and as a result the echo-amplitude is decreased. Based on the diffusion equation, Stjeskal et al. calculated the amount of attenuation of the amplitude of echo signal to be

$$I\max(G)/I\max(0)=\exp[-(\gamma G\delta)^2(\Delta-\delta/3)D], \qquad (5.1)$$

where D is the diffusion coefficient, γ the gyromagnetic ratio of nucleus and G the gradient intensity. Hence, diffusion coefficient can be determined by measuring the echo amplitude as a function of Δ or δ.

Liquid state PFG are now commercially available and one can measure the diffusion coefficient in liquids or solutions without any difficulty. However, it is not commonly used in solid state because of the number of limitation on the experiment. Diffusion coefficients are very small in solids. Even in the case of a typical fast ionic conductor, the ionic diffusion coefficient is usually smaller than $10^{-13}m^2/s$ at room temperatures. Moreover, T_2 is very short, typically 1-2ms. It imposes the upper limit for δ, In the case of liquids the strength of the field gradient of 0.1T/m is sufficient to measure the D. In solid state it should be larger by more than one order larger with good rectangular shape and with good reproducibility. Therefore, the number of the diffusion measurements hitherto done on solids is very few. Several research groups report the diffusion coefficient in solids by PFG by overcoming these problems[5,6,7]

In this chapter, the diffusion coefficient was measured in the present glasses, by an instrument recently developed by Ohishi and Miyajima of the Institute for molecular science. The result will be discussed in relation to the result obtained in the previous chapter.

5-2 Experimental

The details of the instrument is shown in 7. The field gradient coil used is produced by a quadrupolar coil. Coil constant was $0.284T/m^{-1}A^{-1}$. The current supplied is 15.1A and so

G=4.28T/m. The current driver for the coil is equipped with a feed-back circuit to ensure the stable current. Since a slight mismatch of two field-gradient pulses happened, the length of the second pulse was manually adjusted to establish the optimum condition for the measurement. It was adjusted polydimethyl siloxane the diffusion of which is very slow shows the maximum echo amplitude.

The length of $\pi/2$ degrees pulse was 8μs in the spin-echo experimet as shown in Fig.5-1. ^{7}Li NMR spin echo signals were measured at 20MHz. D of lithium ions was measure by changing the value of δ with constant Δ.

5-3 Results and Discussion

The diffusion coefficient of lithium ion in inorganic glassy material in the present work could not be measure at room temperature even under the optimum condition of the apparatus because of small ionic mobility.

For Li_2S-B_2S_3 system, Δ was fixed to 4ms taking account of the fact that T_2 was about 1ms. The attenuation of the echo signal was not observed in $60Li_2S$-$40B_2S_3$ and $65Li_2S$-$35B_2S_3$ because of very short T_2 as well as very small diffusion coefficients in these materials. The echo in $70Li_2S$-$30B_2S_3$ attenuated by applying the PFG only at high temperature at 180°C, which is near T_g. For $6Li_2S$-Ga_2S_3-GeS_2 glasses, T_2 was larger than that in Li_2S-B_2S_3 system allowing to increase Δ up to 12ms. In this case, attenuation was observed at 180°C.

Figure 5-2 shows an example of attenuation of echo amplitude with the duration δ of the gradient pulses.

From eq.(5.1), the logarithmic plot of I versus $\delta^2(\Delta\text{-}1/3\delta)$ gives a straight line with the slope of γ^2G^2D. The plot for $70Li_2S$-$30B_2S_3$ and $6Li_2S$-Ga_2S_3-$6GeS_2$ are shown in 5-3 and 5-4, respectively. Table 5-1 lists the diffusion coefficients of these samples. It was found that in Li_2S-B_2S_3 glass the diffusion coefficient tends to increase on heating.

The diffusion coefficient is related to hopping rate τ^{-1} of ions as follows[8]. Location of ion, R, after n times jumps is written as,

$$\vec{R} = \vec{r}_1 + \vec{r}_2 + \ldots\ldots\ldots\ldots + \vec{r}_n \qquad (5.2)$$

The mean square root of R can be given by,

$70Li_2S\text{-}30B_2S_3$

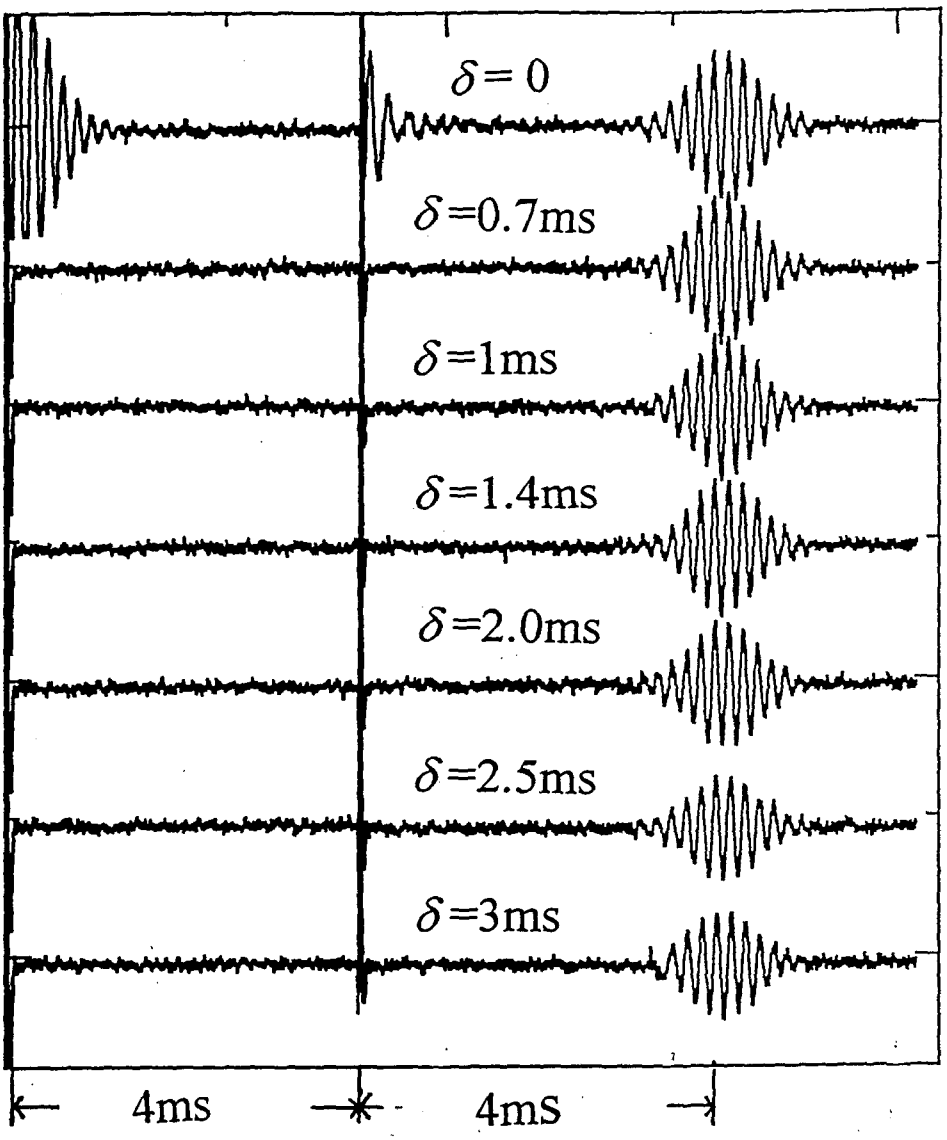

Fig. 5-2 The variation of spin-echo signals with δ for xLi$_2$S-B$_2$S$_3$ at 180°C.

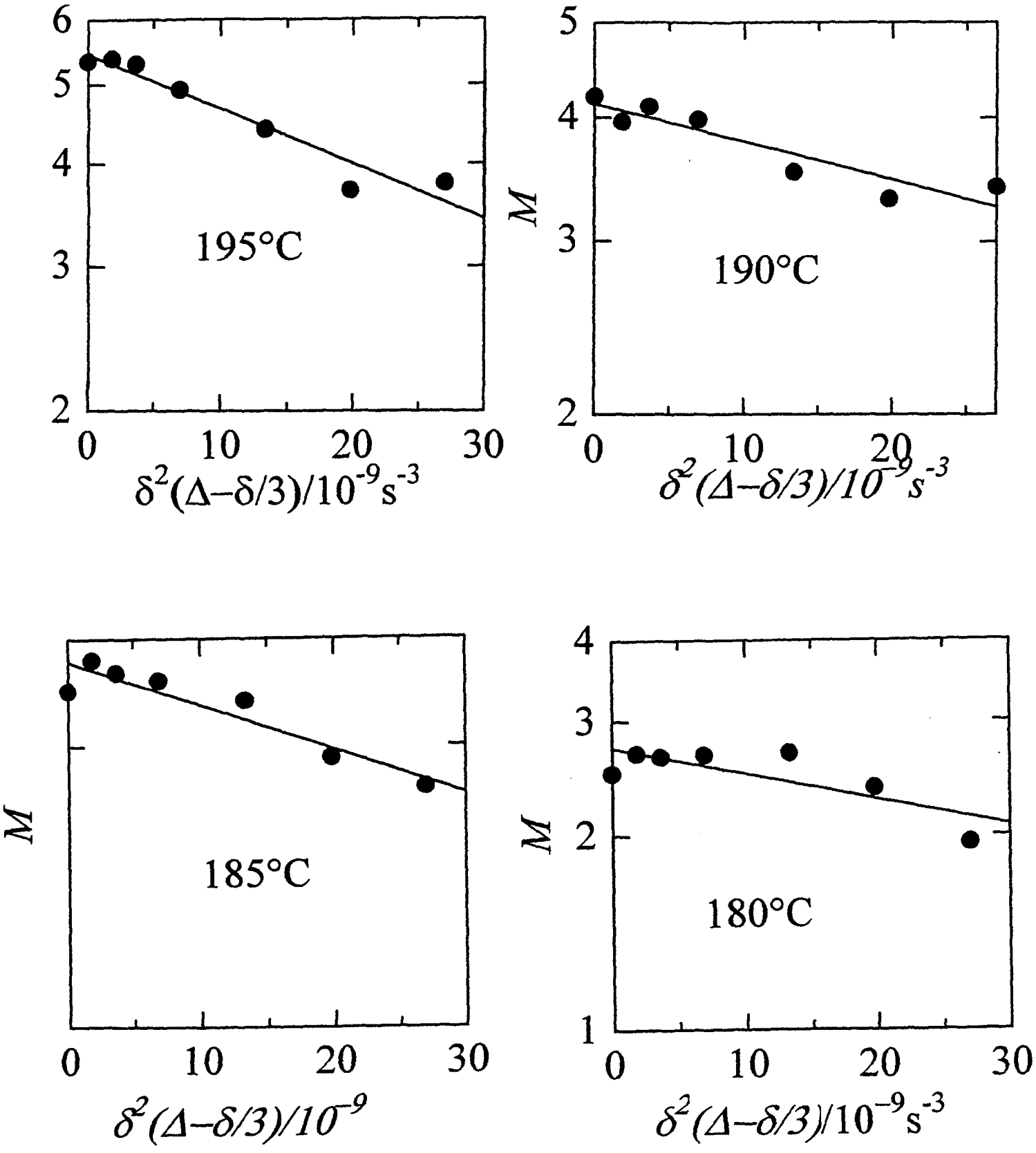

Fig. 5-3 Echo amplitude of Li_2S-B_2S_3 plotted against $\delta^2(\Delta-\delta/3)$. Temperature is shown in the figure.

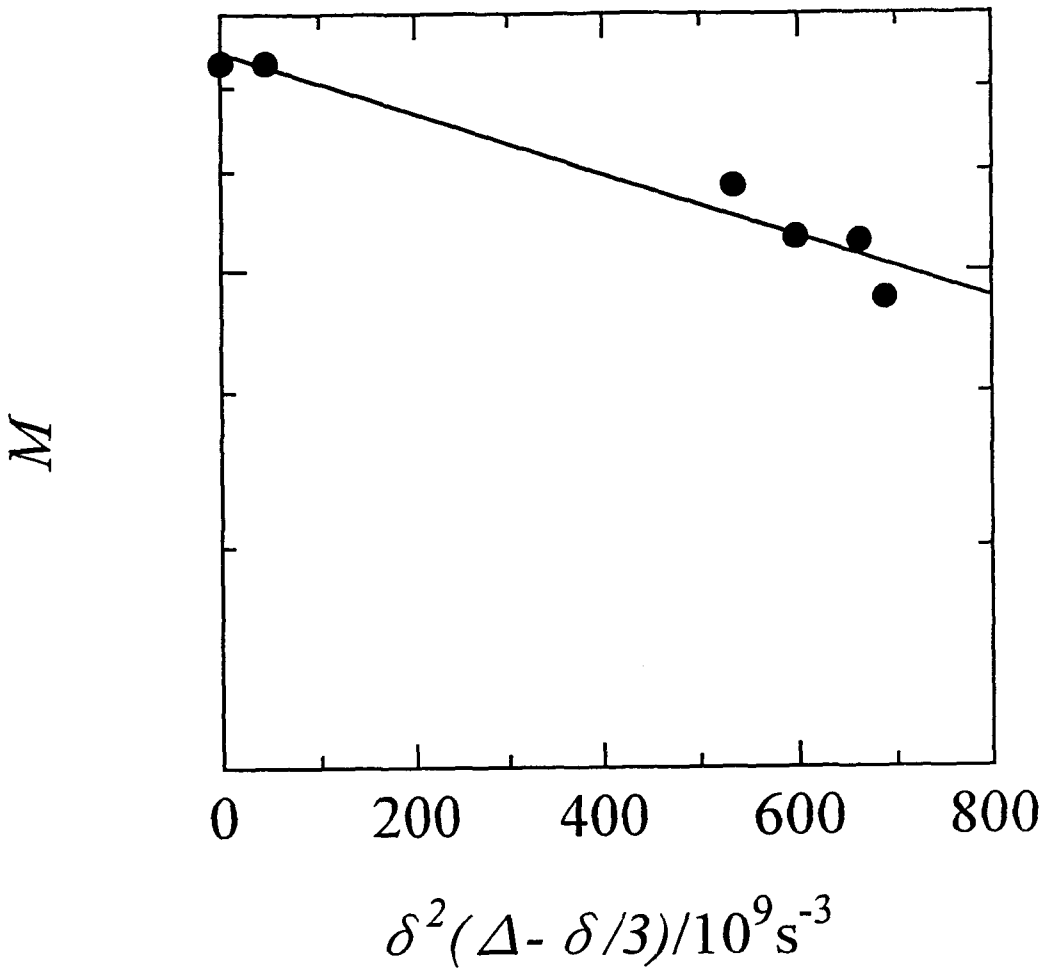

Fig. 5-4 Echo amplitude of $6Li_2S$-Ga_2S_3-$6GeS_2$. plotted against $\delta^2(\Delta-\delta/3)$

Table 5-1 Diffusion coefficient of lithium.

Sample		D/m^{2}s^{-1}
$6Li_2S$-Ga_2S_3-$6GeS_2$	(180°C)	2.8×10^{-12}
$70Li_2S$-$30B_2S_3$	(180°C)	5.5×10^{-11}
	(185°C)	3.7×10^{-11}
	(190°C)	5.0×10^{-11}
	(195°C)	8.2×10^{-11}

$$\langle R^2 \rangle = \sum_{i=1}^{n} < r_i^2 > + 2\sum_{i=1}^{n} \sum_{j=i+1}^{n} < r_i r_j \cos\theta_{ij} >, \qquad (5.3)$$

where θ_{ij} denotes the angle between the direction of i-th jump and that of (i+j)th jump. Assuming the jumping distance of each jump is constant, eq.(5.3) can be written as follows.

$$R^2 = nr^2 + 2r^2 < \cos\theta_{ij} > \; = nr^2 \left\{ \left\{ 1 + \frac{2}{n} < \cos\theta_{ij} > \right\} \right. \qquad (5.4)$$

In the case of random hopping, $<\cos\theta_{ij}>=0$. Hence,

$$R^2 = nr^2 = \frac{t}{\tau} r^2 = \nu r^2 t \qquad (5.5)$$

where $t = n\tau$ and $\nu = 1/\tau$. τ denotes the mean life time of the ions and corresponds to the correlation's of the ionic motion introduced in the previous chapters.

For three dimensional model, it is known that

$$Dt = \frac{1}{6} R^2 \qquad (5.6)$$

From eq. (5.5) and (5.6),

$$D = \frac{1}{6} \nu r^2 \qquad (5.7)$$

When the jump is not random in direction, $<\cos\theta_{ij}>$ remains finite in eq. (5.4). In this case, D is reduced by factor f, so that

$$D = \frac{1}{6} \nu r^2 f \quad . \qquad (5.8)$$

The parameter f depends on the crystal structure.

The jumping distance r is of central interest here because it is directly related with the motions of the lithium ions in our glasses. However, the jumping distance r cannot be defined in a glassy ionic conductor since the lithium ions are considered to be distributed over numerous sites in an amorphous medium. Thus, we estimated r using eq. (5.7) for $70Li_2S$-$30B_2S_3$ and $6Li_2S$-Ga_2S_3-$6GeS_2$ at 180°C to be 0.18nm and 0.17nm, respectively. If we take the jump distance as the sum of atomic radii of lithium and sulfur, it will amount to 0.51nm. The jump distance deduced above are too small compared with the expected one, admitting the experimental uncertainty and possible change in interionic distance for about 0.1-0.2nm If we take f as 0.3, we obtain that r = 0.31nm, which seems to be persistent. Small f means that θ_{ij} is larger than $\pi/2$. This means considerable number of ions hop backward.

The diffusion coefficient of lithium in $70Li_2S$-$30B_2S_3$ is higher by one order than that in $6Li_2S$-Ga_2S_3-$6GeS_2$. This difference in D is comparable to the difference in the

conductivity in these two materials. Hence, it is suggested that the difference in conductivity in high super-ionic conductors may be attributed to the difference in the mobility of ions.

At present the lower limit of measurable diffusion coefficient is about $10^{-12}m^2/s$ and so the diffusion measurements were successful only for relatively "fast" ionic conductor much as sulfide glasses. To examine the mobility of ions in glassy materials with very low conductivity, an apparatus which provide with more intense field gradient pulse and also a probe which can operate at much higher temperature. By doubling the intensity of field gradient, it is possible to measure the diffusion coefficient less than one order. If the temperature is increased up to 400 °C the ionic mobility may be increased by more than 1 or 2 orders. Therefore, it is necessary to develop an apparatus with much higher performance than that applied in the present studies to shed light on the closed mechanism of conduction from the molecular point of view.

References

[1] R. Terai and R. Hayami, J. Non-cryst. solids, 18, 217 (1975).

[2] E. O. Stejeskal and J. E. Tanner, J. Chem. Phys., 42, 288 (1965).

[3] J. Kärger, H. Pfeifer, and W. Heink, Adv. Magn. Reson., 12, 1 (1988)

[4] P. Stilbs, Progress in NMR Spectroscopy., 19, 1 (1987).

[5] W. Heik, J. Kärger, G. Seifert, G. Gliescher, and J. Raushfuβ, J. Magn. Reson., Ser. A., 114, 101 (1995).

[6] S. C. Chen, J. C. Traczon, W. P. Halperin and J. O. Brittan, J. Phys. Chem. Solids., 8, 895 (1985).

[7] O. Oishi and S. Miyajima, J. Magn. Reson. Ser. A. to be publilshed.

[8] T. Kudo and K. Fueki, Chapter 4 in Solid State Inonics, kondansha (1990).

Chapter 6 Structural change with doping salt

6-1 Introduction

As already stated in Chapter 1, doping of lithium salt to glassy materials brings about drastic increase in the conductivity. It is a natural question to ask how doping salt changes the structure of glasses. In the case of alkali-borate glasses it is well accepted that short-range structure do not change with the doping of the lithium halides, *i.e.*, and the dopants are merely dissolved in the glass matrix[1,2]. In the case of oxoanion such as Li_2SO_4, there is two contradicting opinions as to the structural change with the addition of the salt. Raman studies show that there may be a slight change in the short-range structure through the relative intensities of several bands originating from different borate structural unit remains unchanged with the addition of Li_2SO_4[3,4]. On the other hand, Mustarelli *et al.* [5] measured ^{11}B NMR spectra and found that the proportion of 4-coordinate boron, BO_4, to 3 coordinate boron, BO_3, (N_4) increases drastically with the addition of Li_2SO_4. Any structural model cannot explain these contradicting results.

^{11}B NMR has frequently been used as a method to determine N_4. The determination of N_4 in glasses was established by Bray in 1960's when the continuous-wave methods were only available for the measurement of the spectra [6]. Recent spectrometers are equipped by the pulse-Fourier transform method to measure NMR spectra and special cares have to be take for the quantitative analysis as in pointed out in the following experimental section.

In this chapter, the existence of any change of short-range structure of borate glasses with the doping of salts was re-examined by ^{11}B NMR spectra. ^{7}Li NMR spectra is also discussed in relation to mid-range structure.

6-2 Experimental

NMR measurements were carried out by a Chemagnetics CMX 200 spectrometer. ^{11}B NMR was measured at 64 MHz using the single pulse method. The nucleus possesses as a quadrupole moment ($I>1/2$) is distorted because of the nutation effect, if the pulse length is long. The duration of the pulse should therefore be set to less than $\pi/8$ pulse. Here, the pulse length used is 0.5μs ($\pi/2$ pulse is 4.5μs). The spectra were obtained by Fourier transforming the free-induction decay signals after the single-pulse.

6-3 Results and Discussion

Fig. 6-1 displays ^{11}B NMR spectra of $(100-x)(0.5Li_2O\text{-}0.5B_2O3)\text{-}xLi_2SO_4$ system. Only the central transition ($-1/2 \leftrightarrow 1/2$) was observed for each sample. Two lines, sharp one and broad one, were observed. Sharp line is assigned to the 4-coordinated boron with the tetrahedral environment, and the broad line is assigned to the 3-coordinate boron with the planer triangle environment. The spectra for all the glasses are identical, implying that the doping of Li_2SO_4 does not bring about any significant change in N_4. This result is consistent with the result of previous Raman spectra but conflict with the results of previous ^{11}B NMR experiment. Mustralli *et al.* used long pulse in the spectrum measurement which certainly distorts the spectrum, resulting in the wrong N_4.

Therefore, the present ^{11}B studies shows that short-range structure is not altered with the addition of Li_2SO_4 and Li_2SO_4 is dissolved in the borate structure. The change with doping salt should be occur in intermidiate structure as suggested by several authors[7].

Interesting behavior of ^7Li NMR spectrum was found at low temperatures. The change of ^7Li NMR spectrum at low temperature with x is shown in figure 6-2 . It is interesting to note that FWHM is not linearly dependent on x (Figure 6-3). Probably this shows that intermediate structure, originated from the arrangement of structural unit, do not continuously change with x. This suggests that ^7Li NMR spectrum is very promising in studying intermediate structure in glasses. To propose a structural model for intermediate structure, the contribution to line width from Li-Li and Li-B should be separated. The measurement of ^7Li in ^{10}B enriched sample would give a better information.

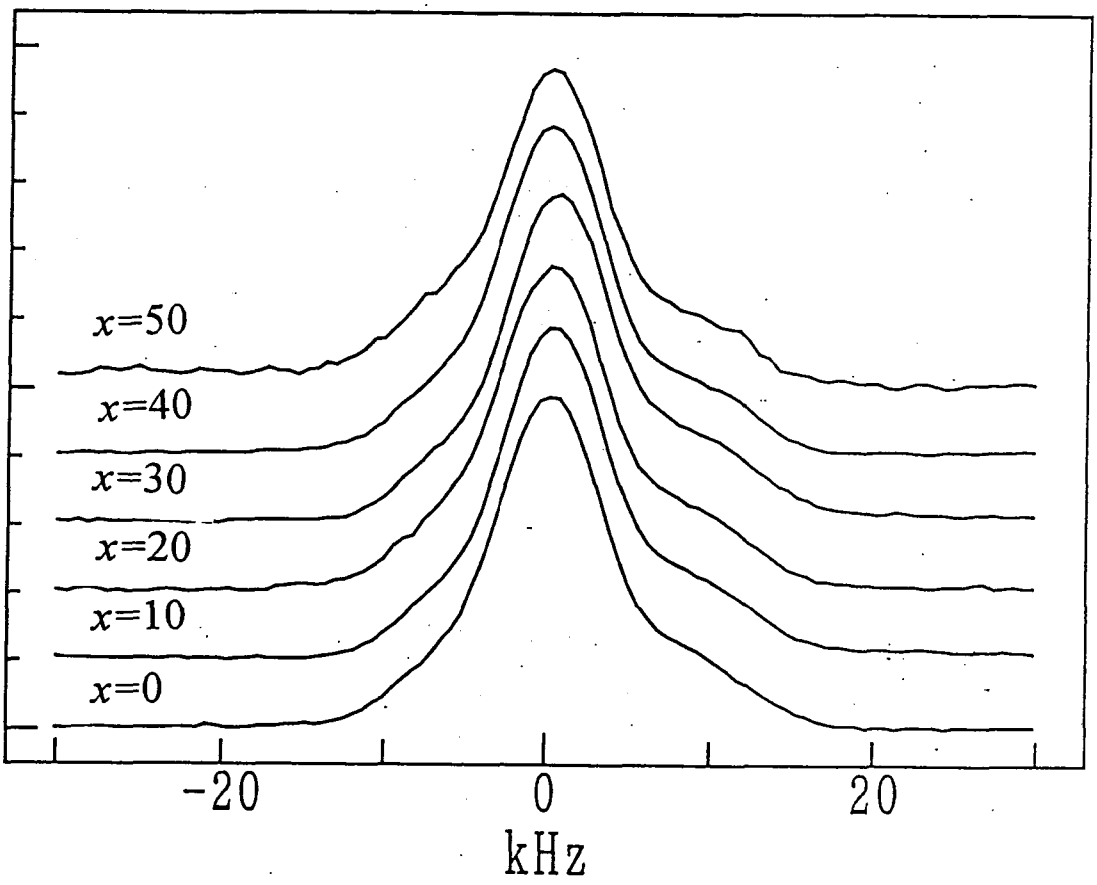

Figure 6-1 ^{11}B NMR spectra of $(100-x)(0.5Li_2O-0.5B_2O_3)-xLi_2SO_4$.

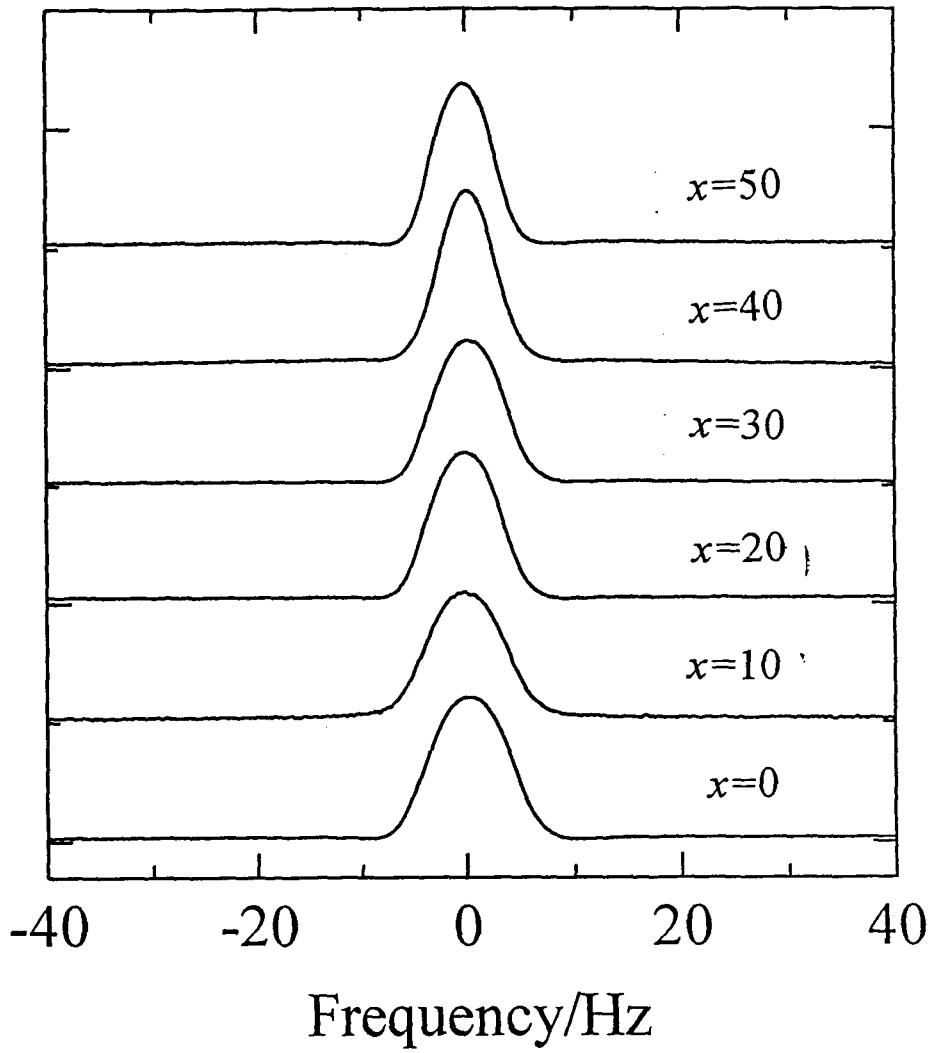

Figure 6-2 ^{7}Li NMR spectra of $(100-x)(0.5Li_2O-0.5B_2O_3)-xLi_2SO_4$ at -120°C.

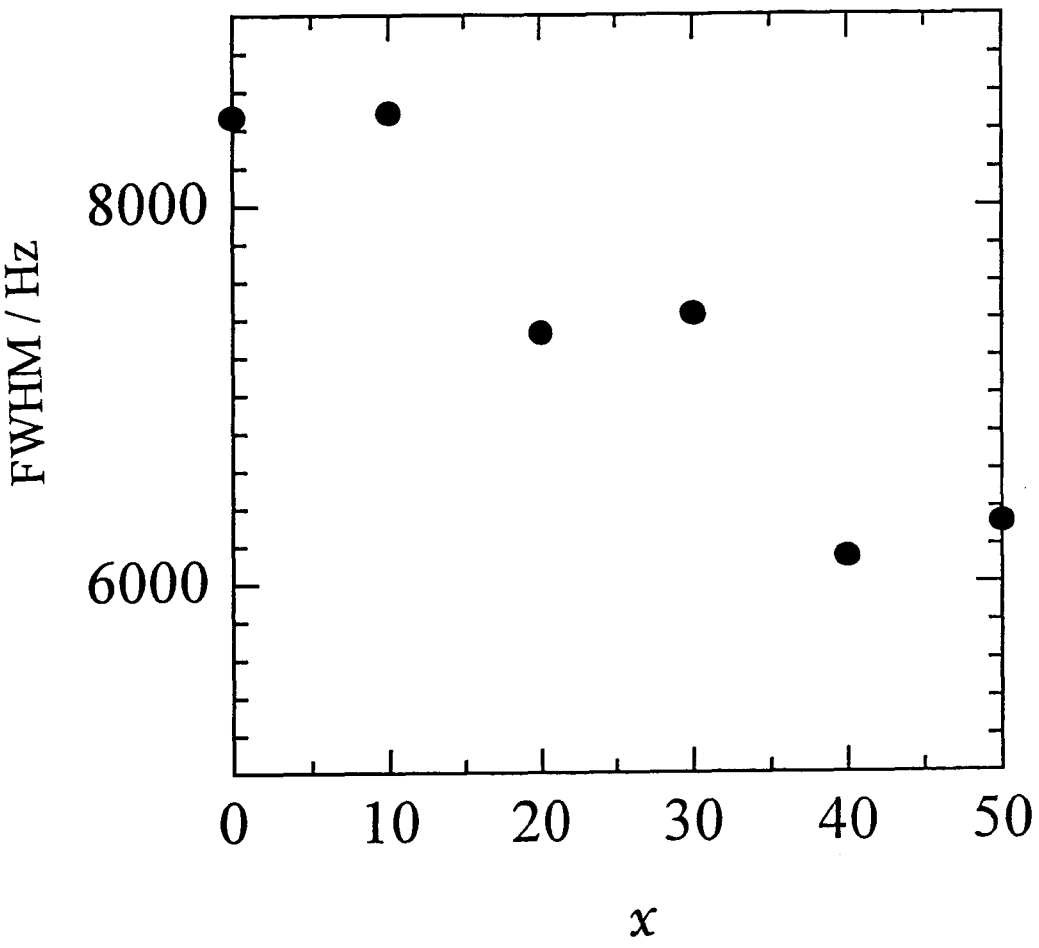

Figure 6-3 ^{7}Li FWHM in the rigid lattice in (100-x)(0.5Li_2O-0.5B_2O_3)-$x$$Li_2SO_4$.

References

[1] A. Levasseur, M. Kbala, P. Hagenmuller, G.Couturier and Y. Danto, Solid State Ion, 9-10, 1439 (1983).

[2] A. E. Geissberger, F. Bucholtz and P. J. Bray, J. Non-cryst solids 49, 117 (1982).

[3] M. Yamashita and R.Terai, Glastech. Ber., 63, 13 (1990).

[4] A. Levasseur, M. Kbala, and J. C. Brethous, Solid State Commun, 32, 839 (1979).

[5] P. Mustarelli, S. Scotti, M. Villa and P. R. Gandhi, Solid State Ionics, 39, 217 (1990).

[6] P. J. Bray and J. G. O'Keefe, Phys. Chem. Glasses, 4, 37 (1963).

[7] L. Borjesson and L. M. Torell, Solid State Ionics., 25, 85 (1987).

Chapter 7 Discussion and summary

In the present study, low frequency motion of lithium in some glassy-ionic conductors, *i.e*, Li_2O-B_2O_3-Li_2SO_4, Li_2S-B_2S_3, Li_2S-Ga_2S_3-GeS_2 systems, were investigated by ^7Li NMR.

Detailed procedures of preparation were shown in Chapter 2. Oxide glasses were prepared by melt-quench method. Sulfide glasses were melted and quenched in a sealed quartz tube under inert atmospheres. The glass transition temperatures of these glasses were determined.

In Chapter 3, electrical properties of these glasses were measured. DC conductivities were measured for several glasses. Modulus of some glasses were also measured. The data were analyzed on the bases of the Kohlraush-Williams-Watt function by least-squares' method. From the temperature dependence of the modulus activation parameters were determined to be τ_0=2.52x10^{-15}s, E_a=52kJ/mol and β=0.54 for 50Li_2O-50B_2O_3.

In Chapter 4, the methods of the Bloembergen-Pound-Purcell and Hendrickson-Bray of the analysis of motional-narrowing line width were reviewed and shortcomings of these methods were pointed out. A new method to calculate the ^7Li linewidth incorporating the KWW function was proposed. Theoretical relaxation function of magnetization, *G(t)*, incorporating KWW function was calculated by the numerical computation method, and digitally Fourier transformed to yield the spectrum; it enables for us to calculate the LW. This new method makes it possible to evaluate activation parameters E_a and τ_0 by measuring temperature dependence of line width. Assuming E_a=E_σ, τ_0 for each glass was estimated for all glasses from the experimental MNLW. For 50Li_2O-50B_2O_3, it was found that the MNLW cannot be reproduced with the same τ_0, E_a and β determined by the conductivity measurements. The data can only be reproduced by setting τ_{0NMR} and β to be 6.0x10^{-14} s and 0.33, respectively. This degree of discrepancy in three parameters between the NMR measurement and conductivity measurement is similar to that for super-ionic glasses.

The probable interpretation for the discrepancy is that the number of mobile ion which causes the long range ionic transport is much less than the whole number of ions in

motion. As was discussed in Chapter 4, some works state that only a small number of mobile ions can find some preferred path for the long-distance transport. These favorite paths are possibly originated from inhomogenity of the system in the molecular level, or intermediate structure. The author believes that this explanation is natural, considering that alkali rich phases can easily be phase-separated from alkali-containing glasses. It is interesting to investigate how τ_{NMR}/τ_{cond} changes with the alkali concentration. Another interesting topic is so-called the mixed-alkali effect which is one of the long-standing problems in glass science. There is a trend to consider that mixed-alkali effect is caused by the formation of different species of alkali ion pairs, resulting in the disappearance of preferred long-range migration path. The quantitative examination of τ_{NMR}/τ_{cond} will shed a new light on this problems. If the still unknown "intermediate structure" is related to such a phenomena the investigation of static ^{7}Li NMR is also important as well as MNLW to study such intermediate structure from the molecular point of view.

As to the parameter β, its physical meaning is not distinct but it is considered to be a measure of the extent of distribution of the correlation time τ_c for the ionic motion: That the values of β is small means that τ_c is distributed over wide range. Very small value of β_{NMR} implies that there is a lot of short-range migration of lithium ions with different τ_c, in significantly different environment. The fact that β_σ is larger than β_{NMR} suggests that among such stochastic random migration of the ions only a small fraction can find their path over long-distance and contribute to the electric conduction, supporting the above statement that the long-range ionic transport takes place *via.* "intermediate structure" of glass in which most of ions feels similar environment.

Alkali oxide glasses show also similar discrepancy in τ_{NMR}/τ_{cond} as that in alkali sulfide glasses though the typical conductivity differs more than 2 orders. In essence, ionic conduction is represented by the product of transport number n and the mobility of ions μ. Hence, the direct measurements of the diffusion coefficients were carried out by pulsed-field gradient spin echo method to derive the quantitative information on μ. In chapter 5 the diffusion coefficients in some glassy inorganic conductors were first measured by the PGSE method. By applying the very large magnetic field gradients, it was successful to measure the diffusion coefficients of Li ions in $70Li_2S$-$30B_2S_3$ and $6Li_2S$-Ga_2S_3-$6GeS_2$; The diffusion coefficients thus obtained were $5.5x10^{-11}m^2s^{-1}$ and

$2.8x10^{-12}m^2s^{-1}$, respectively, at 180°C. The difference between the diffusion coefficient is comparable with that in the conductivities, suggesting that the difference in these conductivity between these glasses is originated from ionic mobility. The diffusion coefficient was also discussed in relation to τ_c obtained in chapter 4: it was suggested that the considerable large fraction of ions hop backward and so only a small fraction of ions can contribute to the long-distance ion transport..

Diffusion coefficient of ions in these glasses is expected to be 10 to 100 times lower than those in the sulfide glasses from the view point of the conductivity data. It is, however, very important to measure the diffusion coefficient using very high field gradient to establish microscopic mechanism of the ionic conduction in various kinds of glasses.

In summary, this work proposed the methods to estimate n and μ independently in inorganic glasses by ^{7}Li NMR. It was indicated that the ^{7}Li NMR experiments over wide temperature range is promising in the study of the ionic conduction mechanism and probably intermediate structure of the glass.

It has long been accepted that glasses do not have any long-range order. In the last few decades, various spectroscopic methods, *i.e.*, XAFS, X-ray, NMR, Raman, IR, XPS and so on revealed that the short range order, related to the nature of chemical bonding and for small structural units, can essentially be described by those which are recognized in "highly ordered " structure, *i.e.*, crystals. These methods have clarified the relation between the physical properties and short-range order. However, there are number of physical properties that cannot be explained only by the short-range order in glasses. One such example is well-known "boron anomalies" in borate glasses which is still controversial in glass science. Such a phenomenon should be attributed to the "intermediate structure". "What is the intermediate structure in glass? "or "how do these structural units connect each other and what is their arrangement in nm scale?". These are the essential problem which most glass scientists now face.

It often happens that the intermediate structure, which denotes an inhomogenity in nm scale, develops to form a microphases over some μm region through ionic conduction with the heat-treatment of the glass. A phenomenon which is known as the phase separation in glass has also been an important subject in glass science and

technology. The shape and size of microphases complexly varies with heat-treatment temperature and time and with the concentration of doping salt. The nature of the phase separation is not well understood from the molecular point of view, especially on the process of structural evolution. It is often stated that two factors play key roles in the evolution of microstructure - the inhomogenities in nm range exist originally in glasses and the other ionic conduction which drives the development of microstructure-.

This work proposed a simple but effective approach to the basic problems in glass science, *i.e*, "ionic conduction and intermediate structure" through the studies of ^{7}Li NMR. It is also of significance from the standpoint of glass industry since it will certainly provide with a key to control the intermediate structure and the evolution of microphases.

Appendix A

```
10 'PROGRAM MODULUS
20 '    Modulus fitting by using stretched-exponential relaxation
30 '    programmed by T. Akai (Osaka National Research Institute)
40 '    If there is any problem, please contact akai@onri.go.jp
50 '    data--- 100 point modulus from frequency 0 to 107 Hz
60 '
70 N=14 'No. of variable
71 M=101 'no. of function (data number used for stretch fitting)
72 N1=N+1:N2=N+2:M1=M+N+1:M2=M1+1:M3=M2+1
80 DIM X(N),F(M),B(M3,N2),AAA(M),BBB(M)
90 DIM MR(70),MI(70),TAUI(40),OMEGA(70),FREQ(70)
100 DIM FACTOR(20),W(100),ZR(100),ZI(100),MRE(100),MIE(100)
110 GOSUB *READDATA
120 '
130 '
140 '*****Program for Modulus fit
150 INPUT "TAUC";TAUC
160 INPUT "beta";BETA
170 SCREEN 3,0,0,1:CLS 3
180 GOSUB *STRETCH
190 GOSUB *MODULUS
200 GOSUB *DISPLAY
210 PRINT "tauc,beta";TAUC,BETA
220 '
230 INPUT "CHANGE PARAMETER (Y/N)?";Q5$
240 IF Q5$="Y" THEN GOTO 140
250 '
260 PRINT "save data?(Y/N)";Q1$
270 IF Q1$="N" THEN GOTO 330
280 INPUT "datafilename?(drive:fn)";FFF2$
290 '
300 FFF3$=FFF2$+".DAT"
310 FFF4$=FFF2$+".PRM"
320 OPEN FFF3$ FOR OUTPUT AS #1
```

```
330      FOR I=1 TO 70
340        WRITE #1, FREQ(I),MIEMAX/MIMAX*MR(I),MIEMAX/MIMAX*MI(I)
350      NEXT I
360 CLOSE #1
370 OPEN FFF4$ FOR OUTPUT AS #1
380      FOR I=1 TO 14
390         WRITE #1, I,TAUI(I),X(I)
400      NEXT I
410 CLOSE #1
420 '
430 '
440 '
450 '
460 END
470 '
480 '
490 '
500 '
510 '
520 '
530 '
540 '
550 '-------    subroutin list ----------------
560 *READDATA
570    INPUT "Modulus data file name";FFF1$
580    OPEN FFF1$ FOR INPUT AS #1
590       FOR I=1 TO 100
600          INPUT #1, W(I),ZR(I),ZI(I),MRE(I),MIE(I)
610       NEXT I
620    CLOSE #1
630    MIEMAX=MIE(0)
640 FOR II=1 TO 100
650    IF MIEMAX<MIE(II) THEN MIEMAX=MIE(II)
660 NEXT II
670 RETURN
680 '
```

```
690 '
700 *MODULUS
710 '
720 '-----Modulus CALCULATION BY USING FITTED X(J)--------
730 SCREEN 3,0,0,1:CLS 3
740      FOR I=1 TO 70
750          FREQ(I)=10^(.1*I)
760          OMEGA(I)=2*3.14*FREQ(I)
770         MR(I)=0: MI(I)=0
780         FOR J=1 TO N
790          PRODUCT=OMEGA(I)*TAUI(J)
800              MR(I)=MR(I)+X(J)*PRODUCT^2/(1+PRODUCT^2)
810              MI(I)=MI(I)+X(J)*PRODUCT/(1+PRODUCT^2)
820         NEXT J
830    NEXT I
840 RETURN :STOP
850 '
860 '
870 '
880 *DISPLAY
890 '------DATA DISPLAY. THE SCALE IS DETERMINED BY THE MAX VALUE
900 'OF THEORETICAL AND EXEPRIMENTAL VALUE----------------
910 '
920      SCREEN 3,0,0,1:'CLS 3
930      MIMAX=MIMAX(0):MIMIN=MIMIN(0)
940        FOR II=1 TO 69
950            IF MIMAX<MI(II) THEN MIMAX=MI(II)
960        NEXT II
970 '
980        LINE(10,10)-(10,200):LINE(10,10)-(300,10)
990        LINE(300,10)-(300,200):LINE(10,200)-(300,200)
1000         WINDOW(0,-1)-(7,0)
1010         VIEW(10,10)-(300,200)
1020 '
1030 FOR J=1 TO 69
1040            LINE      (LOG(FREQ(J))/LOG(10),-MR(J))-(LOG(FREQ(J+1))/LOG(10),-
```

```
MR(J+1)),2
1050   LINE (LOG(FREQ(J))/LOG(10),-MI(J))-(LOG(FREQ(J+1))/LOG(10),-MI(J+1)),5
1060 NEXT J
1070 '
1080   FOR J=1 TO 100:PRINT MIMAX,MIEMAX
1090            CIRCLE (LOG(W(J))/LOG(10),-MIMAX/MIEMAX*MRE(J)),.01,2
1100            CIRCLE (LOG(W(J))/LOG(10),-MIMAX/MIEMAX*MIE(J)),.01,5
1110            PRINT MIE(J)
1120        NEXT J
1130 RETURN
1140 '
1150 '
1160 '
1170 *STRETCH
1180 '----------Exapansion of stretche exponential using non-linear
1190 'least square method.X(I)is the weighed factor.'TAUI used for
1200 ' expansion is shown in the part ¥¥¥¥function. INITIAL CONDITION
1210 ' is in ¥¥¥¥¥initial
1220 '
1230 N=14' "no of variables=";N
1240 M=101 'NT "no of functions";M
1250 IMAX=400*M*N
1270 PRINT "max no of function evaluation=";IMAX
1280 INPUT "EPS initial(=0.1)";EPS
1290 H=.000001
1300 PRINT "step size in numerical differentiation"
1310 PRINT "h=";H
1320 PRINT "convergence criterion"
1330 PRINT "epsilon=";EPS
1340 PRINT
1350 NIT=0:RINCR=1.5:RDECR=.5
1360 NF=0
1370 '
1380 '
1390 '¥¥¥¥¥¥¥¥ set initial i
1400 'NEXT I
```

```
1410 FOR I=1 TO 14
1420     X(I)=.001
1430 NEXT
1440     X(8)=.6
1450     X(7)=.3
1460     X(9)=.1
1470 NIT=NIT+1
1480 GOSUB 3740
1490 NF=NF+1
1500 S=0
1510 FOR I=1 TO M
1520 S=S+F(I)^2
1530 NEXT I
1540 SUMSQ=S
1550 FOR I=1 TO M
1560 'PRINT "f(";I;")=";F(I):B(I,N1)=F(I)
1570 NEXT I
1580 PRINT:PRINT "sumsq=";SUMSQ
1590 GOSUB 2530
1600 IF NIT>1 THEN 1650
1610 S=0:FOR I=1 TO M:FOR J=1 TO N
1620 S=S+B(I,J)^2
1630 NEXT J,I
1640 V=SQR(S/(N*M))
1650 IC=0
1660 FOR I=1 TO N:FOR J=1 TO N1
1670 B(M+I,J)=0:NEXT J
1680 B(M+I,I)=V:NEXT I
1690 GOSUB 3500
1700 GOSUB 2890
1710 GOSUB 3090
1720 P=ABS(X(1)):PP=ABS(B(1,N2))
1730 IF N=1 THEN 1780
1740 FOR I=2 TO N
1750 IF ABS(X(I))>P THEN P=ABS(X(I))
1760 IF ABS(B(I,N2))>PP THEN PP=ABS(B(I,N2))
```

```
1770 NEXT I
1780 IF P<1 THEN P=1
1790 IF PP < EPS*P THEN 2000
1800 IF SW=0 THEN 1860
1810 IC=IC+1
1820 GOSUB 3150
1830 V=RINCR*V
1840 IF V>1E+6 THEN 2510
1850 GOTO 1700
1860 JS=0
1870 IF PP<EPS*P*100 THEN JS=1
1880 FOR I=1 TO N
1890 X(I)=B(M3,I):NEXT I
1900 SUMSQ=SN
1910 PRINT "----------"
1920 PRINT "no of iterations=";NIT:PRINT
1930 FOR I=1 TO N:PRINT "x(";I;")=";X(I):NEXT I
1940 IF IC>0 THEN 1960
1950 V=V*RDECR
1960 IF NF>IMAX THEN 2520
1970 NIT=NIT+1
1980 FOR I=1 TO M:B(I,N1)=F(I):NEXT I
1990 GOTO 1580
2000 PRINT "----------"
2010 PRINT "optimal solution":PRINT
2020 IF SW=1 THEN SN=SUMSQ:GOTO 2060
2030 FOR I=1 TO N
2040 X(I)=B(M3,I)
2050 NEXT I
2060 FOR I=1 TO N
2070 PRINT "x(";I;")=";X(I)
2080 NEXT I
2090 PRINT
2100 FOR I=1 TO M
2110 'PRINT "f(";I;")=";F(I)
2120 NEXT I
```

```
2130 PRINT
2140 PRINT "sum of squares=";SN
2150 PRINT "no of iterations=";NIT
2160 PRINT "no of function evaluations=";NF
2170 SCREEN 3,0,0,1:'CLS 3
2180 WINDOW (0,-1)-(100,0)
2190 VIEW (10,10)-(200,200)
2200 LINE(0,-1)-(0,0):LINE(0,-1)-(100,-1)
2210 LINE(100,-1)-(100,0):LINE(100,0)-(0,0)
2220 FOR I=0 TO M-1
2230      CIRCLE (I,-AAA(I)),.5,2
2240 NEXT
2250 FOR I=0 TO M-2
2260      LINE (I,-BBB(I))-(I+1,-BBB(I+1))
2270 NEXT I
2280 '
2290 WINDOW(-4,-1)-(3,0)
2300 VIEW (200,10)-(410,200)
2310 LINE(-4,-1)-(-4,0):LINE(-4,-1)-(3,-1)
2320 LINE(-4,0)-(3,0):LINE(3,-1)-(3,0)
2330 FOR I=1 TO N-1
2340     LINE (-4+.5*I,-X(I))-(-4+.5*(I+1),-X(I+1))
2350 NEXT I
2360 CLS
2370 LOCATE 25,15:
2380 '
2390 TOTAL=0
2400 FOR I=1 TO N
2410     TOTAL=TOTAL+X(I)
2420 NEXT I
2430 PRINT "TOTAL"; TOTAL
2440 INPUT "Calculate modulus(M) and change ESH(E)";QQ1$
2450 IF QQ1$="E" THEN GOTO 1280
2460 RETURN 'end of the main subroutine *stretch
2470 '
2480 '---subroutine in *stretch
```

```
2490 '
2500 PRINT:PRINT "too small ep sr":STOP
2510 PRINT :PRINT "too big v":STOP
2520 PRINT :PRINT "no convergence within ";NF;" function call":STOP
2530 FOR I=1 TO M
2540 B(I,N1)=F(I)
2550 NEXT I
2560 IF JS=1 THEN 2700
2570 FOR I=1 TO M
2580 B(I,N2)=F(I)
2590 NEXT I
2600 FOR J=1 TO N
2610 X(J)=X(J)+H
2620 GOSUB 3740
2630 NF=NF+1
2640 FOR I=1 TO M
2650 B(I,J)=(F(I)-B(I,N1))/H
2660 NEXT I
2670 X(J)=X(J)-H
2680 NEXT J
2690 RETURN
2700 FOR J=1 TO N
2710 X(J)=X(J)-H
2720 GOSUB 3740
2730 NF=NF+1
2740 FOR I=1 TO M
2750 B(I,N+2)=F(I)
2760 NEXT I
2770 X(J)=X(J)+2*H
2780 GOSUB 3740
2790 NF=NF+1
2800 FOR I=1 TO M
2810 B(I,J)=(F(I)-B(I,N2))/(2*H)
2820 NEXT I
2830 X(J)=X(J)-H
2840 NEXT J
```

```
2850 FOR I=1 TO M
2860 F(I)=B(I,N1)
2870 NEXT I
2880 RETURN
2890 B(N,N2)=B(N,N1)/B(M1,N)
2900 IF N=1 THEN 2980
2910 FOR K=N-1 TO 1 STEP -1
2920 B(K,N2)=B(K,N1)
2930 FOR J=K+1 TO N
2940 B(K,N2)=B(K,N2)-B(K,J)*B(J,N2)
2950 NEXT J
2960 B(K,N2)=B(K,N2)/B(M1,K)
2970 NEXT K
2980 FOR I=1 TO N
2990 B(M3,I)=X(I)-B(I,N2)
3000 NEXT I
3010 FOR I=1 TO N
3020 B(M2,I)=X(I):X(I)=B(M3,I)
3030 NEXT I
3040 GOSUB 3740
3050 NF=NF+1
3060 FOR I=1 TO N:X(I)=B(M2,I)
3070 NEXT I
3080 RETURN
3090 SN=0
3100 FOR I=1 TO M
3110 SN=SN+F(I)^2
3120 NEXT I
3130 IF SUMSQ <SN THEN SW=1: RETURN
3140 SW=0:RETURN
3150 RR=RINCR*RINCR-1
3160 V2=V*V
3170 IF IC>1 THEN 3280
3180 FOR I=1 TO N
3190 B(I,I)=B(M1,I)
3200 NEXT I
```

```
3210 FOR I=1 TO N:FOR J=N1 TO I STEP -1
3220 S=0
3230 FOR K=1 TO I
3240 S=S+B(K,I)*B(K,J)
3250 NEXT K
3260 B(J+1,I)=S
3270 NEXT J,I
3280 RV=RR*V2
3290 FOR I=1 TO N
3300 B(I+1,I)=B(I+1,I)+RV
3310 NEXT I
3320 FOR K=1 TO N
3330 S=B(K+1,K)
3340 IF K=1 THEN 3380
3350 FOR I=1 TO  K-1
3360 S=S-B(I,K)*B(I,K)
3370 NEXT I
3380 B(K,K)=SQR(S)
3390 B(M1,K)=B(K,K)*SGN(B(M1,K))
3400 FOR J=K+1 TO N1
3410 S=B(J+1,K)
3420 IF K=1 THEN 3460
3430 FOR I=1 TO K-1
3440 S=S-B(I,K)*B(I,J)
3450 NEXT I
3460 B(K,J)=S/B(M1,K)
3470 NEXT J
3480 NEXT K
3490 RETURN
3500 FOR K=1 TO N:BK=B(K,K)
3510 S=0
3520 FOR I=K TO M+K
3530 S=S+B(I,K)^2
3540 NEXT I:S=SQR(S)
3550 BT=1/(S*(S+ABS(BK)))
3560 IF BK=0 THEN B(M1,K)=-S:B(K,K)=S:GOTO 3590
```

```
3570 B(M1,K)=- SGN(BK)*S
3580 B(K,K)=BK+SGN(BK)*S
3590 FOR J=K+1 TO N1
3600 S=0
3610 FOR L=K TO M+K
3620 S=S+B(L,K)*B(L,J)
3630 NEXT L
3640 S=S*BT
3650 FOR I=K TO M+K
3660 B(I,J)=B(I,J)-S*B(I,K)
3670 NEXT I
3680 NEXT J
3690 NEXT K
3700 RETURN
3710 '
3720 '
3730 '
3740 '¥¥¥¥¥ Function ¥¥¥¥¥¥¥¥¥¥¥¥¥¥¥
3750 FOR I=1 TO N
3760   FACTOR(I)=-4+.5*I
3770     TAUI(I)=TAUC*10^(FACTOR(I))
3780 NEXT I
3790 '
3800 FOR II=0 TO M-2
3810    T=TAUC*10/100*II
3820    AAA(II)=EXP(-(T/TAUC)^BETA)
3830        BBB(II)=0
3840        FOR JJ=1 TO N
3850            BBB(II)=BBB(II)+X(JJ)*EXP(-T/TAUI(JJ))
3860        NEXT JJ
3870 '
3880    F(II)=AAA(II)-BBB(II)
3890 NEXT
3900 '
3910 SUMX=0
3920 FOR II=1 TO N
```

```
3930     SUMX=SUMX+X(II)
3940 NEXT II
3950    F(100)=1-SUMX
3960 RETURN
3970 ' End of subroutine stretch
□
```

Appendix B

```
10 '
20 '*********************************************************
30 '   Numerical Calculation of Motional Narrowing
40 '   of the Line Width by using stretched exponential
50 '   relaxation
60 '      For detailed inforamation, refer to J.Mag. Reson.
70 '
80 '            programmed by T. Akai
90 '
100 '           1996
110 '*********************************************************
120 '
130 SCREEN 3,0,0,1: CLS 3
140 DEF FNRELAX(T,T1,TAUC,BETA)=(T-T1)*EXP(-(T1/TAUC)^BETA)
150 '**************Main**********************************
160 DIM XF#(1024),YF#(1024),ZF(1024),CP#(1024),S(512),C(512),XINI#(1024)
170 DIM G#(1024),INTEG#(1024)
180 DIM TEMP(50),TAUC(50),FWHM(50),TDATA(100),FWDATA(100)
190 '
200 CS=1024
210 TAU0=1E-14'INPUT "TAU0";TAU0
220 EA=30 'INPUT "Activation Energy";EA
230 RL=24000'INPUT "RIGID LATTICE LINE WIDTH";RL
240 BETA=.5'INPUT "BETA";BETA
250 PRINT BETA
260 '
270 INITEMP=13:FLTEMP=INITEMP
280 FOR II=INITEMP TO 100
290     TEMP(II)=10*II
300     TAUC(II)=TAU0*EXP(EA*1000/8.32/TEMP(II)):PRINT TAUC(II)
310     IF TAUC(II)<7E-7 THEN GOTO 340
320     FLTEMP=FLTEMP+1
330 NEXT II
340 '
```

```
350 '
360 '
370 '
380 GOSUB *DISPLAY
390 '
400 '
410 '
420 '
430 FOR II=INITEMP TO FLTEMP
440     TAUC=TAUC(II)
450     GOSUB *DELDET :PRINT DELTA#
460     GOSUB *MNFORM
470     GOSUB *DATAFORM
480     GOSUB   *FFT
490     GOSUB   *FWHM
500   FWHM(II)=FWHM
510     GOSUB *PLOT :PRINT G#(100),INTEG#(100)
520 '
530 NEXT II
540 '
600 '
720    PRINT "TAU0,EA,BETA"; TAU0,EA,BETA
730 '
740 '
750 GOSUB *DATASAVE
760 END
770 '
780 '
790 '
800 '
810 '
820 '
830 '-----subroutine list----------
840 '
850 '*****SUBROUTINE FOURIER TRANSFORM
860 *FFT
```

```
870 CLS 1
880 M=LOG(CS)/LOG(2)
890 A=0:B=3.14159*2/CS
900 FOR I=0 TO CS/2:S(I)=SIN(A):C(I)=COS(A):A=A+B:NEXT I
910 L=CS:H=1
920 FOR G=1 TO M:L=L/2:K=0
930 FOR Q=1 TO H:P=0
940 FOR I=K TO L+K-1:J=I+L
950 A=XF#(I)-XF#(J):B=YF#(I)-YF#(J)
960 XF#(I)=XF#(I)+XF#(J):YF#(I)=YF#(I)+YF#(J)
970 IF P=0 THEN XF#(J)=A:YF#(J)=B:GOTO 990
980 XF#(J)=A*C(P)+B*S(P):YF#(J)=B*C(P)-A*S(P)
990 P=P+H:NEXT I
1000 K=K+L+L:NEXT Q
1010 H=H+H:NEXT G
1020 J=CS/2
1030 FOR I=1 TO CS-1:K=CS
1040 IF J<I THEN SWAP XF#(I),XF#(J):SWAP YF#(I),YF#(J)
1050 K=K/2:IF J>=K THEN J=J-K:GOTO 1050
1060 J=J+K
1070 NEXT I
1080 FOR I=0 TO CS-1:XF#(I)=XF#(I)/CS:YF#(I)=YF#(I)/CS:NEXT I
1090 CLS 1
1100 RETURN
1110 '
1120 '
1130 '
1140 '***** data form routine*************
1150 *DATAFORM
1160 FOR I=0 TO 1023
1170      PERIOD =4
1180       XF#(I)=COS(2*3.14159/PERIOD*I)*G#(I)
1190       XINI#(I)=XF#(I)
1200 NEXT I
1210 '
1220 RETURN
```

```
1230 '
1240 '
1250 '@@@@@@@@@ subroutine display @@@@@@@@@@@@
1260 *DISPLAY
1270   LINE (10,10)-(600,10): LINE (10,10)-(10,300)
1280   LINE (10,300)-(600,300):LINE (600,10)-(600,300)
1290   WINDOW(50,-RL/2)-(500,0)
1300   VIEW(10,10)-(600,300)
1310    FOR III=5 TO 50 STEP 5
1320     LINE(TEMP(III),0)-(TEMP(III),-RL/100)
1330     LINE(TEMP(III),-RL/100*99)-(TEMP(III),-RL)
1340    NEXT III
1350 RETURN
1360 '
1370 '
1380 '
1390 '@@@@@@@@@ evaluation of correlation function @@@@@@@@@@
1400 *MNFORM
1410 '
1420 '====== calculation of G#(i) by numerical calculation=======
1430 FOR I=1 TO 1024
1440       T#=DELTA#*I :DIV=20
1530 '        G2#(I)=EXP(-RL^2*TAUC^2*(EXP(-T#/TAUC)-1+T#/TAUC))
1540 '       G#(I)=EXP(-T#/TAUC)
1550 '
1560 ' SYMPSON
1570        SA#=0 : SB=T#
1580        SH#=T#/(2!*DIV)
1590        SS#=FNRELAX(T#,SA#,TAUC,BETA)+FNRELAX(T#,SB#,TAUC,BETA)
1600 '
1610        FOR SI=1 TO DIV
1620         SJ=2*SI-1
1630         SX#=SA#+SJ*SH#
1640         SS#=SS#+4!*FNRELAX(T#,SX#,TAUC,BETA)
1650        NEXT SI
1660 '
```

```
1670        FOR SI=2 TO DIV
1680          SJ=2*SI-2
1690          SX#=SA#+SJ*SH#
1700          SS#=SS#+2!*FNRELAX(T#,SX#,TAUC,BETA)
1710        NEXT SI
1720        SS#=SS#*SH#/3!
1721         G#(I)=EXP(-RL^2*SS#)
1740 '
1750 NEXT
1760 RETURN
1770 '
1780 '
1790 '@@@@@@ determination of delta @@@@@@@@@@@@@@@@@@@@
1800 *DELDET
1810 '--------Determination of DELTA----------
1820   DELTA#=.000006#
1830   T#=DELTA#*125
1840   G#=EXP(-RL^2*TAUC^2*(EXP(-T#/TAUC)-1+T#/TAUC))
1850   IF G#<.1 THEN GOTO 1880
1860   IF G#>.1 THEN DELTA#=DELTA#*1.5
1870   GOTO 1830
1880   IF G#>.08 THEN 1900
1890    DELTA#=DELTA#/2:GOTO 1830
1900   RETURN
1910 '
1920 '
1930 '@@@@@@@@ Calculation of FWHM by interpolation @@@@@@@
1940 *FWHM
1950 '-----MINIMUM AND MAXIMUM SEARCH----------
1960        YMIN=XF#(0):YMAX=XF#(0)
1970       FOR I=0 TO 512
1980          IF YMIN>XF#(I) THEN YMIN=XF#(I)
1990          IF YMAX<XF#(I) THEN YMAX=XF#(I)
2000       NEXT I
2010 '-------FWHM calculation by interpolation
2020       MIDY=(YMAX+YMIN)/2
```

```
2030      FOR I=O TO 511
2040        IF XF#(I)>MIDY THEN I1=I-1
2050        IF XF#(I)>MIDY THEN GOTO 2070
2060      NEXT I
2070      FOR I=I1+2 TO 511
2080        IF XF#(I)<MIDY THEN I2=I-1
2090        IF XF#(I)<MIDY THEN GOTO 2110
2100      NEXT I
2110 '
2120        XL=I1+(MIDY-XF#(I1))*(I1+1-I1)/(XF#(I1+1)-XF#(I1))
2130        XH=I2+(MIDY-XF#(I2))*(I2+1-I2)/(XF#(I2+1)-XF#(I2))
2140        FWHM=(XH-XL)/DELTA#/1024
2150        PRINT "FWHM";
2160 RETURN
2170 '
2180 *PLOT
2190        CIRCLE(TEMP(II),-FWHM(II)),.5,2,,,,F,2
2200 RETURN
2210 '
2220 '
2230 *DATASAVE
2240   FFF4$="e:ea30.dat" 'INPUT "DATAFILE TO SAVE";FFF4$
2250   OPEN FFF4$ FOR OUTPUT AS #1
2260    FOR II=INITEMP TO FLTEMP
2270       WRITE #1, TEMP(II), FWHM(II)
2280   NEXT II
2290 CLOSE #1
2300 RETURN
```